STUDIES ON THE NANOCELLULOSE FILLED POLYLACTIDE BASED BIOCOMPOSITES

A THESIS SUBMITTED TO
THE GRADUATE SCHOOL OF NATURAL AND APPLIED SCIENCES OF
MIDDLE EAST TECHNICAL UNIVERSITY

BY

BURCU SARI

IN PARTIAL FULFILLMENT OF THE REQUIREMENTS FOR
THE DEGREE OF DOCTOR OF PHILOSOPHY IN
POLYMER SCIENCE AND TECHNOLOGY

MARCH 2024

Approval of the thesis:

STUDIES ON THE NANOCELLULOSE FILLED POLYLACTIDE BASED BIOCOMPOSITES

submitted by **BURCU SARI** in partial fulfillment of the requirements for the degree of **Doctor of Philosophy in of Polymer Science and Technology Department, Middle East Technical University** by**,**

Prof. Dr. Naci Emre Altun
Dean, Graduate School of **Natural and Applied Sciences** _____

Prof. Dr. Necati Özkan
Head of Department, **Polymer Science and Technology** _____

Prof. Dr. Cevdet Kaynak
Supervisor, **Metallurgical and Materials Eng. Dept., METU** _____

Examining Committee Members:

Prof. Dr. Necati Özkan
Polymer Science and Technology Dept., METU _____

Prof. Dr. Cevdet Kaynak
Metallurgical and Materials Engineering Dept., METU _____

Prof. Dr. Bora Maviş
Mechanical Engineering Dept., Hacettepe University _____

Assoc. Prof. Dr. Simge Çınar Aygün
Metallurgical and Materials Engineering Dept., METU _____

Assist. Prof. Dr. Salih Ertan
Chemical Engineering Dept., Atılım University _____

Date: 14.03.2024

I hereby declare that all information in this document has been obtained and presented in accordance with academic rules and ethical conduct. I also declare that, as required by these rules and conduct, I have fully cited and referenced all material and results that are not original to this work.

Name, Last Name : Burcu Sarı

Signature :

ABSTRACT

STUDIES ON THE NANOCELLULOSE FILLED POLYLACTIDE BASED BIOCOMPOSITES

Sarı, Burcu
Ph.D., Department of Polymer Science and Technology
Supervisor: Prof. Dr. Cevdet Kaynak

March 2024, 128 pages

In the first part of this dissertation, the main purpose of the first step was to obtain and characterize cellulose nanocrystal (CNC) particles by applying sulfuric acid hydrolysis method to the starting material of microcrystalline cellulose (MCC) fibrils. After obtaining CNC particles via acid hydrolysis procedure, various analyses conducted revealed that average size of round shaped CNC particles was 38 nm with -30.4 mV Zeta potential value. They have monoclinic *Cellulose-I* crystal structure with *Crystallinity Index* of 80.6% and *Crystallite Size* of 3.39 nm. Their maximum thermal degradation temperature was 307ºC with 23 wt% residue at 800ºC. In the second step, the main aim was to investigate contribution of these obtained CNC particles when they were used as nano-reinforcement in polylactide (PLA) matrix biocomposites produced by industrially compatible melt mixing and shaping techniques. Mechanical tests revealed that when only 1 wt% CNC particles were incorporated into PLA matrix, increases in flexural strength and modulus were 29% and 51%, respectively, while increases in fracture toughness values were as much as 105%.

In the second part of this dissertation, the main purpose was to use “green materials” approach by investigating effects of only 1 wt% Cellulose Nanofibrils (CNF) on the strengthening and toughening of neat and blended polylactide (PLA) biopolymer matrix. For this purpose, first of all, effects of CNF were investigated in PLA/CNF biocomposite specimens. After blending of PLA with 10 phr bio-based thermoplastic polyester (b-TPE) elastomer, effects of CNF were investigated also for this PLA/b-TPE/CNF ternary biocomposite specimens. Mechanical tests revealed that due to the efficient strengthening and toughening mechanisms, CNF increased flexural strength of PLA by 33%, while b-TPE increased fracture toughness of PLA by 104%. When

CNF and b-TPE were incorporated together, synergism in the strength and toughness values occurred. All bioblend and biocomposite specimens were produced by using the same “melt mixing” technique in a laboratory size twin-screw extruder, and their test specimens were shaped by conventional “compression molding”. Since shaping by “3D-printing” is frequently used in the biomedical sectors, another distinctive aim of this part was to reveal whether there were any differences in the strength and toughness values of specimens after their 3D-printing. It was observed that due to the “textured” structure of 3D-printed specimens, their flexural strength values were approximately 20% lower, while fracture toughness values were approximately 20% higher.

In the third part of this dissertation, the main purpose was to investigate effects of various electrospinning parameters on the morphology and diameter of cellulose nanofibril (CNF) filled polylactide (PLA) nanofibers. For this purpose, first of all, effects of three important electrospinning parameters; polymer “Solution Concentration”, “Solution Feeding Rate” and “Collector Distance” to feeding tip were studied. Then, effects of using higher amount of CNF, effects of using cellulose nanocrystal (CNC) particles, and effects of adding potassium chloride salt were also investigated. It was observed that when optimum electrospinning parameters were determined, then it was possible to obtain almost “bead-free” morphology and “finest” average diameter of 232 nm for PLA/CNF electrospun fibers. Increasing values of Feeding Rate and Collector Distance parameters resulted in bead formation and thicker diameters. On the other hand, increasing CNF amount, using CNC particles and adding KCl salt, all resulted in further decreases in the diameter down to 152 nm; mainly due to increased charge density of the polymer solution. Moreover, *in vitro* degradation analysis of all types of electrospun nanofiber mats in a simulated body fluid revealed that increasing the immersion period increased their degradation rate in terms of “% weight loss”. It was also observed that mats with fine diameter fibers had higher degradation rate.

Keywords: Cellulose Nanocrystals, Cellulose Nanofibrils, Polylactide, Sulfuric Acid Hydrolysis, 3D-Printing, Electrospinning

ÖZ

NANOSELÜLOZ PARÇACIKLARI İÇEREN POLİLAKTİT BAZLI BİYOKOMPOZİTLER ÜZERİNE ÇALIŞMALAR

Sarı, Burcu
Doktora, Polimer Bilim ve Teknolojisi Bölümü
Tez Yöneticisi: Prof. Dr. Cevdet Kaynak

Mart 2024, 128 sayfa

Bu tezin ilk bölümündeki birinci amaç, başlangıç malzemesi olan mikrokristalin selüloz (MCC) fibrillerine sülfürik asit hidroliz yöntemi uygulanarak selüloz nanokristal (CNC) parçacıklarının elde edilmesi ve karakterize edilmesidir. Asit hidroliz işlemi ile CNC parçacıkları üretildikten sonra yapılan analizler, yuvarlak şekilli CNC parçacıklarının ortalama boyutunun 38 nm ve Zeta potansiyel değerinin ise -30,4 mV olduğunu ortaya çıkarmıştır. Bu parçacıklar %80,6 *Kristallik İndeksi*ne ve 3,39 nm *Kristalit Boyutu*na sahip monoklinik *Selüloz-I* kristal yapısına sahiptirler. Maksimum termal bozunma sıcaklığı 307°C, 800°C'deki kütlece kalıntı oranıysa %23 bulunmuştur. İkinci amaç ise, elde edilen CNC parçacıklarının endüstriyel üretime uyumlu eriyik karıştırma ve şekillendirme teknikleriyle üretilen polilaktit (PLA) matris biyokompozitlerinde nano takviye olarak kullanıldığında katkılarının araştırılmasıdır. Mekanik testler, PLA matrisine ağırlıkça yalnızca %1 CNC parçacıkları eklendiğinde, eğme mukavemeti ve modülündeki artışların sırasıyla %29 ve %51 olduğunu, kırılma tokluğu değerlerindeki artışlarınsa %105'e ulaştığını ortaya çıkarmıştır.

Bu tezin ikinci bölümündeki amaç, ağırlıkça sadece %1 Selüloz Nanofibrillerin (CNF) saf ve harmanlanmış PLA biyopolimer matrisinin güçlendirilmesi ve toklaştırılması üzerindeki etkilerini araştırmaktır. Bu amaçla hem PLA/CNF biyokompozit numunelerinde hem de 10 phr biyo bazlı termoplastik polyester (b-TPE) elastomer ile harmanlanmış PLA/b-TPE/CNF üçlü biyokompozit numunelerde CNF'nin etkileri araştırılmıştır. Mekanik testler, etkili güçlendirme ve toklaştırma mekanizmaları nedeniyle CNF'nin PLA'nın eğme mukavemetini %33 oranında arttırdığını, b-TPE'nin ise PLA'nın kırılma tokluğunu %104 arttırdığını ortaya çıkarmıştır. CNF ve b-TPE bir

araya getirildiğinde mukavemet ve tokluk değerlerinde sinerji oluşmuştur. Tüm biyo-harman ve biyo-kompozit numuneleri, laboratuvar boyutunda çift vidalı ekstruderde aynı "eriyik karıştırma" tekniği kullanılarak üretilmiştir ve test numuneleri, geleneksel "basınçlı kalıplama" ile şekillendirilmiştir. Biyomedikal sektöründe “3D baskı” ile şekillendirme sıklıkla kullanıldığı için bu çalışmanın bir diğer amacı da numunelerin 3D baskı sonrasında dayanım ve tokluk değerlerinde herhangi bir farklılık olup olmadığını ortaya çıkarmaktır. 3D baskılı numunelerin eğme mukavemet değerlerinin yaklaşık %20 daha düşük, kırılma tokluk değerlerinin ise yaklaşık %20 daha yüksek olduğu gözlemlenmiştir.

Bu tezin üçüncü bölümünde amaç, çeşitli elektroeğirme parametrelerinin CNF dolgulu PLA nanoliflerinin morfolojisi ve çapı üzerindeki etkilerini araştırmaktır. Bu amaçla öncelikle üç temel elektroeğirme parametresinin etkileri; polimer “Çözelti Konsantrasyonu”, “Çözelti Besleme Hızı” ve besleme ucuna “Kollektör Mesafesi” incelenmiştir. Ayrıca, daha yüksek miktarda CNF kullanımı, CNC kullanımı ve potasyum klorür tuzu ilavesinin etkileri de araştırılmıştır. Optimum elektroeğirme parametreleri belirlendiğinde, PLA/CNF elektroeğirme lifleri için neredeyse “boncuksuz” morfoloji ve 232 nm “en ince” ortalama çap elde etmenin mümkün olduğu gözlenmiştir. Besleme Hızı ve Kolektör Mesafesi parametrelerinin değerlerinin artması, boncuk oluşumuna ve daha kalın çaplara neden oldu. Öte yandan, hem CNF miktarının arttırılması, hem CNC parçacıkları kullanılması, hem de KCl tuzu ilave edilmesi, fiber çapının 152 nm'ye kadar azalmasını sağlamıştır. Ayrıca, simüle edilmiş vücut sıvısına daldırılmış nanofiber matların *in vitro* bozunma analizi, daldırma süresinin arttırılmasının "ağırlık kaybı yüzdesi" açısından bozunma oranlarını arttırdığını ortaya çıkarmıştır. İnce çaplı liflere sahip matların bozunma oranının daha yüksek olduğu da gözlenmiştir.

Anahtar Kelimeler: Selüloz Nanokristalleri, Selüloz Nanofibriller, Polilaktit, Sülfürik Asit Hidrolizi, 3-Boyutlu Baskı, Elektroeğirme,

To all living and non-living beings who struggle to coexist despite the plunder of nature...

ACKNOWLEDGEMENTS

The motivation behind this academic journey and exploring green material science has been a strong desire to solve one of the most critical problems of today, environmental crisis which is getting worse day by day. The main idea of this dissertation was born through the belief that materials science is the key to avoiding the harms of traditional products. This research is just a tiny contribution to the collective efforts to guide us to coexist more harmoniously with our fragile planet.

Journeys in the pursuit of knowledge and the achievement of academic goals often cannot be done alone. This thesis was shaped and enriched by the support of many people and institutions to whom I owe my gratitude. Foremost, I would like to express my deepest gratitude to my supervisor Prof. Dr. Cevdet Kaynak, whose guidance has been decisive in shaping this work, for his deep insight, constructive criticism and unremitting encouragement. I would also like to thank members of my thesis committee, Prof. Dr. Necati Özkan and Assoc. Prof.Dr. Simge Çınar Aygün, for their invaluable feed-back and scientific mentorship. Their insightful comments and meticulous review have undoubtedly strengthened the scientific background of this work. My heartfelt appreciation has gone out to my lab mates Deniz Varsavaş and Ulaş Can, who contributed to the progress of this thesis by sharing their fruitful insights. I am very satisfied to have experienced the culture of collective work in the Polymers and Nanocomposites Laboratory, with a special mention to my dear colleague Yelda Meyva Zeybek.

Of course, this academic journey extended beyond the boundaries of the academic community. My family and friends have been safe havens, providing support and encouragement during all stormy moments. Your support has been the wind beneath my wings and encouraged me to reach this milestone. This journey is as much yours as it is mine.

With sincere appreciation,

TABLE OF CONTENTS

ABSTRACT v
ÖZ vii
ACKNOWLEDGEMENTS x
TABLE OF CONTENTS xi
LIST OF TABLES xiv
LIST OF FIGURES xv
LIST OF NOMENCLATURE xviii
CHAPTERS 1
1. INTRODUCTION 1
1.1 Nanocellulose Structures 1
1.2 Use of Cellulose Nanostructures as Reinforcement in Polymer Matrix Composites 4
1.3 Polylactide / Nanocellulose Biocomposites 8
1.4 Three Main Objectives of This Dissertation 10
2. USE OF ACID HYDROLYSIS TO OBTAIN CELLULOSE NANOCRYSTALS FOR REINFORCING POLYLACTIDE BIOCOMPOSITES 11
2.1 Obtaining Cellulose Nanocrystal (CNC) Particles by Sulfuric Acid Hydrolysis 14
2.2 Characterization of CNC Particles 17
2.3 Production and Analyses of PLA/CNC Biocomposites 18
2.4 Characteristics of CNC Particles Obtained 19
2.5 Use of CNC Particles as Reinforcement in PLA Biocomposites 29
3. USE OF CELLULOSE NANOFIBRILS FOR STRENGTHENING AND TOUGHENING OF NEAT AND BLENDED POLYLACTIDE BIOCOMPOSITES 39
3.1 Ingredients of the Bioblends and Biocomposites 41
3.2 Production of Bioblends and Biocomposites 43
3.3 Shaping of Test Specimens by Compression Molding 43
3.4 Shaping of Test Specimens by 3D-Printing 45
3.5 Testing and Analyses of the Specimens 45

3.6 Fracture Surface Morphology of Bioblends and Biocomposites 47
3.7 Thermal Behavior of Bioblends and Biocomposites 49
3.8 Contribution of CNF on the Strengthening of Neat and Blended PLA ... 53
3.9 Contribution of CNF on the Toughening of Neat and Blended PLA 56
3.10 Differences in Strengthening and Toughening of Specimens After 3D-Printing 58
4. USE OF CELLULOSE NANOFIBRILS AND NANOCRYSTALS IN ELECTROSPINNING OF POLYLACTIDE NANOFIBERS 65
4.1 Materials Used 68
4.2 Electrospinning Procedures 69
4.3 Diameter Analysis of Electrospun Fibers 71
4.4 *In Vitro* Degradation Analysis of Electrospun Fibers 72
4.5 Effects of PLA/CNF Concentration in the Solution 74
4.6 Effects of Solution Rate and Collector Distance on the Bead-Free PLA/CNF Fibers 77
4.7 Effects of Solution Rate and Collector Distance on the Diameter of PLA/CNF Fibers 79
4.8 Effects of 3 wt% CNF Use Compared to 1 wt% on the Diameter of Electrospun Fibers 82
4.9 Effects of CNC Use Compared to CNF on the Diameter of Electrospun Fibers 84
4.10 Effects of KCl Salt Addition on the Diameter of Electrospun Fibers 84
4.11 Effects of Electrospun Fiber Diameters on the *In Vitro* Degradation Rate 86
5. CONCLUSIONS AND FUTURE RECOMMENDATIONS 89
5.1 Use of Acid Hydrolysis to Obtain Cellulose Nanocrystals for Reinforcing Polylactide Biocomposites 89
5.2 Effects of Cellulose Nanofibrils on the Strengthening and Toughening of Neat & Blended Polylactide 90
5.3 Use of Cellulose Nanofibrils and Nanocrystals in Electrospinning of Polylactide Nanofibers 92

5.4 Future Recommendations 93
REFERENCES 95
CURRICULUM VITAE 125

LIST OF TABLES

TABLES

Table 2.1 Flexural Strength (σ_{Flex}), Flexural Modulus (E_{Flex}) and Fracture Toughness (K_{IC} and G_{IC}) Values of PLA/CNC Biocomposites.....32

Table 2.2 Values of the thermal degradation temperatures and *%residue* of neat PLA and PLA/CNC biocomposites determined from TGA curves.....37

Table 3.1 Values of the transition temperatures, enthalpies and crystallinity amounts of bioblend and biocomposite specimens determined from first heating DSC thermograms.....50

Table 3.2 Values of the thermal degradation temperatures and *%residue* of the bioblend and biocomposite specimens determined from thermogravimetric curves...52

Table 3.3 Differences in the values of all mechanical properties of 3D-printed and compression molded specimens.....61

Table 4.1 Effects of average fiber diameters on the *in vitro* degradation degree of all electrospun fiber mats after each month.....88

LIST OF FIGURES

FIGURES

Figure 1.1 Scales of cellulose structure.....2
Figure 1.2 Three structures of nanocellulose.....4
Figure 1.3 Application areas of nanocellulose.....5
Figure 1.4 Estimates of nanocellulose production.....6
Figure 1.5 Production methods of polymer matrix nanocomposites.....7
Figure 2.1 Schematic of the sulfuric acid hydrolysis method to obtain cellulose nanocrystal (CNC) particles.....12
Figure 2.2 Images of the set-ups of each step to obtain CNC particles; (a) sulfuric acid hydrolysis, (b, c) dilution and washing, (d, e) dialysis, (f, g) sonication and filtering, (h) freeze drying and (i) solid particles of CNC.....16
Figure 2.3 SEM images showing size range and morphology of MCC fibrils and CNC particles.....21
Figure 2.4 Size distribution of CNC particles determined by DLS analyses.....22
Figure 2.5 FTIR spectrums of MCC fibrils and CNC particles.....24
Figure 2.6 X-ray diffractograms showing *Cellulose I* crystal structure of MCC fibrils and CNC particles.....26
Figure 2.7 TG and DTG curves for MCC fibrils and CNC particles.....28
Figure 2.8 Flexural stress-strain curves of PLA/CNC biocomposites.....30
Figure 2.9 Effects of CNC content on the flexural strength and modulus of PLA biocomposites.....31
Figure 2.10 Effects of CNC content on the fracture toughness of PLA biocomposites.....33
Figure 2.11 SEM images showing fracture surface morphology of PLA/CNC biocomposites.....35
Figure 2.12 Thermogravimetric curves of PLA/CNC biocomposites.....36
Figure 3.1 Molecular structure of the ingredients (PLA, b-TPE, CNF) used in the bioblends and biocomposites.....42
Figure 3.2 General views of the equipment used during production of bioblends and biocomposites by melt mixing; and their specimen shaping by conventional molding

and additive manufacturing technique.....44
Figure 3.3 General and closer view SEM images showing fracture surface morphology of bioblend and biocomposite specimens.....48
Figure 3.4 First heating DSC thermograms of bioblend and biocomposite specimens.....50
Figure 3.5 Thermogravimetric curves of bioblend and biocomposite specimens.....52
Figure 3.6 Flexural stress-strain curves of bioblend and biocomposite specimens....54
Figure 3.7 Contribution of CNF on the strengthening and stiffening of neat and blended PLA.....55
Figure 3.8 Contribution of CNF on the toughening of neat and blended PLA.....57
Figure 3.9 Differences in the flexural strength and modulus values of 3D-printed and compression molded specimens.....59
Figure 3.10 Differences in the fracture toughness values of 3D-printed and compression molded specimens.....60
Figure 3.11 Images of the semi-transparent neat PLA mechanical test specimens showing rather textured structure of 3D-printed ones compared to compression molded ones.....63
Figure 4.1 Two different nanocellulose structures (CNF and CNC) used as fillers in biocomposites.....65
Figure 4.2 Typical electrospinning system indicating important processing parameters.....67
Figure 4.3 General view of the electrospinning equipment used.....70
Figure 4.4 General and closer views of *in vitro* degradation of electrospun fiber mats.....72
Figure 4.5 Images showing effects of PLA/CNF concentration or viscosity of the solution on the formation of Taylor Cone and polymer Solution Jet.....75
Figure 4.6 SEM images showing effects of solution concentration on the formation of PLA/CNF “droplets” or “beaded fibers” 76
Figure 4.7 SEM images showing effects of solution rate and collector distance on the formation of “beaded” and “bead-free” electrospun PLA/CNF fibers.....78
Figure 4.8 General and closer SEM images showing effects of Solution Rate on the average diameter of PLA/CNF electrospun fibers when Collector Distance was kept

as 15 cm.....80
Figure 4.9 General and closer SEM images showing effects of Collector Distance on the average diameter of PLA/CNF electrospun fibers when Solution Rate was kept as 1.5 mL/h.....81
Figure 4.10 SEM images showing effects of higher CNF amount on the diameter of PLA/CNF electrospun fibers.....83
Figure 4.11 SEM images showing effects of CNC use and KCl salt addition on the diameter of electrospun fibers.....85
Figure 4.12 Increase of degradation degrees with increasing PBS immersion period for all electrospun fiber mats.....87

LIST OF NOMENCLATURE

NOMENCLATURE

CNC	**:**	cellulose nanocrystal
CNF	**:**	cellulose nanofibril
BNC	**:**	bacterial nanocellulose
MCC	**:**	microcrystalline cellulose
PLA	**:**	poly(lactic acid) or polylactide
b-TPE	**:**	bio-based thermoplastic polyester
CF	**:**	chloroform
DMF	**:**	dimethyl formamide
KCl	**:**	potassium chloride
TEMPO:		(2,2,6,6-Tetramethylpiperidin-1-yl)oxyl
PBS	**:**	phosphate buffered saline
pH	**:**	potential for hydrogen
ISO	**:**	International Organization for Standardization
ATR	**:**	attenuated total reflectance
FTIR	**:**	Fourier transform infrared spectroscopy
DSC	**:**	differential scanning calorimetry
DLS	**:**	dynamic light scattering
XRD	**:**	x-ray diffraction
SEM	**:**	scanning electron microscopy
TGA	**:**	thermogravimetric analysis
TG	**:**	thermogravimetric
DTG	**:**	differential thermogravimetric
2θ	**:**	XRD diffraction angle
σ_{Flex}	**:**	flexural strength
E_{Flex}	**:**	flexural modulus
G_{ic}	**:**	fracture toughness as critical strain energy release rate
K_{ic}	**:**	fracture toughness as critical stress intensity factor
$T_{5\%}$	**:**	thermal degradation temperature at 5 wt% mass loss

$T_{10\%}$	:	thermal degradation temperature at 10 wt% mass loss
$T_{25\%}$	:	thermal degradation temperature at 25 wt% mass loss
T_{max}	:	thermal degradation temperature of maximum mass loss rate
T_g	:	glass transition temperature
T_{cc}	:	cold crystallization temperature
T_m	:	melting temperature
ΔH_{cc}	:	heat of crystallization
$\Delta H_m°$	:	melting enthalpy of 100% crystalline PLA
X_c	:	degree of crystallinity
CrI	:	crystallinity index
I	:	peak intensity
D_{hkl}	:	crystallite size
k	:	Scherrer's constant
λ	:	X-ray wavelength
θ	:	Bragg's angle
β	:	full width at half maximum

CHAPTER 1

INTRODUCTION

Derived from renewable sources such as plants, algae or tunicates, nanocellulose has grown in popularity owing to its exceptional properties for diverse applications. Some of the indispensable properties of cellulose-based materials such as functionality, uniformity, and durability can be improved by transforming macro and micro cellulose structures into nanocellulose structures which present enhanced mechanical properties due to their high surface area, large water-holding capacity and reactive hydroxyl side groups, where almost any desired functional group can be attached. As seen in Figure 1.1, cellulose has different structures at different scales such as micron-sized cellulose and nano-sized cellulose structures [1].

1.1. Nanocellulose Structures

As illustrated in Figure 1.2, nanocellulose structures can be mainly in cellulose nanocrystal (CNC), cellulose nanofibril (CNF) and bacterial nanocellulose (BNC) forms [1, 2]. These materials exhibit distinct properties that make them suitable for various applications, and ongoing research aims to optimize their production processes and expand their applicability.

(i) Cellulose Nanocrystals (CNC)

Cellulose nanocrystals (CNC) are rod-like nanoparticles produced by breaking down the larger cellulose fibers into tiny crystalline structures. The geometrical dimensions of CNCs are “all nano”, with diameter in the range of 5–50 nm and length in the range of 100–300 nm [3].

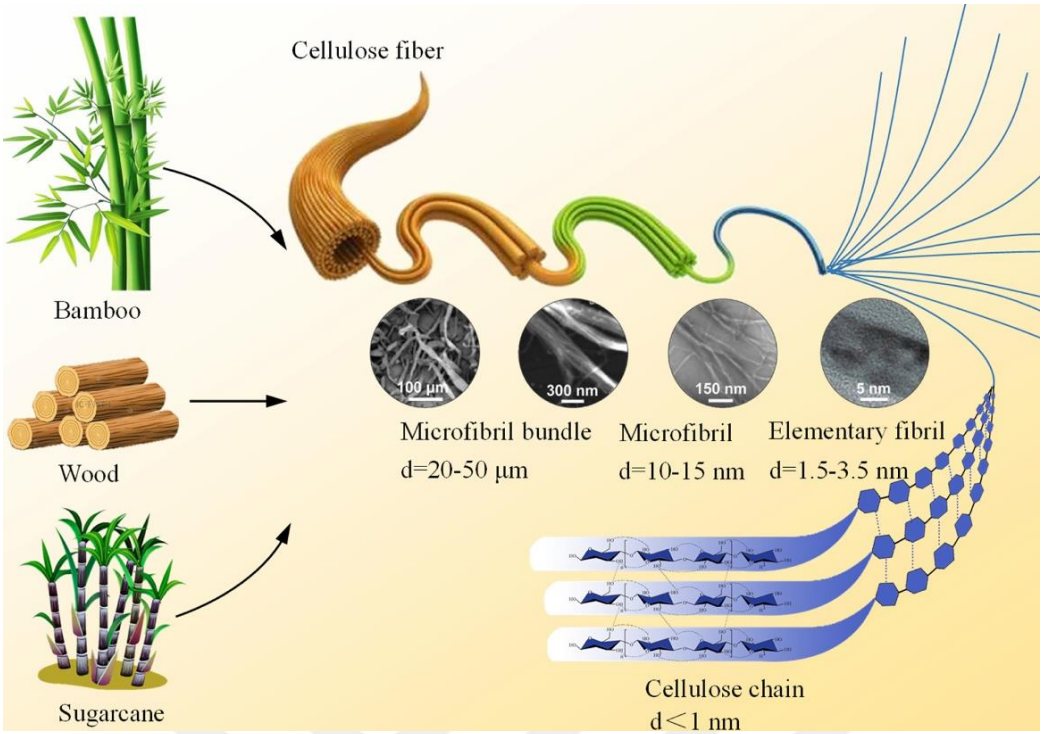

Figure 1.1 Scales of cellulose structure [1]

The extraction process involves breaking down the amorphous regions of cellulose, leaving behind the crystalline segments. The resulting CNCs possess unique mechanical, thermal, and optical properties owing to their nanoscale dimensions, large surface area, highly crystalline structure, transparency and chemical purity. The most common CNC production technique is acid hydrolysis [4] and various strong acids such as hydrochloric, phosphoric and sulfuric acids have been studied in the literature [3].

In this technique, amorphous regions of the cellulose microfibrils are eliminated by introducing acid attacks under controlled conditions such as the nature of the acid, the concentration of acid, the temperature, the mixing rate, the reaction time, and the cellulose fibers-to-acid solution ratio. The hydronium ions slip into the amorphous regions of the cellulose structure and induce the hydrolytic degradation of the glycosidic bonds.

(ii) Cellulose Nanofibrils (CNF)

Cellulose nanofibrils (CNF) consist of stretched aggregates of elementary nanofibrils that consist of both crystalline and amorphous domains. Their diameter is in the 5-50 nm range and lengths extend into the micrometer scale [5]. The production of CNFs involves mechanical, chemical or enzymatic processes to separate and disentangle cellulose fibers at the nanoscale. CNF extraction from micron-sized cellulosic fibrils is mainly obtained by mechanical treatments such as homogenization, grinding, and milling; chemical treatments such as TEMPO oxidation and enzymatic hydrolysis; or a combination of these methods. During mechanical treatment, CNFs are generally produced from wood-pulp fibrils by using high-pressure homogenizers.

(iii) Bacterial Nanocellulose (BNC)

Bacterial nanocellulose (BNC) is produced through a bottom-up approach, the biosynthesis of cellulose by bacterial fermentation, typically strains of Acetobacter [6]. BNC possesses a highly crystalline structure and high purity, offering exceptional mechanical properties and biocompatibility. However, production is time-consuming and costly compared to CNC and CNF. In order to isolate bacterial nanocellulose (BNC), certain bacteria, such as Acetobacter xylinum, are cultured in a suitable medium that supports cellulose production. The bacterial culture medium plays a crucial role in supporting bacterial growth and cellulose production. It typically consists of carbon and nitrogen sources, minerals, and other nutrients. The fermentation conditions, including temperature, pH, and agitation, are carefully controlled to optimize cellulose production [7].

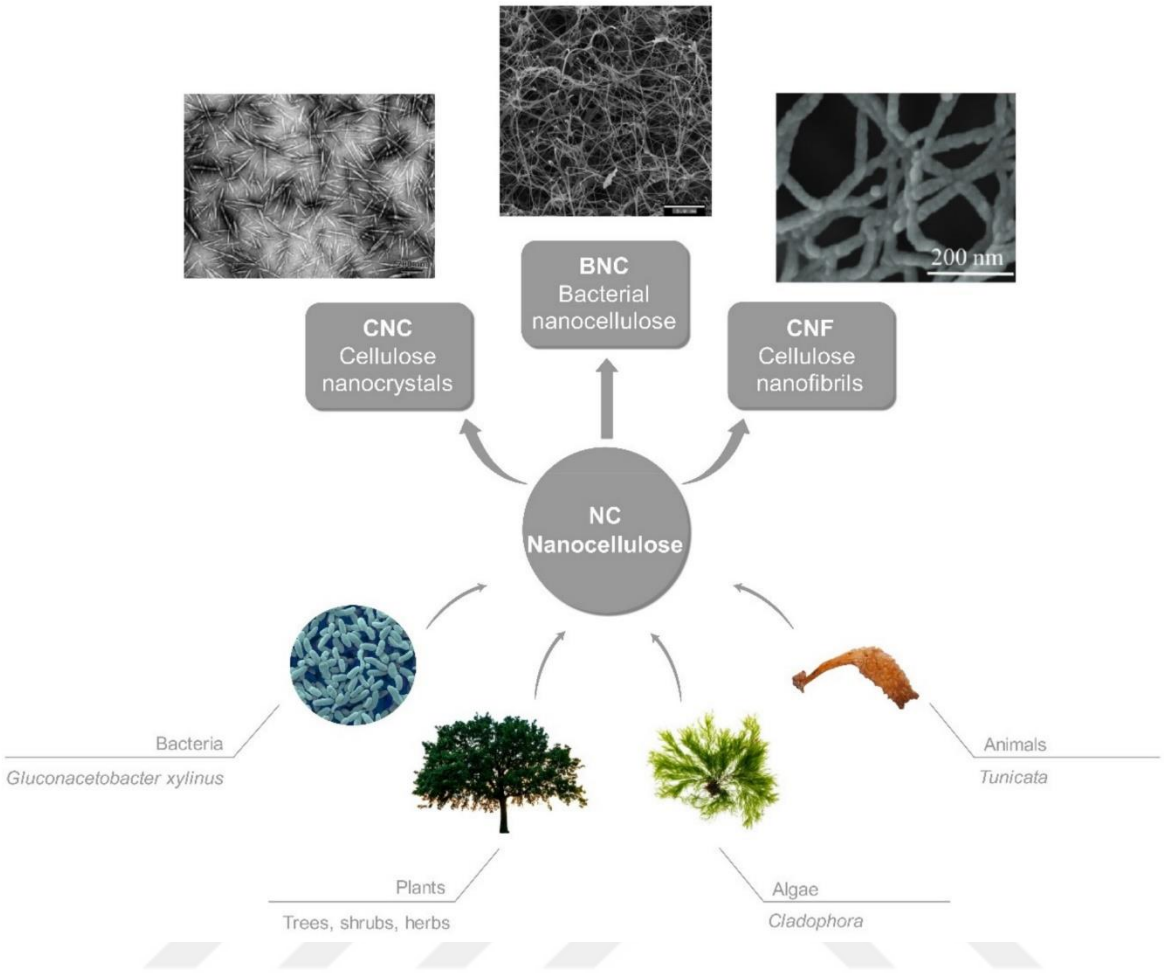

Figure 1.2 Three structures of nanocellulose [8]

1.2. Use of Cellulose Nanostructures as Reinforcement in Polymer Matrix Composites

At the point where material technologies have come, it is not easy to meet complex end-product requirements with a single material. We can see that both academia and various industries' orientation towards composite materials is increasing day by day. Composite materials can be described as the combination of two or more distinct constituents with different physical and chemical properties to enhance material properties compared to individual constituents alone. These constituents are mainly described as matrix phase and reinforcement (filler) phase.

Cellulose nanostructures have a wide range of applications due to their unique properties as shown in Figure 1.3. While nanocellulose can be used alone in applications such as drug delivery systems [9], tissue scaffolds [10], biosensors [11], food [12], supercapacitors [13], printed electronics [14]; they are generally used as a reinforcing material in polymer composites such as epoxy [15], polyethylene (PE) [16], polypropylene (PP) [17] and polystyrene (PS) [18] matrix nanocomposites.

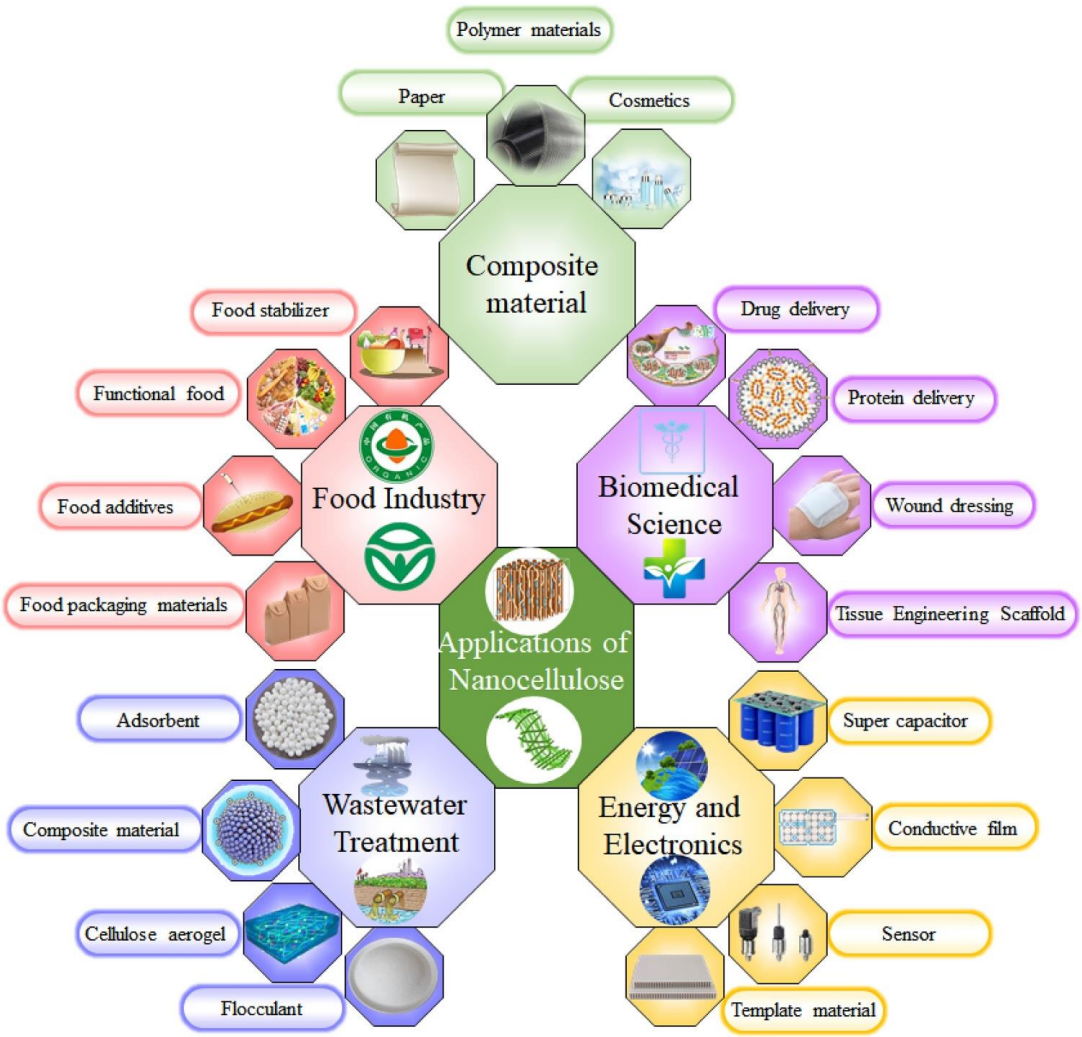

Figure 1.3 Application areas of nanocellulose [1]

As seen in Figure 1.4, the nanocellulose market is experiencing strong growth driven by the increasing demand for environmentally friendly materials in various industries. Technological developments in nanotechnology and the interest of academia in this

field have also expanded the potential applications. At the same time, government regulations aimed at encouraging the use of green materials are also accelerating the growth in the market.

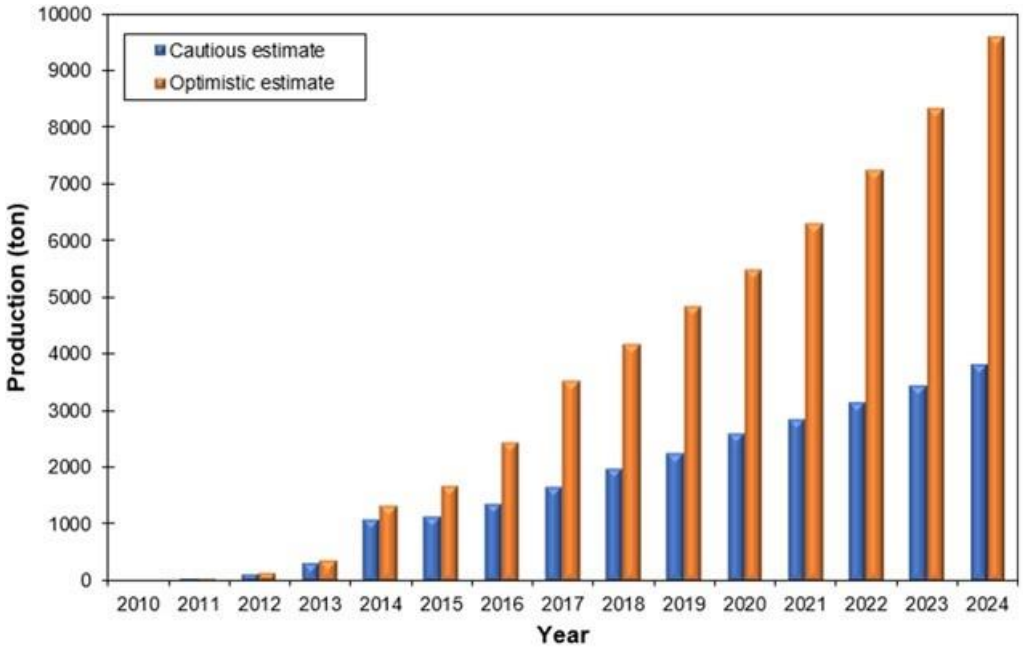

Figure 1.4 Estimates of nanocellulose production [19]

In order to produce polymer matrix nanocomposite with cellulose nanostructures, three main production routes shown in Figure 1.5 have been used: "Solution Mixing", "*In situ* Mixing" and "Melt Mixing" [20]. Solution mixing is a method used to prepare composite materials where the nanocellulose is dispersed in a solvent along with the matrix material. The process involves dissolving, dispersal and solvent removal steps. In this method, homogenous nanocellulose dispersion and process of temperature-sensitive composites can be easily obtained. However, the solvent removal step can be toxic and energy-intensive. Also, solvent alternatives are limited for polymers.

On the other hand, *in situ* mixing involves the creation of composite materials within the matrix material itself, typically during the manufacturing process. The reinforcing phase is generated or introduced *in situ*, providing a seamless integration of nanocellulose with the matrix. In this method, enhanced interfacial bonding between

matrix and reinforcing phases, and improved mechanical properties due to a homogeneous distribution of reinforcements can be obtained. However, the process is complex and suitable for small-batch systems.

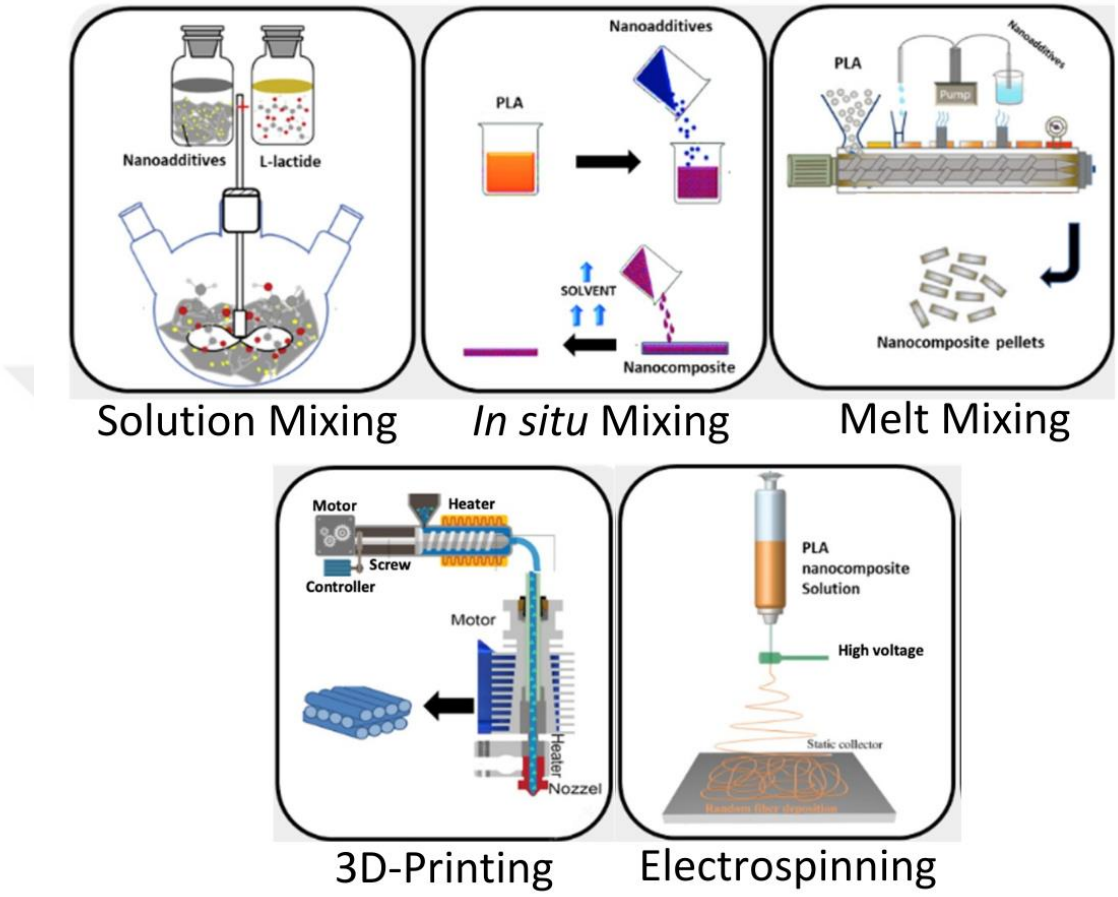

Figure 1.5 Production methods of polymer matrix nanocomposites [20]

Melt mixing is the third and the most common method in industry to produce polymer matrix composites, where nanocellulose particles are added to the molten polymer. This method provides high-volume production with various nanocellulose structures. One of the most used melt mixing equipment is twin-screw extruder, which has two intermeshing screws housed within a barrel. The rotation of the screws imparts shear forces on the materials and facilitates the transport, melting, and mixing of materials within the extruder.

Apart from these three main methods, new polymer nanocomposite production and shaping methods such as electrospinning and 3D-printing have revolutionized the field of composite technologies. Both of these methods expand the application areas of traditional production methods and contribute to the use of polymer nanocomposites in areas such as smart textiles, packaging, tissue engineering and prototyping:

Additive manufacturing, commonly known as 3D-printing [21], involves layer-by-layer deposition of material by melt blending process to build a three-dimensional object. 3D-printing enables the fabrication of complex geometries and customization of the final product. This method is the best candidate for rapid prototyping, custom prosthetics and implants.

Another remarkable method is electrospinning which is a fiber production method that uses an electric field to draw nanoscale fibers from a solution [22]. This method allows high surface area fibers. Application areas of electrospun nanocellulose biocomposites are mainly tissue engineering, drug delivery, protective gear membranes and sensors.

1.3. Polylactide / Nanocellulose Biocomposites

As a result of the destruction of nature at a faster rate than its renewal rate, the sustainability debates, which are getting hotter day by day, have opened the door to new directions in the field of materials science. Of course, the leading of these trends is the production of green materials and multiplication of their application areas. Green material refers to a substance that is characterized by its minimalized environmental impact in terms of resource use, energy consumption, and waste generation.

Two important trends in material science discussed above, green material and composite material approaches, come together in the concept of "fully green composite". Fully green composites prioritize the use of environmentally friendly matrix and reinforcements to achieve eco-friendly end products, which are a specific

subset of material science that combines the principles of green chemistry and materials in the realm of composite materials.

As explained above, nanocellulose as a reinforcement material is used in a wide variety of polymer matrices. However, cellulose nanostructures have recently been used with biopolymer matrices for the fully green composite approach. For these purposes, various biopolymers are used as matrix materials such as chitosan [23], polyhydroxybutyrate (PHB) [24], poly (3-hydroxybutyrate-co-3-hydroxyvalerate (PHBV) [25], polybutylene succinate (PBS) [26], natural rubber [27], etc. However, the most promising polymer is polylactide or poly(lactic) acid (PLA) for cellulose nanostructure-filled nanocomposites [28], for which 3D-printing [29] and electrospinning [30] methods have also been frequently used to produce PLA/nanocellulose composites, recently.

PLA has been synthesized from renewable sources, such as corn starch, sugarcane or other carbohydrate sources and today it is one of the most significant biopolymers with comparable mechanical, thermal, and chemical properties with traditional thermoplastics. Moreover, due to its biocompatibility and biodegradability characteristics, PLA attracts a lot of attention in food packaging, drug delivery, biomedical and tissue engineering. However, the production of PLA based products is limited due to several disadvantages such as brittleness, low service temperature and slow crystallization rates. To overcome these problems of PLA, nanoparticles such as nanocellulose have been a functional reinforcement. Overall, PLA/nanocellulose composites offer synergistic effects that can lead to improved mechanical, thermal biocompatible, and biodegradable properties, making them attractive candidates for various engineering applications in textile, packaging, automotive, biomedical, and other industries.

1.4. Three Main Objectives of This Dissertation

As would be discussed in the further chapters of this dissertation, although there are certain numbers of studies conducted on the various aspects of polylactide filled with nanocellulose structures CNC and CNF, there are still certain aspects to be contributed. Therefore, three main objectives selected in this dissertation were as follows.

In Chapter 2, the main objective was to obtain and characterize CNC particles produced by sulfuric acid hydrolysis method and to reveal effects of CNC particles on the mechanical performance including fracture toughness of PLA biocomposites.

In Chapter 3, the main objective was to investigate degree of strengthening and toughening of neat and bioelastomer blended PLA when reinforced with only 1 wt% CNF; and to reveal whether there were any differences in the strength and toughness values of specimens after their 3D-printing, compared to their compression molded counterparts.

In Chapter 4, the main objective was to investigate effects of various parameters on the diameter of CNF and CNC filled PLA electrospun nanofibers; and their *in vitro* degradation behaviour in a simulated body fluid.

CHAPTER 2

USE OF ACID HYDROLYSIS TO OBTAIN CELLULOSE NANOCRYSTALS FOR REINFORCING POLYLACTIDE BIOCOMPOSITES

Cellulose, being the main building block of all plants, is the most abundant natural polymer structure. Due to its many particular properties including mechanical performance and biocompatibility, it is used for various purposes in many sectors. Although cellulose has been used in the form of macro-sized fibers or micron-sized fibrils for various applications, today there are many technological expectations if cellulose could be obtained as the nano-sized structure efficiently and economically.

There have been a tremendous number of investigations to obtain nano-sized cellulose structures by using various combinations of mechanical, chemical and biological techniques. Depending on the structure, morphology and production technique, these nano-sized structures are classified as “Cellulose Nanocrystals” (CNC) or “Cellulose Nanofibrils” (CNF) and sometimes as “Bacterial Nanocellulose” (BNC) [31-33].

Generally, as shown in Figure 2.1, cellulose nanocrystal (CNC) particles were isolated from certain micron-sized cellulosic resources by concentrated “acid hydrolysis” procedure. When process parameters are carefully determined during acid hydrolysis method, not only does reduction in size take place; but also, amorphous and paracrystalline domains are eliminated.

Although various strong acids have been used for the production of CNC particles including hydrochloric acid [34], phosphoric acid [35], hydrobromic acid [36], and maleic acid [37]; the most effective one is reported as sulfuric acid [38-47]. Because, when CNC particles were obtained via sulfuric acid hydrolysis, there would be formation of negatively charged sulfate groups (such as $R–OSO_3^-$) on their surfaces leading to homogeneous and more stable suspensions due to enhanced electrostatic

repulsion [41-43].

In the literature, to obtain CNC particles, various studies were reported in which their starting materials were macro-sized cellulose resources, such as cotton [38], bamboo [39], sugarcane [40], jute [41], hemp [42], kenaf [43], tunicates [44] and so on. On the other hand, before obtaining nano-sized cellulose structures, it was generally required to conduct many further processes to obtain micron-sized structures first. Consequently, starting from macro-sized resources takes much longer periods and lower degree of repeatability.

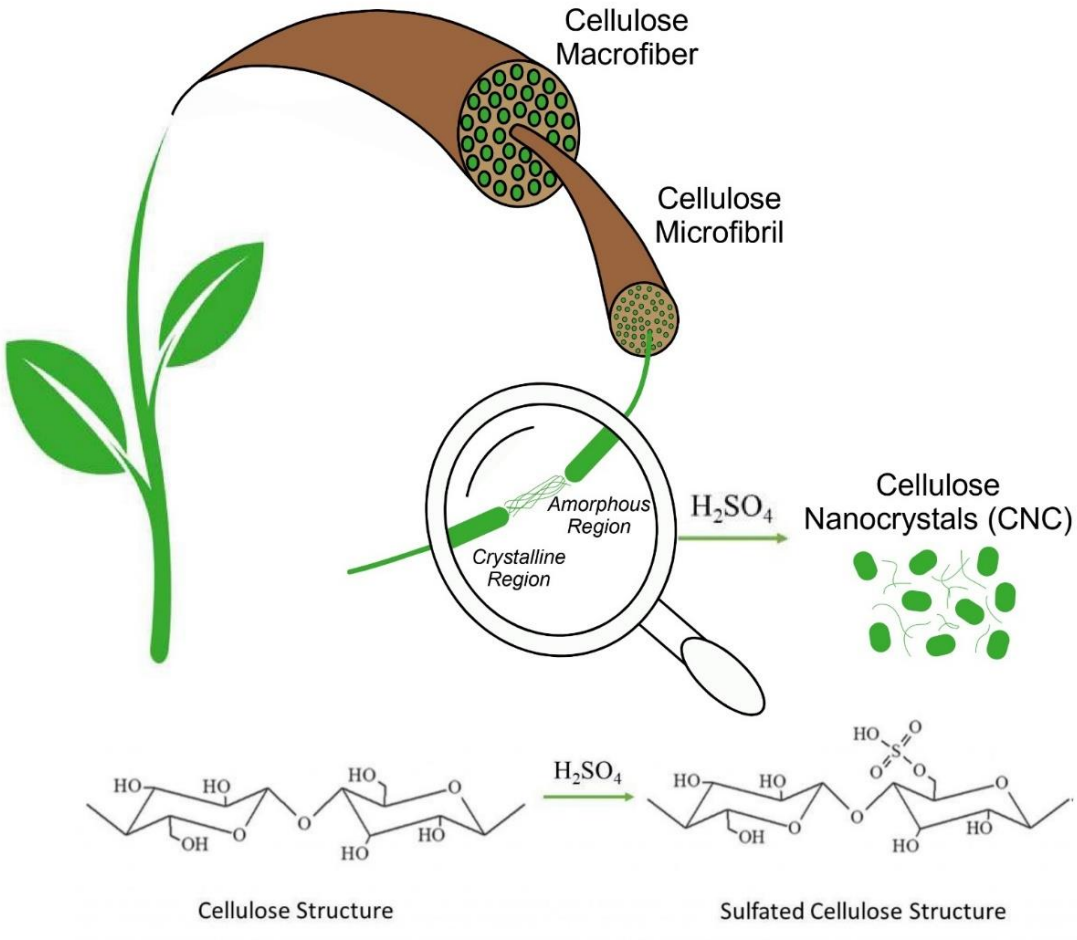

Figure 2.1 Schematic of the sulfuric acid hydrolysis method to obtain cellulose nanocrystal (CNC) particles

Thus, for practical reasons and much higher repeatability, to obtain CNC particles via acid hydrolysis method, many researchers [45-48] used microcrystalline cellulose (MCC) fibrils as the starting material. Since MCC fibrils are available commercially, they have been chosen as the starting material in this study, too.

After obtaining CNC particles, although they might be used for many other purposes, they have been generally considered as the filler material in the production of biocomposites. For this purpose, as the matrix material, various biopolymers including poly(hydroxybutyrate) (PHB) [49, 50], poly(butylene succinate) (PBS) [51, 52], poly(epsilon-caprolactone) (PCL) [53, 54] have been used. Of course, due to its higher mechanical performance, and its commercial mass production, poly(lactic acid) also named as polylactide (PLA) is the most preferable biopolymer matrix material.

Literature survey on PLA/CNC biocomposites [55-64] revealed that, in many of them biocomposites were generally evaluated in terms of thermal and biomedical behaviors including tensile and flexural mechanical properties, but not fracture toughness performance. Moreover, to the best of our knowledge, in none of these PLA/CNC biocomposite studies, CNC particles were obtained not from MCC fibrils; their CNC particles were either supplied commercially, or their starting materials used during acid hydrolysis method were other cellulose resources.

Therefore, after obtaining CNC particles from MCC fibrils by sulfuric acid hydrolysis method, and producing PLA/CNC biocomposites by industrially compatible melt mixing and shaping techniques; the main contribution of this chapter would be to reveal effects of CNC particles on the mechanical performance including fracture toughness of PLA biocomposites, which is considered as the most dominant property required in structural components.

After obtaining and characterizing CNC particles, they were used as the reinforcement material in PLA matrix biocomposites. Experimental procedures conducted for these steps were as follows.

2.1 Obtaining Cellulose Nanocrystal (CNC) Particles by Sulfuric Acid Hydrolysis

In this study, the starting material used during acid hydrolysis procedure was "micron-sized crystalline cellulose fibrils" (purchased from Sigma-Aldrich, USA). That kind of cellulose structure is generally named as "microcrystalline cellulose", and designated with MCC. Following steps applied to obtain CNC particles via sulfuric acid hydrolysis were based on the related studies cited in the literature [65, 66]:

(i) Acid Hydrolysis

In this step, the strong acid used was 97% purity sulfuric acid (H_2SO_4) (Fluka, Germany). The suspensions of distilled water with micron-sized crystalline cellulose (MCC) fibrils were continuously stirred at 45°C for 120 minutes (Figure 2.2(a)). During stirring, sulfuric acid concentration was arranged as 64%. Then, acid-to-cellulose ratio was 8.75 mL/g.

(ii) Dilution and Washing

In order to stop acid hydrolysis, suspensions were diluted with 10-fold distilled water and left overnight for decantation (Figure 2.2(b)). Then, repeated washing steps were applied in centrifuge (Nüve NF 200, Turkey) at 5000 rpm for 5 min (Figure 2.2(c)).

(iii) Dialysis

For the removal of free acid molecules (i.e., sulfate ions) and to neutralize suspensions; dialysis with distilled water was applied for one week (Figure 2.2(d)). A special dialysis membrane (14 kDA, Viskase Membra-Cel, USA) was used, and the procedure was continued until obtaining a constant value of pH, measured by using a digital pH meter (Hanna, HI 211, USA) (Figure 2.2(e)).

(iv) Sonication and Filtering

To achieve stable and homogenous colloidal suspensions with cellulose particles, sonication was applied by using an ultrasonic homogenizer (Bandelin Sonopuls HD3200, Germany) for 15 minutes at 75 W. In order to prevent overheating, sonication was performed in an ice bath (Figure 2.2(f)). Then, larger cellulose particles and other impurities that might left in suspensions were filtered through a special filtering medium (Macherey-Nagel, MN640m-125mm, Germany) with the help of a vacuum pump (Millipore, 230 V, Germany) (Figure 2.2(g)).

(v) Freeze Drying

Freeze drying also known as “lyophilization” was the last step for the complete removal of water molecules by sublimation so that a pile of solid particles of nanocellulose crystals could be obtained. It was applied by using a freeze dryer (Christ, Alpha 2-4 LDplus, Germany) under 0.05 mbar for two days (Figure 2.2(h)). After freeze drying, a certain degree of grinding was necessary to get CNC particles in the form of fine powders (Figure 2.2(i)).

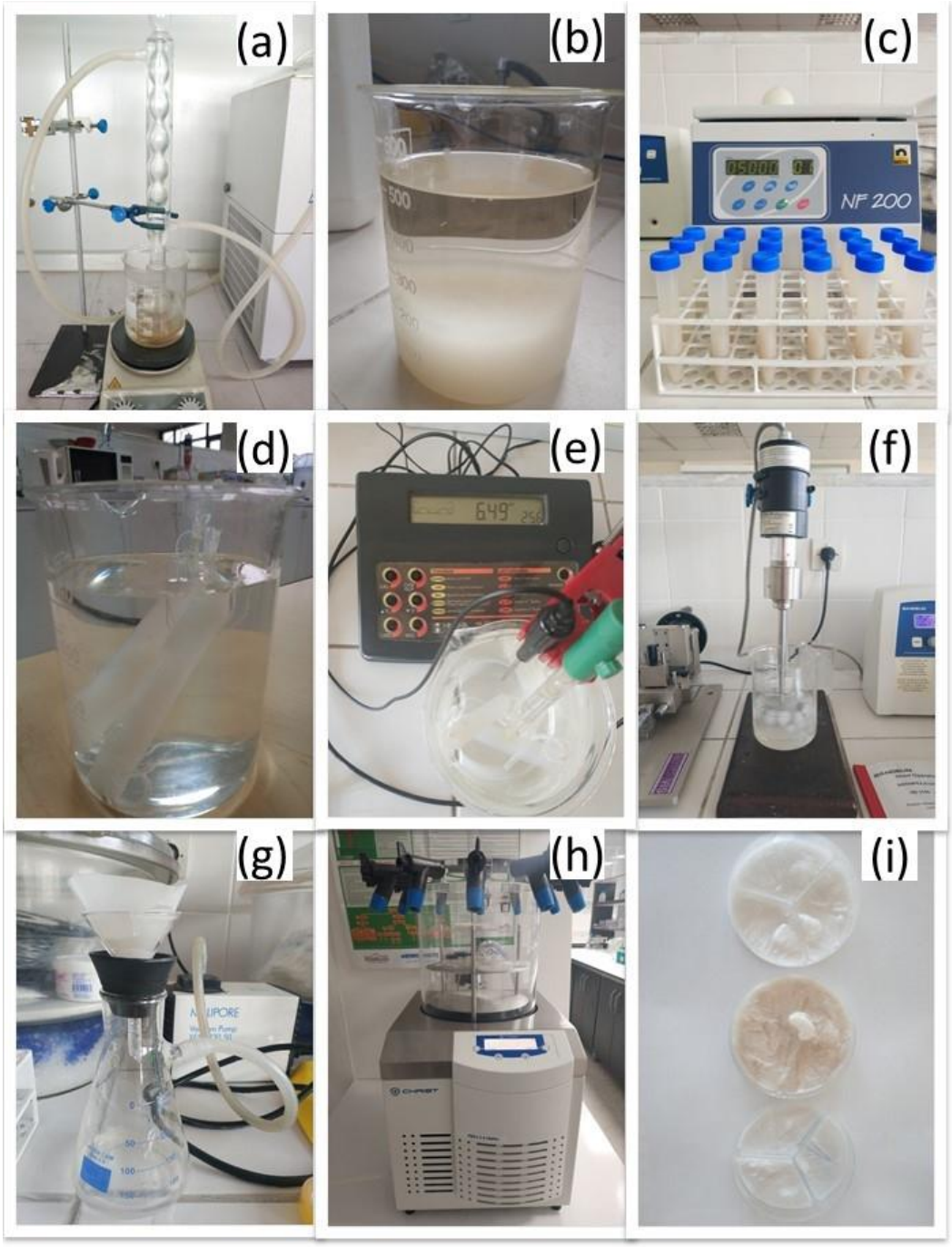

Figure 2.2 Images of the set-ups of each step to obtain CNC particles; (a) sulfuric acid hydrolysis, (b, c) dilution and washing, (d, e) dialysis, (f, g) sonication and filtering, (h) freeze drying and (i) solid particles of CNC

2.2 Characterization of CNC Particles

After obtaining CNC particles via sulfuric acid hydrolysis, their structure was investigated by using the following analyses. For comparison, these characterization techniques were also applied to MCC fibrils.

(i) Scanning Electron Microscopy (SEM)

The first analysis to investigate size range and morphology of CNC particles was SEM analysis (FEI, Nova Nano 430, Japan). For this purpose, particles were adhered to conductive two-sided carbon tape.

(ii) Dynamic Light Scattering (DLS)

The second analysis conducted to determine size distribution and Zeta potential of CNC particles obtained was DLS analysis (Malvern, Zetasizer Nano ZS, UK). All measurements were carried out in triplicate, at room temperature, by using 633 nm red laser. Samples of the CNC water solutions were prepared with 0.1 mg/mL concentration. During size distribution calculations, the values of refractive index and absorption coefficient used for the nanocellulose particles were 1.49 and 0.01, respectively. According to Smoluchowski's approximation, Henry's function “F(κa)” was used as 1.5.

(iii) Fourier-Transform Infrared Spectroscopy (FTIR)

Chemistry of the CNC particles obtained was evaluated by FTIR spectroscopy (Bruker, Alpha 25, USA). For this purpose, attenuated total reflectance (ATR) unit of the equipment was utilized in the wavenumber range from 4000 cm^{-1} to 500 cm^{-1}.

(iv) X-ray Diffraction (XRD)

Crystal structure of CNC particles was observed by XRD analysis (Bruker, D8 Advance A25, USA). For this purpose, CuKα radiation was utilized in the 2Θ range from 5º to 40º.

(v) Thermogravimetric Analysis (TGA)

Moreover, thermal degradation behavior of CNC particles was determined by TGA investigation (SII TG/DTA 7300, Exstar, Japan) under 10°C /min heating rate between 30°-800°.

2.3 Production and Analyses of PLA/CNC Biocomposites

In this study, CNC particles obtained by acid hydrolysis technique were evaluated as the potential reinforcement for the production of "fully green composites". For this purpose, the biopolymer matrix phase chosen was polylactide (PLA) with L-type lactic acid macromolecules (NaturePlast, PLE 001, France) having weight average molecular weight of 10^5 g/mol. In order to reveal effects of CNC amount in the biocomposites, four different loading levels (0.5, 1, 2, 3 wt%) were used. Production techniques and the analyses used for these PLA/CNC biocomposites were as follows.

(i) Mixing and Shaping of PLA/CNC Biocomposites

Biocomposites were produced by using the "melt mixing" method in a laboratory scale "twin-screw extruder" (Rondol, Microlab 300, UK). Typical temperature profile used in the extruder zones were 120°-170°-180°-175°-145°C, while the screw speed was 60 rpm. Before melt mixing, CNC particles and PLA granules were pre-dried in a vacuum oven at certain temperatures for certain periods.

In order to shape mechanical test specimens of PLA/CNC biocomposites, conventional "compression molding" method was used. Before filling the molds prepared according to the related ISO standards with 2-3 mm pellets obtained from the cutter of the twin-screw extruder, these pellets were first dried in an oven at 60°C for 12 hours. Then, test specimens were shaped by using a laboratory-scale hot press (MSE, LP_M2SH05, Turkey) at around 165°C, under 25 kN for 10 minutes.

(ii) Testing and Analyses of PLA/CNC Biocomposites

First of all, the degree of CNC distribution in the PLA matrix was observed by the same SEM equipment explained above. This time, fracture surfaces of the specimens to be examined were gold sputtered. Thermal degradation behavior of the biocomposite specimens was also analyzed by using the same TGA equipment mentioned above, this time between 30°-550°C.

Mechanical properties of the specimens were determined by "Three-Point Bending" and "Fracture Toughness" tests in accordance with ISO 178 and ISO 13586 standards, respectively. These tests were conducted by 5 kN Universal Testing System (Instron, 5565A, USA) for five specimens of each biocomposite composition.

Since this chapter was basically composed of two steps, (i) obtaining cellulose nanocrystals by sulfuric acid hydrolysis, and (ii) using them as reinforcements in polylactide matrix biocomposites; results obtained were discussed in the following two main sections.

2.4 Characteristics of CNC Particles Obtained

In order to characterize and reveal the possible differences in the size, morphology, chemical structure, crystallinity and thermal degradation of cellulose nanocrystal (CNC) particles compared to the starting material microcrystalline cellulose (MCC) fibrils; results of all analyses were evaluated for each cellulose structure.

(i) Size Range and Morphology of CNC Particles

It was stated in the data sheet of commercially available MCC fibrils that their average size was 20 μm. As shown in Figure 2.3, SEM analysis conducted to reveal details of size range and morphology of MCC fibrils indicated that their diameter range was 10-

15 μm, while their length range was 20-50 μm. That is, they have fibrillar morphology with an approximate aspect ratio of three.

On the other hand, Figure 2.3 clearly revealed that when CNC particles were obtained from MCC fibrils by sulfuric acid hydrolysis method, morphology changed from "fibrillar" geometry into rather "round" geometry. It was discussed in the literature [67-70] that rod-like and round morphology of CNC particles especially depends on the degree of "ultrasonication" and "acid-to-cellulose" ratio used during acid hydrolysis method.

SEM analysis also indicated that diameter range of these round shaped CNC particles was 15-55 nm. Thus, it could be stated that sulfuric acid hydrolysis method used in this study was successful in achieving nano-sized cellulose particles, so that, due to their very high surface area/volume ratio, they could be considered as a reinforcement phase for the production of polymer matrix biocomposites.

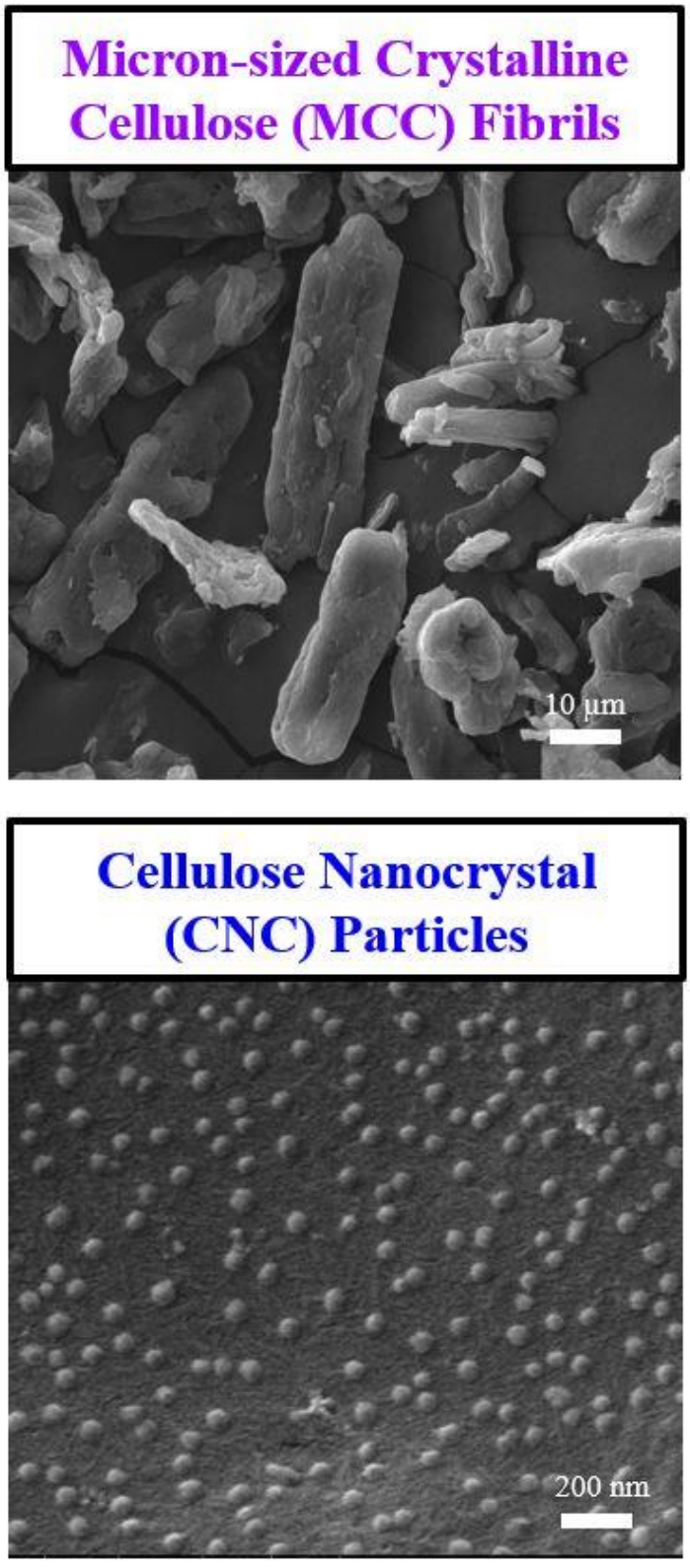

Figure 2.3 SEM images showing size range and morphology of MCC fibrils and CNC particles

(ii) Size Distribution and Zeta Potential of CNC Particles

Results of DLS analysis in the form of size distribution histograms given in Figure 2.4 revealed that the average size of CNC particles obtained was 38 nm, which was consistent with the size range observed under SEM analysis. DLS analysis also indicated that CNC particles obtained by sulfuric acid hydrolysis method had arithmetic mean of Zeta potential value as -30.4±1.4 mV, which might be considered as a sufficient value to obtain stable dispersion in water.

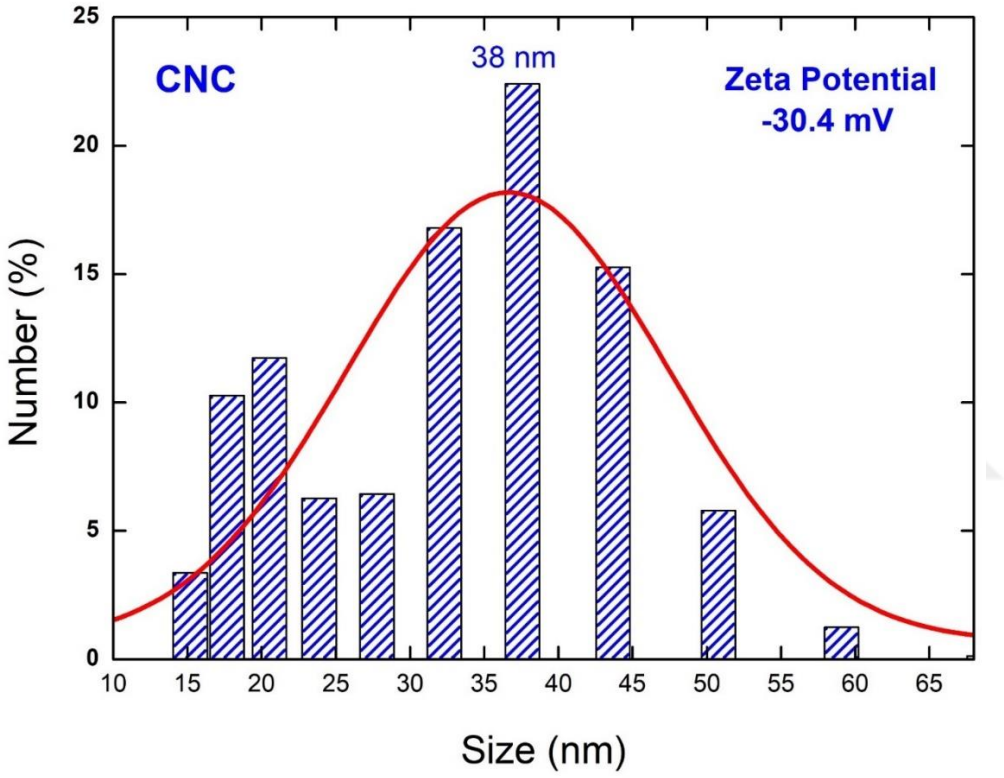

Figure 2.4 Size distribution of CNC particles determined by DLS analyses

It was discussed that [69-71] this rather sufficient value of Zeta potential could be due to the formation of anionic sulfate ester groups on the surfaces of CNC particles during sulfuric acid hydrolysis. They indicated that when Zeta potential value was less than -30 mV, CNC particles would have sufficient surface charges to repel each other, hence preventing agglomeration in water.

(iii) Chemical Structure of CNC Particles

It is known that [72-76] typical IR bands observed in the cellulose structure were –OH free stretching of CH_2–OH vibration at around 3279 cm^{-1} which corresponds to intra and intermolecular hydrogen bonds present;–CH stretching at around 2875 cm^{-1} corresponding to symmetric and asymmetric vibration of CH_2 in the aliphatic glucose unit; bending vibrations of the –OH groups at around 1595 cm^{-1} due to absorbed water; –CH cellulose mainchain bands between 1415 cm^{-1} and 1317 cm^{-1}; C–O–C elongations of the characteristic β (1→4) glycosidic ether linkage bands at 1052, 1027 and 892 cm^{-1}.

As shown in Figure 2.5, these typical IR bands appeared in the structure of MCC fibrils and CNC particles. On the other hand, compared to the –OH peaks of MCC fibrils at around 3279 and 1595 cm^{-1}, the first one was broader while the second one had very high intensity in the spectrum of CNC particles.

It is known that [76-78] after sulfuric acid hydrolysis, new IR peaks at around 815 and 1250 cm^{-1} would appear due to the presence of sulfate half-ester S=O and C–O–S in $O{-}SO_3^-$ groups, respectively. In this study, these tiny peaks were overlapped by the other dominant larger peaks.

Thus, it could be stated that these hydroxyl and sulfate ester groups might play a significant role in the polar interactions between the polymer matrix and CNC particles when used as reinforcement phase.

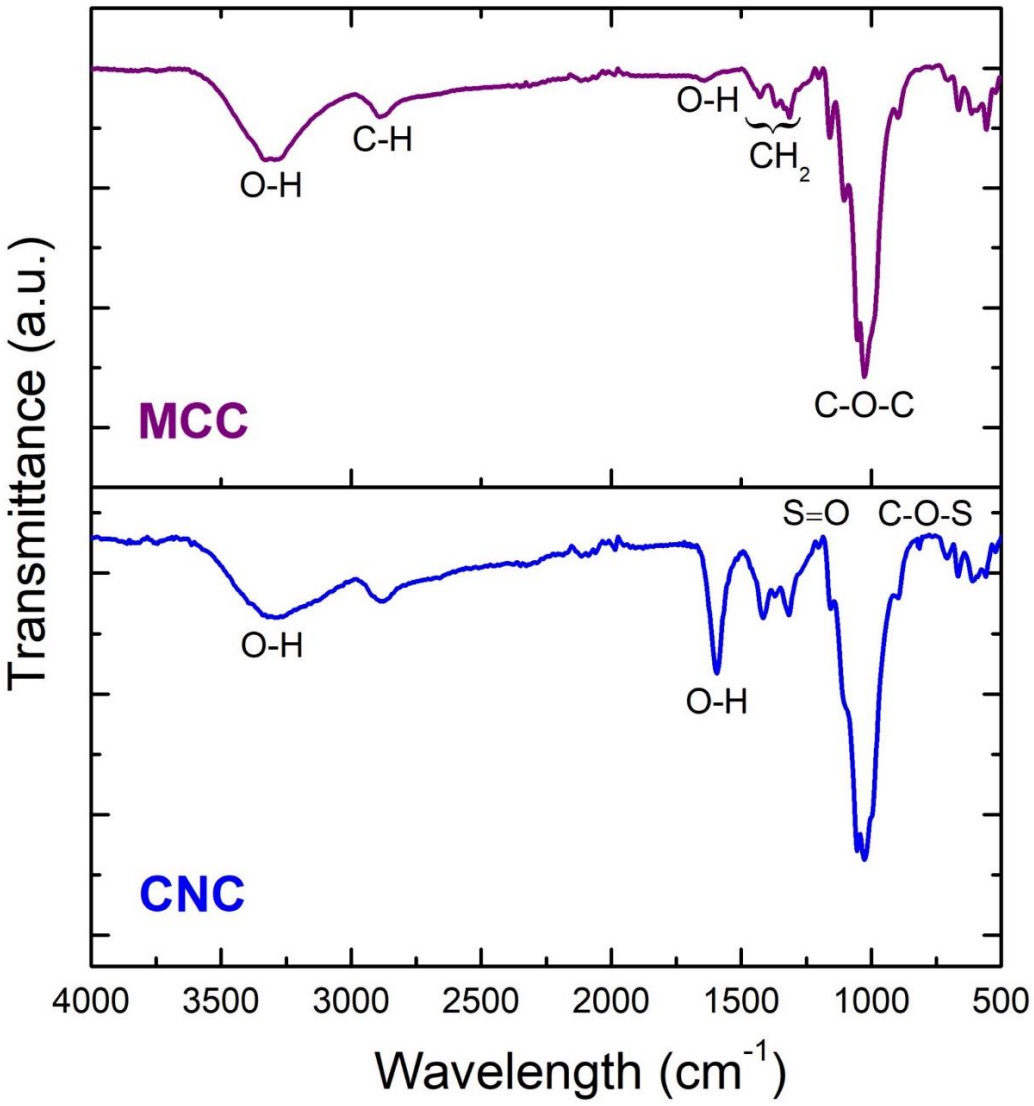

Figure 2.5 FTIR spectrums of MCC fibrils and CNC particles

(iv) Crystal Structure of CNC Particles

Cellulose is a semicrystalline material composed of amorphous and crystalline regions. Depending on the processing conditions different crystal structures could be formed designated as *Cellulose I, Cellulose II, Cellulose III, Cellulose IV* and *Cellulose V.* The most native one having monoclinic structure is *Cellulose I* with X-ray diffractions at 2θ = 14.8˚, 16.5˚, 22.6˚ and 34.5˚; which corresponds to crystal planes of $(1\ \overline{1}\ 0)$, (110), (200) and (004), respectively [73-76].

X-ray diffractograms shown in Figure 2.6 indicated that all these characteristic peaks of *Cellulose I* crystal structure appeared for MCC fibrils and CNC particles obtained. The very broad amorphous reflection at $2\theta \approx 18^{\circ}$ was completely overlapped by the peaks of crystalline planes.

In the cellulose related studies [73, 75, 77], the degree of crystallinity was measured by using *"Segal's Equation"*; and the parameter is named as *"Crystallinity Index" (CrI)* :

$$\boldsymbol{CrI = \frac{I_{200} - I_{amorphous}}{I_{200}} * 100}$$

where I_{200} is the peak intensity of (200) plane at 2θ = 22.6˚, while $I_{amorphous}$ is the peak intensity of broad amorphous structure at $2\theta \approx 18^{\circ}$.

By using these peak intensities in Figure 2.6, *CrI* of MCC fibrils and CNC particles were determined as 76.7% and 80.6%, respectively. Thus, higher crystallinity index of CNC particles could be interpreted as stronger structure compared to MCC fibrils. Then, it would be an advantage to use CNC particles as the reinforcement phase in polymer matrix biocomposites.

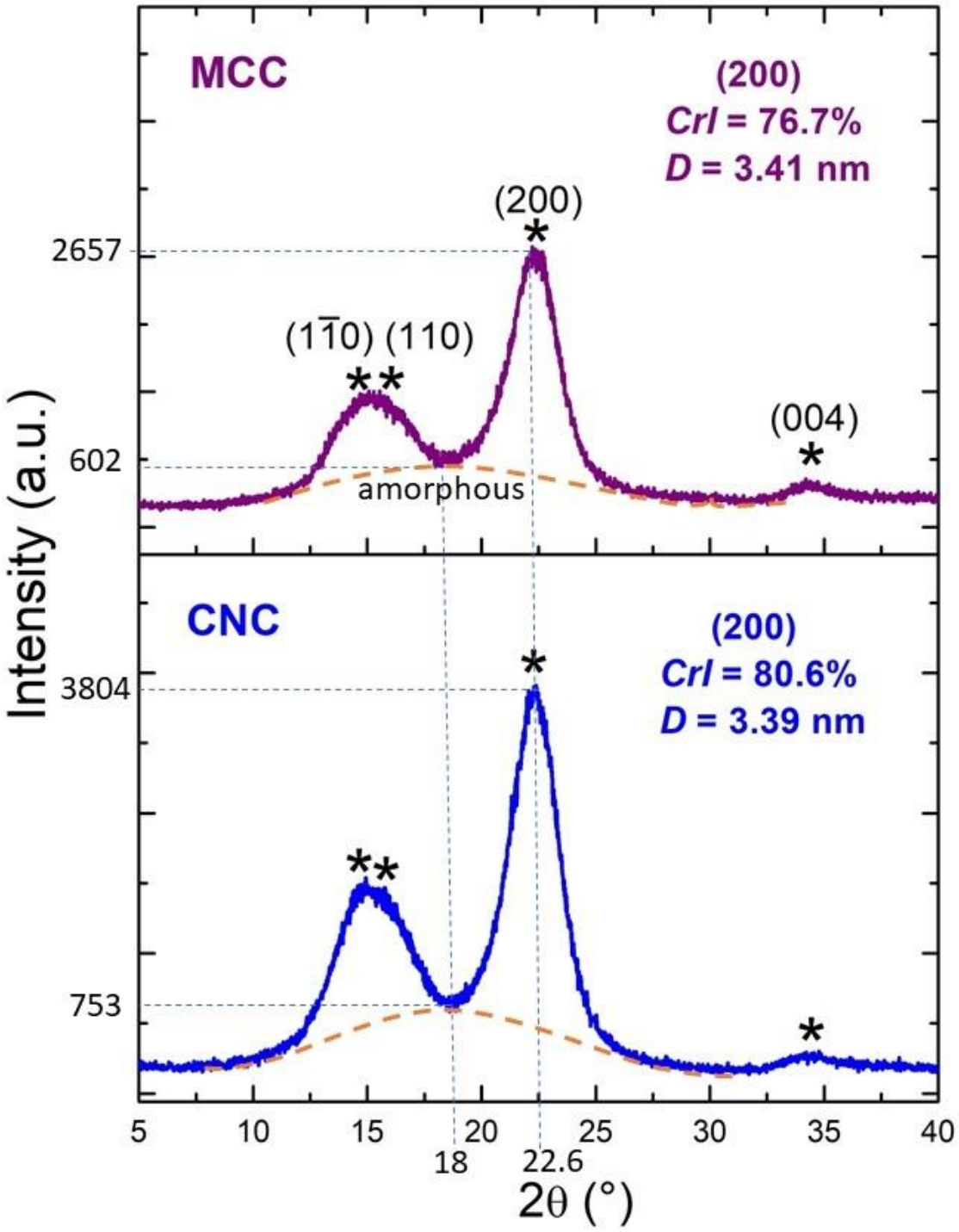

Figure 2.6 X-ray diffractograms showing *Cellulose I* crystal structure of MCC fibrils and CNC particles

Moreover, in the cellulose related studies [77, 78], size of the crystallites was determined by using *"Scherrer's Equation":*

$$D_{hkl} = \frac{k\lambda}{\beta \cos\theta}$$

For instance, in order to determine "D_{200} Crystallite Size" of (200) plane in nm; k (*Scherrer's constant)* was taken as 0.94, λ (*X-ray wavelength used*) was taken as 0.15418 nm, θ (*Bragg's angle)* was taken as 22.6˚/2=11.3˚, and β *(full width at half maximum of the 200 plane diffraction peak)* was the value in terms of radian for MCC and CNC. Then, crystallite size for MCC fibrils was determined as 3.41 nm, while it was 3.39 nm for CNC particles.

(v) Thermal Degradation of CNC Particles

It is known that [67, 69, 70, 74, 76] mass loss in cellulose structure starts below 100ºC due to removal of adsorbed moisture; while depolymerization, dehydration and decomposition of strong glycosidic linkages of cellulose chains take place between 200-400ºC. Finally, release of gaseous products and char residues form between 400-800ºC. Thermogravimetric (TG) and differential thermogravimetric (DTG) curves given in Figure 2.7 revealed that all these thermal degradation steps occurred both in MCC fibrils and CNC particles.

The main difference in their TG curves was the %Residue at 800ºC; which was 4.21 wt% for MCC fibrils while it was 23.1 wt% for CNC particles. Because, acid hydrolysis technique used for CNC particles resulted in higher crystallinity leading to higher char residue.

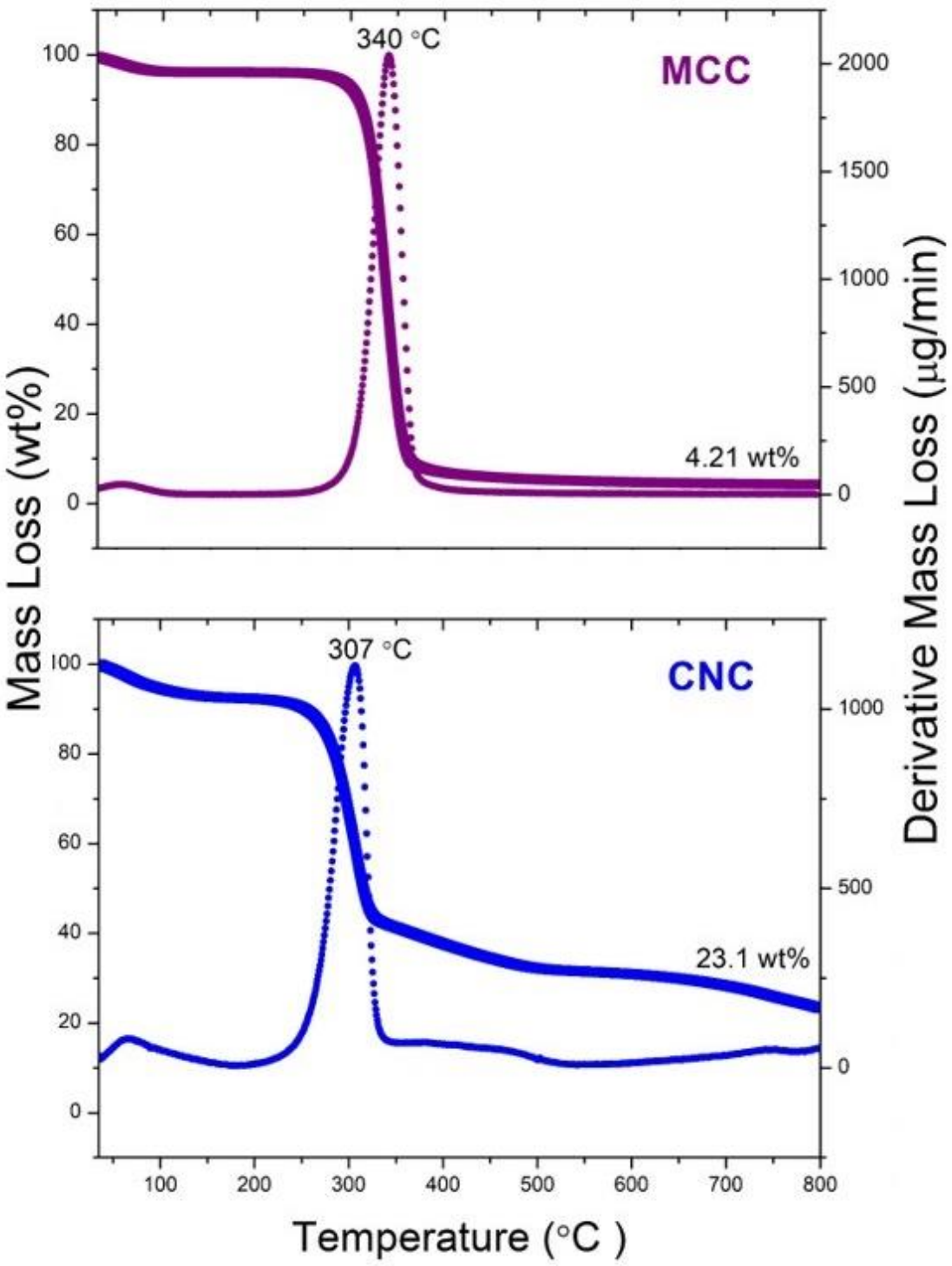

Figure 2.7 TG and DTG curves for MCC fibrils and CNC particles

The main difference in their DTG curves was the maximum thermal degradation peak T_{max} ; which was 340ºC for MCC fibrils while it was 307ºC for CNC particles. One reason for this lower T_{max} value of CNC particles would be their nano-sized structure leading to higher surface area to volume ratio, i.e. higher surface area exposed to heat.

Another reason for the lower T_{max} of CNC particles was attributed to the sulfuric acid hydrolysis method used. It was stated that [67, 70, 76] sulfate half-ester groups introduced to the cellulose chains could catalyze the thermal degradation of reactions.

2.5 Use of CNC Particles as Reinforcement in PLA Biocomposites

After obtaining and characterizing CNC particles, they were used as nano-reinforcement phase in PLA matrix with four different amounts of 0.5, 1, 2 and 3 wt%. Then, effects of these CNC contents on the mechanical and thermal degradation behaviors of PLA biocomposites were investigated.

(i) Effects of CNC Content on the Mechanical Properties

The first mechanical test conducted to reveal effects of CNC content was three-point bending test to compare "Flexural Strength, σ_{Flex}" and "Flexural Modulus, E_{Flex}" values of all specimens. Figure 2.8 indicates flexural stress-strain curves obtained, while effects of CNC content were illustrated in Figure 2.9 and tabulated in Table 2.1.

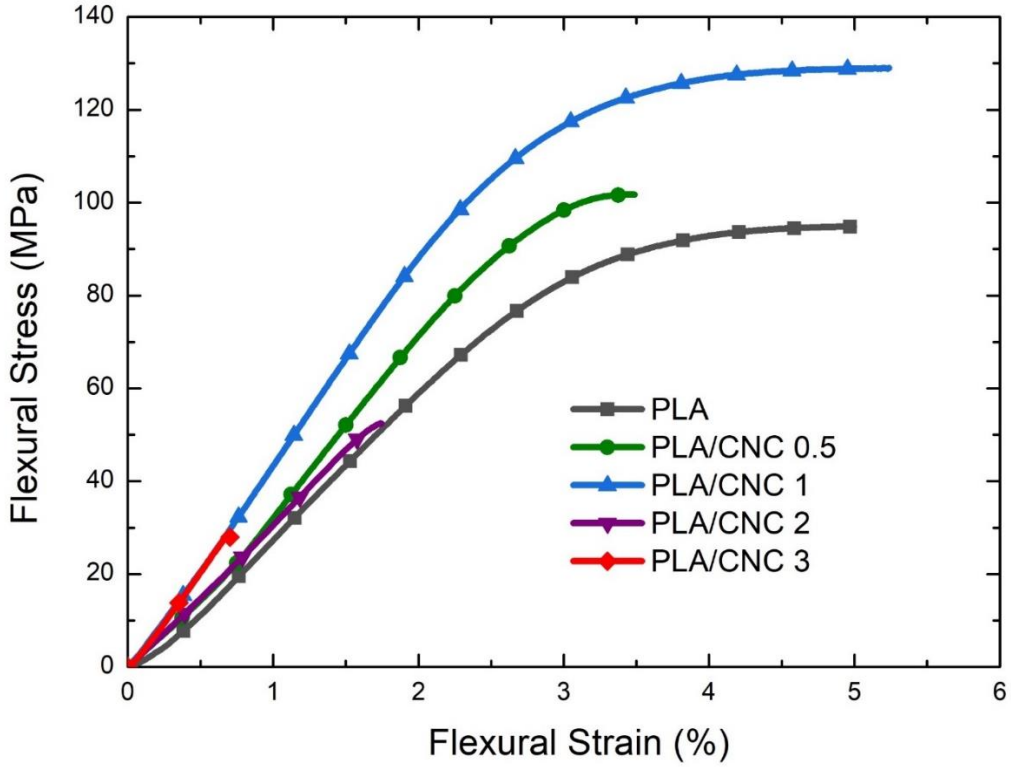

Figure 2.8 Flexural stress-strain curves of PLA/CNC biocomposites

Figure 2.9 revealed that the highest improvement in the strength and modulus values was obtained when CNC content was 1 wt%. The improvement compared to neat PLA matrix was as much as 29% in σ_{Flex} and 51% in E_{Flex} values.

It is known that main mechanisms responsible for the improvement of strength and modulus values were "load transfer from the weak polymer matrix to the stronger reinforcement material", plus "decrease of the mobility of macromolecular chain structure of polymer matrix by the rigid reinforcement phases". Thus, nano-sized CNC particles having extremely high "surface area to volume ratio" were very effective in these strengthening mechanisms.

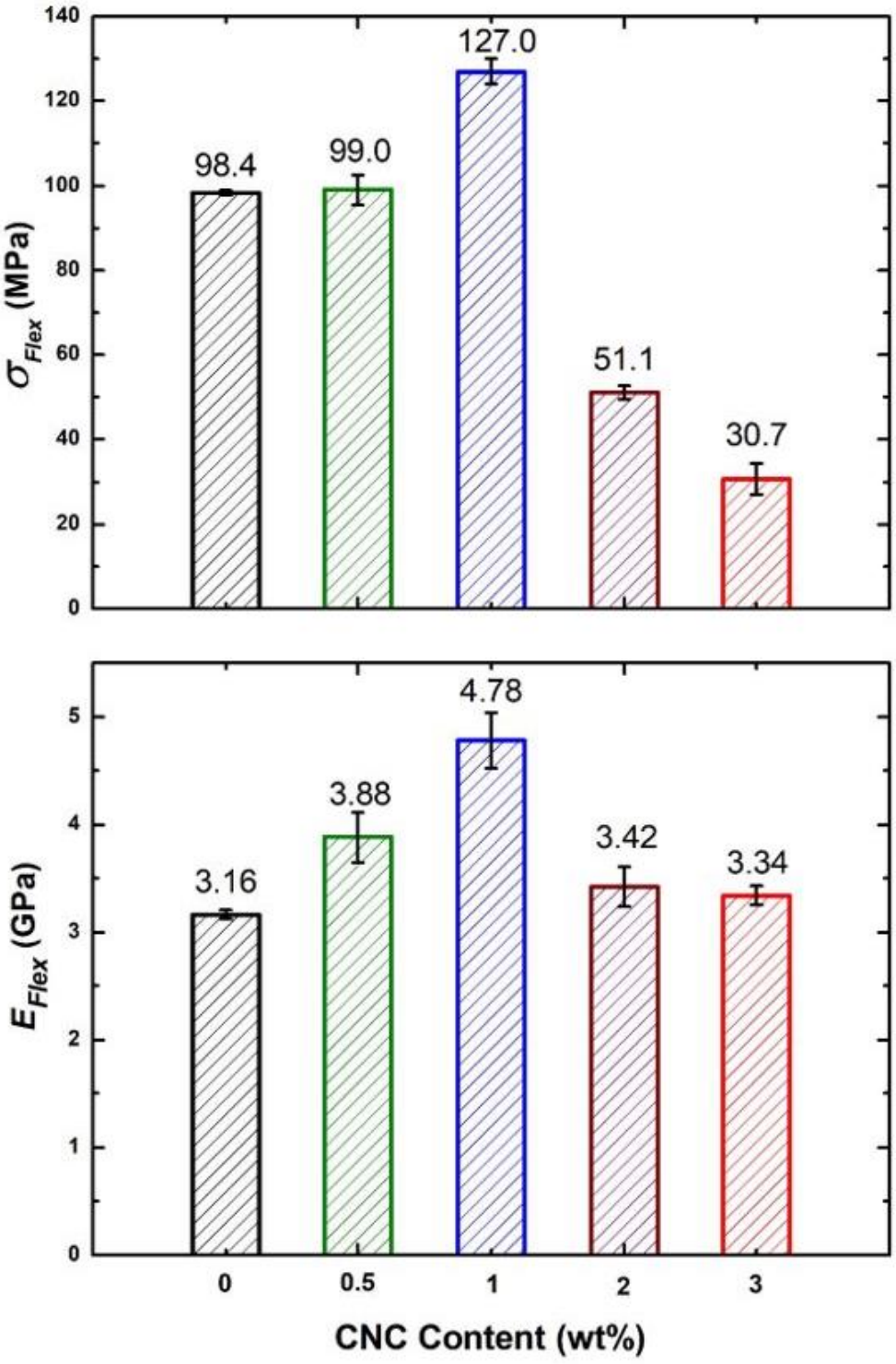

Figure 2.9 Effects of CNC content on the flexural strength and modulus of PLA biocomposites

The second mechanical test conducted to reveal effects of CNC content was fracture toughness test to compare "Critical Stress Intensity Factor, K_{IC}" and "Critical Strain Energy Release Rate, G_{IC}" values of all specimens, as illustrated in Figure 2.10 and tabulated in Table 2.1.

Table 2.1 Flexural Strength (σ_{Flex}), Flexural Modulus (E_{Flex}) and Fracture Toughness (K_{IC} and G_{IC}) Values of PLA/CNC Biocomposites.

Specimens	σ_{Flex} **(MPa)**	E_{Flex} **(GPa)**	K_{IC} **(MPa√m)**	G_{IC} **(kJ/m²)**
PLA	98.41±0.50	3.16±0.04	3.75±0.04	6.28±0.07
PLA/CNC 0.5	99.02±3.51	3.88±0.23	4.94±0.41	11.17±0.36
PLA/CNC 1	127.01±3.07	4.78±0.26	5.31±0.23	12.86±0.47
PLA/CNC 2	51.13±1.52	3.42±0.19	3.80±0.18	5.75±0.57
PLA/CNC 3	30.68±3.67	3.34±0.09	2.68±0.38	5.58±0.26

It was again observed that the highest improvement in the fracture toughness values was obtained when CNC content was 1 wt%. The improvement compared to neat PLA matrix was as high as 42% in K_{IC} and 105% in G_{IC} values. Because, nano-sized CNC particles were also very efficient in the main toughening mechanism of "decreased crack growth rate"; acting as "crack pinning" and "crack deflection" sites in the matrix.

On the other hand, Figures 2.9 and 2.10 revealed that when CNC content was beyond 1 wt%, then all the mechanical properties of PLA/CNC biocomposites started to decline. Since the main reason for this behavior could be non-uniform distribution and certain degree of agglomeration of nano-sized CNC particles, it was necessary to conduct SEM analysis.

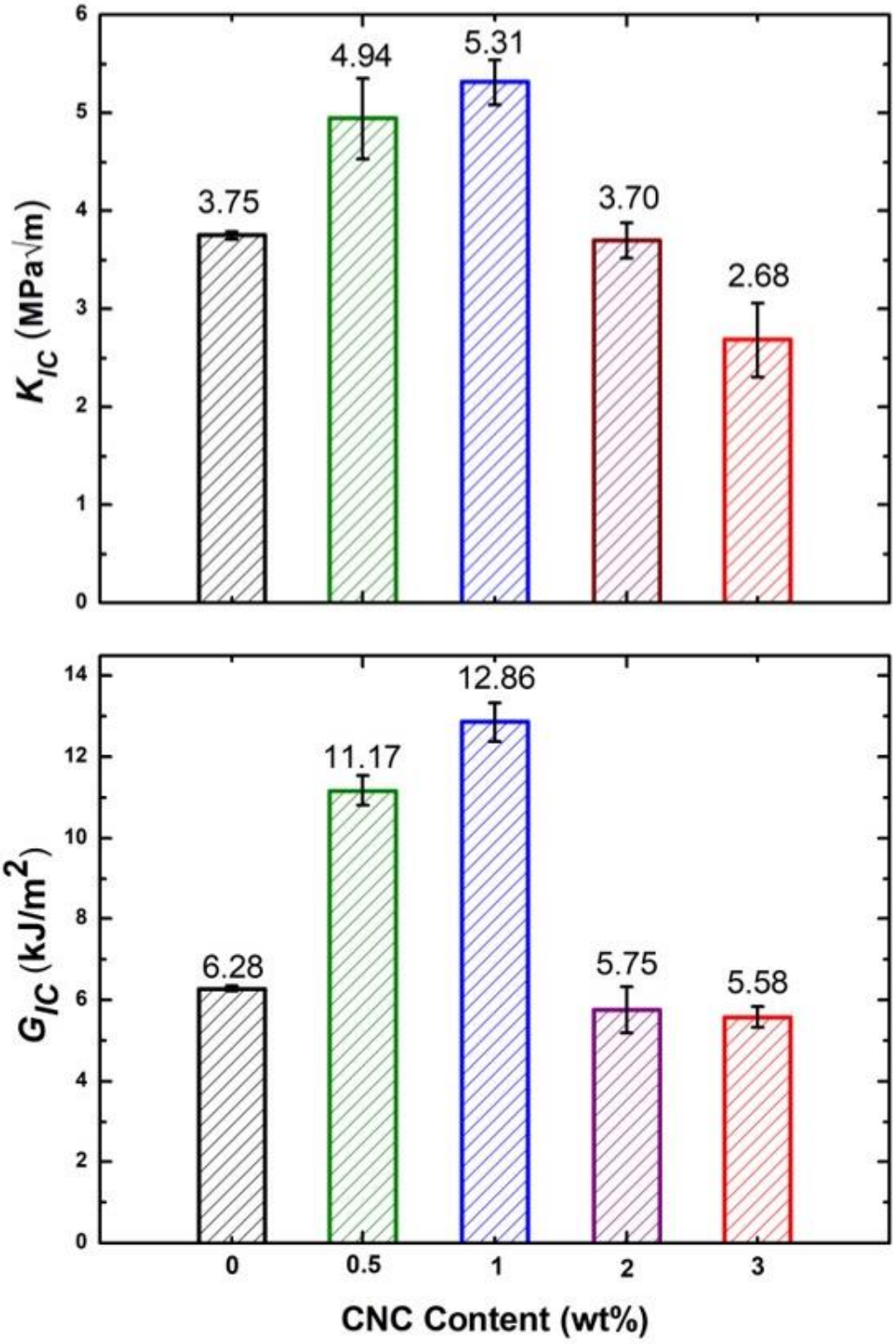

Figure 2.10 Effects of CNC content on the fracture toughness of PLA biocomposites

(ii) Fracture Surface Morphology of PLA/CNC Biocomposites

In order to observe morphological features of PLA/CNC biocomposites, SEM analysis was conducted on the fracture surfaces of the broken specimens after their fracture toughness tests. Figure 2.11 simply showed that due to the inherently brittle nature of PLA matrix, fracture surfaces appeared very smooth without any sign of shear yielding.

SEM fractographs in Figure 2.11 also revealed that there was almost no debonding or separation between the CNC particles and PLA matrix. This could be interpreted as the degree of interfacial adhesion between CNC and PLA was sufficient for the operation of strengthening and toughening mechanisms discussed in the previous section.

Because, as evidenced in the FTIR spectrum of Figure 2.5, there were plenty of hydroxyl groups and negatively charged sulfate groups formed on the surfaces of CNC particles. It is known that [79-81] interfacial polar interactions were possible between the hydroxyl and sulfate groups on the cellulose structure and the functional groups of PLA structure, such as carbonyl groups of PLA backbone and/or hydroxyl and carboxyl groups of PLA chain ends.

On the other hand, as seen in Figure 2.11, there was certain degree of agglomeration problem when CNC particles were incorporated into PLA matrix when more than 1 wt%. This could be the main reason for the decline of all mechanical properties of PLA/CNC 2 and PLA/CNC 3 specimens, discussed in the previous section. Similar observations on the agglomeration of cellulose nanoparticles primarily via Van der Waals forces, during melt mixing of biocomposites, were also reported in the literature [63, 64].

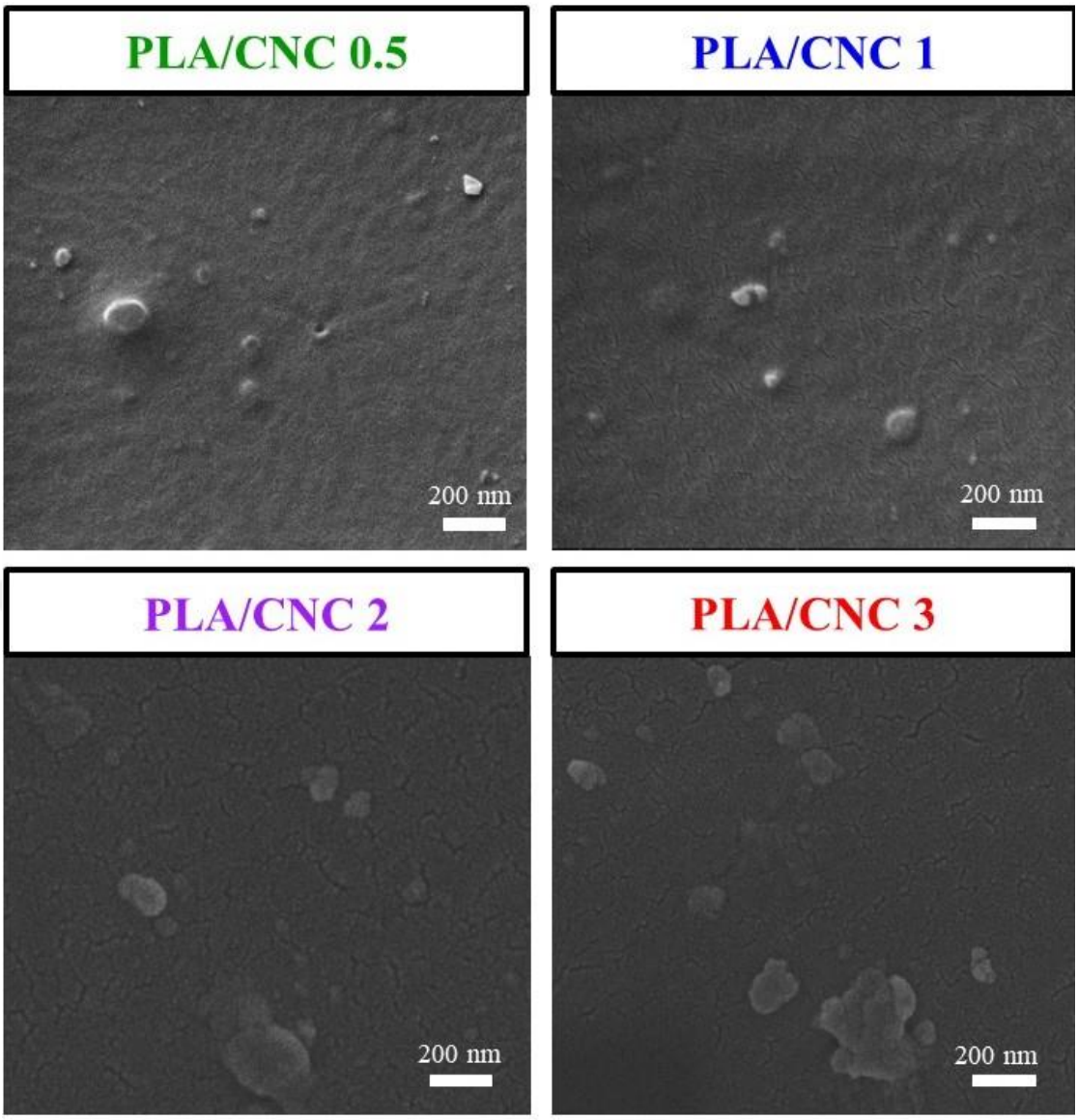

Figure 2.11 SEM images showing fracture surface morphology of PLA/CNC biocomposites

(iii) Thermal Degradation Behavior of PLA/CNC Biocomposites

TGA curves obtained for neat PLA and PLA/CNC biocomposites were shown in Figure 2.12; while the thermal degradation temperatures at 5 wt%, 10 wt%, 25 wt%, and maximum wt% losses ($T_{5\%}$, $T_{10\%}$, $T_{25\%}$, T_{max}) determined were tabulated in Table 2.2, including the %residue at 550ºC data. It was observed that incorporation of CNC particles into PLA matrix resulted in no improvements in the thermal degradation temperatures of the biocomposite specimens. Because, as evidenced in Figure 2.7 before, CNC particles had lower thermal degradation temperatures compared to PLA matrix. Similar observations were cited in the literature [62, 64].

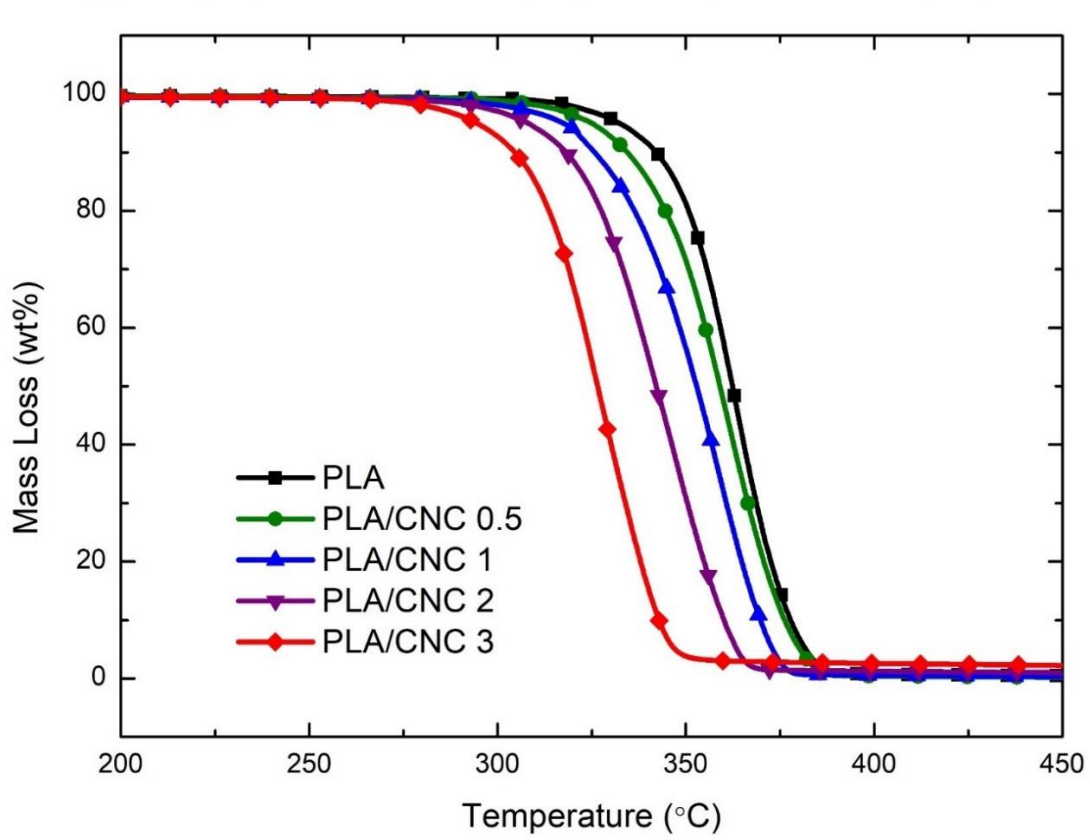

Figure 2.12 Thermogravimetric curves of PLA/CNC biocomposites

Table 2.2 Values of the thermal degradation temperatures and %residue of neat PLA and PLA/CNC biocomposites determined from TGA curves.

Specimens	$T_{5\%}$ **(°C)**	$T_{10\%}$ **(°C)**	$T_{25\%}$ **(°C)**	T_{max} **(°C)**	**%Residue at 550ºC**
PLA	332	342	353	366	0.19
PLA/CNC 0.5	324	334	348	365	0.10
PLA/CNC 1	317	325	340	361	0.71
PLA/CNC 2	308	316	328	348	1.03
PLA/CNC 3	294	304	316	331	2.34

CHAPTER 3

USE OF CELLULOSE NANOFIBRILS FOR STRENGTHENING AND TOUGHENING OF NEAT AND BLENDED POLYLACTIDE BIOCOMPOSITES

Although use of petroleum-based traditional polymers is still dominating in various sectors of industry, consideration of bio-based polymers from the point of "green materials" approach is becoming an important necessity. Among other alternative biopolymer macromolecules, poly(lactic acid) simply named as polylactide (PLA) is becoming one of the best candidates due to its available mass production method from corn-starch and its thermoplastic character leading to efficiency in many industrial processing techniques such as melt mixing and conventional molding for shaping.

Performance of neat PLA in terms of mechanical and thermal properties could be sufficient for many ordinary components used at around room temperature. On the other hand, for the applications requiring higher degree of strength and toughness; reinforcing and blending will be required.

In order to improve strength of PLA, composite making with conventional fibers, macro and/or micro-fillers could be used. In the academia, researchers especially used nano-size reinforcing agents such as nanoclays, carbon nanotubes, graphene and various inorganic fillers [82-84] due to their efficiency in the main polymer strengthening mechanisms of "load transfer from the matrix" and "decreased mobility of matrix macromolecules" by their very high surface area to volume ratios.

For the "fully green composites" approach, it is important that not only bio-based polymer matrix, but nano-sized reinforcing agents should be also bio-based; such as Cellulose Nanofibrils (CNF). There are certain number of studies [85-96] conducted to observe influences of CNF on the certain mechanical properties of PLA matrix

biocomposites. These studies generally indicated that use of around 1 wt% CNF could result in improvement in strength values; while certain melt mixing problems would occur when higher amounts of CNF were incorporated. Thus, one of the purposes of this chapter was to contribute to these studies by investigating effects of using only 1 wt% CNF on the strengthening mechanism of PLA matrix.

In order to improve toughness of PLA, the general approach is using "rubber toughening" method which is very efficient for the main toughening mechanism of "shear yielding". For this purpose, blending of PLA with various traditional elastomers including natural rubber, isoprene rubber, butadiene-based rubbers and many ethylene-copolymers was used [97-100]. For the "green blends" approach, PLA was blended with bio-based elastomers, such as bio-based thermoplastic vulcanizates (TPVs) [101-108], poly(butylene adipate-co-terephthalate) (PBAT) [109, 110], starch [111-113], poly-(3-hydroxybutyrate-co-3-hydroxyvalerate) (PHBV) [114], lignin [115, 116], poly(butylene succinate) (PBS) [117], bio-based poly(ethylene terephthalate) [118] and polycaprolactone (PCL) [119].

It is known that block-copolymer elastomer structures having thermoplastic character due to their hard and soft segments could be also efficient in balancing strength and toughness values in the PLA blends. In the literature, blending of PLA with bio-based thermoplastic polyurethane (b-TPU) elastomer was reported by only three studies [120-122]; while blending with bio-based thermoplastic polyester (b-TPE) elastomers by only two studies [123, 124]. These studies generally indicated that blending of PLA with around 10 phr thermoplastic elastomers would result in improvement in toughness values without too much decrease in strength values. Thus, another purpose of this chapter was to contribute to these very limited number of studies by investigating effects of blending PLA with only 10 phr b-TPE on the toughening mechanisms.

In order to get optimum degree of strength and toughness, "ternary systems" could be also produced; that is PLA matrix could be blended with a bio-based elastomer together with reinforcing with a cellulose nano-filler, simultaneously. From this point

of view, a few studies were reported for the ternary systems of PLA/elastomer/CNF [125-127]. However, to the best of our knowledge, no studies on the ternary systems of PLA/b-TPE/CNF were cited in the literature. Thus, the most distinctive aim of this chapter was to investigate the degree of strengthening and toughening of PLA biopolymer when reinforced with only 1 wt% CNF and blended with only 10 phr b-TPE, simultaneously.

Although shaping of the components made from bio-blends and biocomposites could be achieved by traditional injection or compression molding techniques, use of additive manufacturing techniques such as 3D-printing in the biomedical sectors is on the rise due to various advantages. Significant number of 3D-printer studies [128-140] on the PLA/Cellulose biocomposites were already cited in the literature. However, only two of them [129, 132] compared changes in the mechanical properties of specimens. Thus, another distinctive aim of this chapter was to reveal whether there were any differences in the strength and toughness values of all groups of PLA, b-TPE, CNF specimens after their 3D-printing, compared to their compression molded counterparts.

In this chapter, in order to fulfill these distinctive aims following experimental procedures were conducted.

3.1 Ingredients of the Bioblends and Biocomposites

The main biopolymer matrix used was polylactide (PLA) with L-type lactic acid macromolecules. According to the supplier (NaturePlast PLE 001, France), its density was 1.25 g/cm^3, melting temperature range was 145-155°C, melt flow index range at 190°C under 2.16 kg was 2-8 g/10 min, while the weight average molecular weight was 101x10^3 g/mol.

For toughening purposes, inherently brittle PLA matrix was blended with a bio-based Thermoplastic Polyester Elastomer (b-TPE). According to the supplier (Dupont,

Hytrel RS 40F3 NC010, USA), soft segments were composed of at least 50% renewably sourced bio-ingredients by weight. Its block copolymer structure consists of poly(tetramethylene ether) glycol terephthalate soft segments and poly(butylene terephthalate) hard segments. Its density, Shore-D hardness, stress and strain at break values were 1.11 g/cm^3, 37, 26 MPa and 650%, respectively.

For reinforcing purposes of neat PLA and PLA/b-TPE blends, cellulose nanofibrils (CNF) were used. According to the supplier (Guilin Qihong Technology, China) diameter range of these CNF particles was 20-100 nm. Molecular structures of these three ingredient materials are given in Figure 3.1.

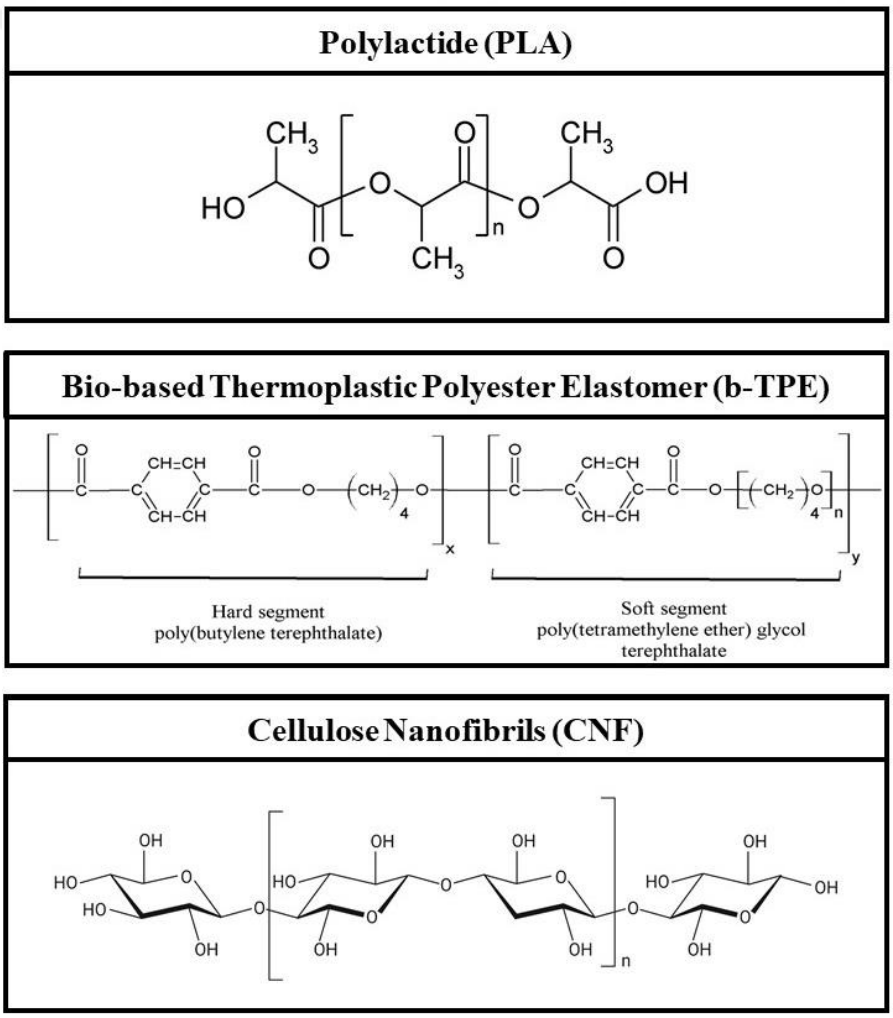

Figure 3.1 Molecular structure of the ingredients (PLA, b-TPE, CNF) used in the bioblends and biocomposites

3.2 Production of Bioblends and Biocomposites

Both bioblends (PLA/b-TPE) and biocomposites (PLA/CNF and PLA/b-TPE/CNF) were produced by using the same “melt mixing” technique in a laboratory size twin-screw extruder (Rondol Microlab 300, UK) (Figure 3.2). For all compositions, typical temperature profile and screw speed used were 115°-170°-180°-175°-150°C and 70 rpm, respectively. Before melt-mixing, all ingredients (PLA, b-TPE, CNF) were pre-dried in a vacuum oven at certain temperatures for certain periods.

Literature survey indicated that typical elastomer amount used for toughening of PLA with little decrease in strength was around 10 phr; while typical amount of nano-reinforcements used in nanocomposite studies was around 1 wt%. Thus, in this study, PLA/b-TPE bioblends were produced by using 10 phr b-TPE; while PLA/CNF and PLA/b-TPE/CNF biocomposites were produced by incorporating 1 wt% CNF particles.

3.3 Shaping of Test Specimens by Compression Molding

The first technique used to shape test specimens of all bioblends and biocomposites was the conventional “compression molding”. Before filling the molds prepared according to related ISO standards with 2-3 mm pellets obtained from the cutter of the twin-screw extruder; these pellets were first dried in an oven at 60°C for 12 hours. Then, specimens were shaped by using a laboratory-scale hot press (MSE LP_M2SH05, Turkey) (Figure 3.2) at 160°C, under 25 kN for 5-6 min.

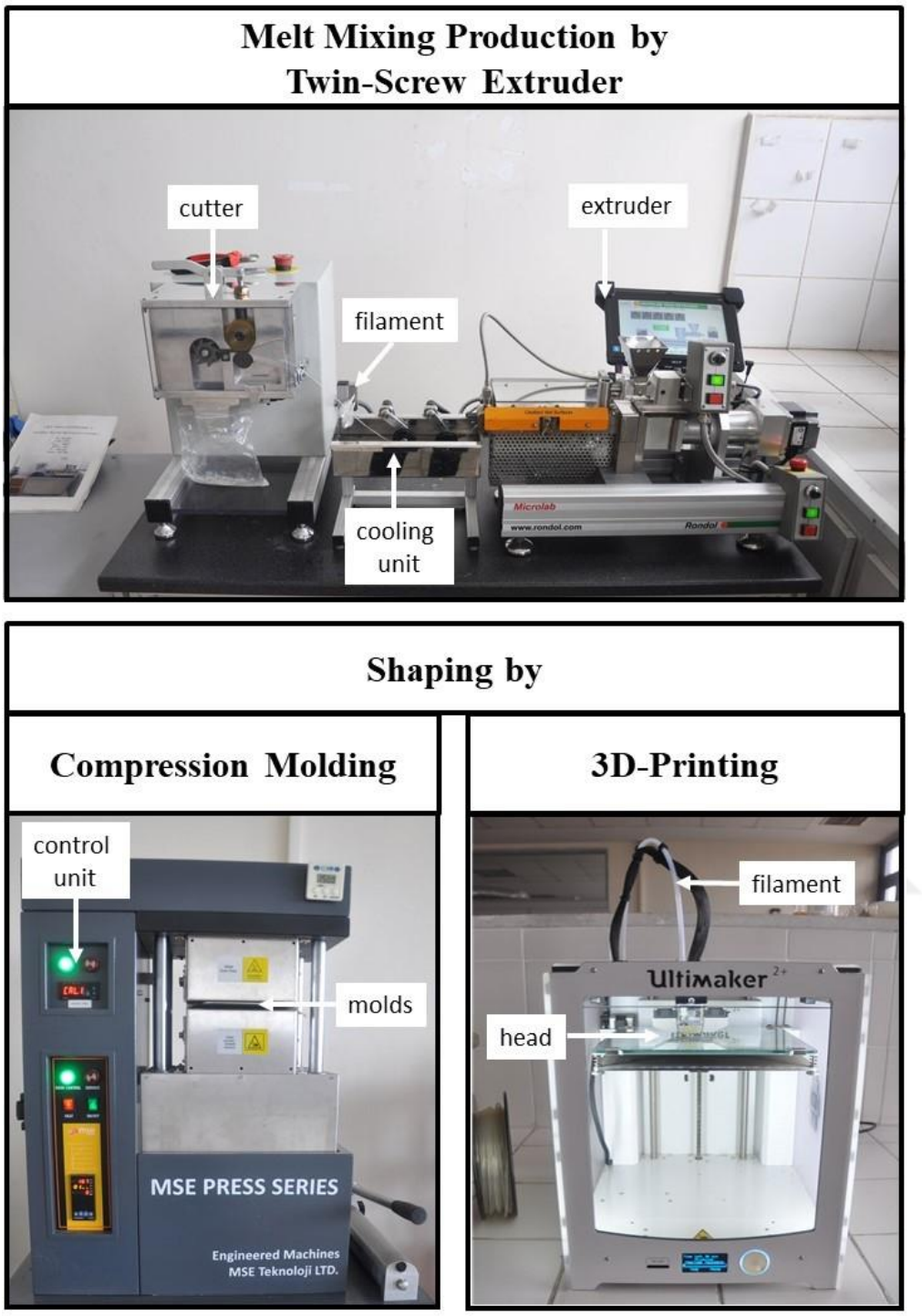

Figure 3.2 General views of the equipment used during production of bioblends and biocomposites by melt mixing; and their specimen shaping by conventional molding and additive manufacturing technique

3.4 Shaping of Test Specimens by 3D-Printing

In order to observe whether there would be any differences in the mechanical properties of bioblends and biocomposites when their test specimens were shaped by an additive manufacturing technique compared to conventional molding technique; a Fused Deposition Modeling (FDM) type table-top 3D-printer (Ultimaker 2+, Netherlands) (Figure 3.2) was used. For this purpose, 2 mm diameter continuous filaments obtained from the twin-screw extruder were fed into the 3D-printer head at 190ºC having 0.4 mm nozzle.

Specimen geometries in accordance with related ISO standards were obtained by using a drawing software (SolidWorks) and then G-code slicing software (Cura 2.3.1). After determining all the required hardware parameters and software parameters by conducting various trials, test specimens were printed with lay-down position and ±45º raster orientation.

3.5 Testing and Analyses of the Specimens

(i) Electronmicroscopy Analyses

Morphology and distribution of b-TPE domains and CNF particles in PLA matrix were observed by using a field emission scanning electron microscope (SEM) (FEI Nova Nano 430, Japan) under an accelerating voltage of 15 kV with a working distance of 5 mm. Fracture surfaces of the specimens to be examined were first gold sputtered.

(ii) Thermal Analyses

Thermal behaviors of the bioblend and biocomposite specimens were analyzed by both Differential Scanning Calorimetry (SII X-DSC 700 Exstar, Japan) and Thermogravimetric Analyses (SII TG/DTA 7300 Exstar, Japan) under a heating rate of

10°C /min. Heating profile used during DSC analyses was from -80° to 220°C, while during TGA analyses it was from 30° to 550°C.

(iii) Mechanical Tests

Strength and stiffness of the bioblend and biocomposite specimens were determined by conducting "Three-Point Bending" tests in accordance with ISO 178 standard, while toughness values of the specimens were determined by conducting "K_{IC} and G_{IC} Fracture Toughness" tests in accordance with ISO 13586 standard. Tests were performed by using a 5 kN Universal Testing System (Instron 5565A, USA) for at least five specimens in each group.

In this chapter, after fracture surface morphology observations in the compression molded bioblend and biocomposite specimens, effects of CNF reinforcements on the thermal and mechanical properties were discussed. Moreover, differences observed when the specimens were shaped by 3D-printing were also reported.

3.6 Fracture Surface Morphology of Bioblends and Biocomposites

As shown in Figure 3.3, SEM analyses on the fracture surface of the specimens were conducted under two different magnifications; i.e., "general view" with 1000X magnification and "closer view" with 5000X magnification.

General view image of PLA/CNF biocomposite specimen revealed very smooth fracture surface with certain degree of craze bands, which was due to the inherently brittle behavior of PLA matrix. Closer view image of this biocomposite specimen indicated that use of 1 wt% CNF particles was rather randomly and uniformly distributed in PLA matrix. As would be discussed later, even distribution of CNF reinforcements played a critical role in the improvement of mechanical properties.

On the other hand, general view image of PLA/b-TPE bioblend specimen revealed excessively rough fracture surface which was due to the shear yielding occurred with very high degree of plastic deformation. Due to the immiscibility of PLA with b-TPE, closer view image of this bioblend specimen indicated that use of 10 phr b-TPE resulted in homogeneously distributed round "domains" with diameters less than 10 microns. As would be discussed later, these elastomer domains played a critical role in the rubber toughening mechanism of specimens.

For the specimen of PLA/b-TPE/CNF, general view image in Figure 3.3 again revealed excessively rough fracture surface due to the shear yielding occurred. However, in the closer view image, it was not possible to recognize CNF particles which were obscured by the large amount of b-TPE domains formed.

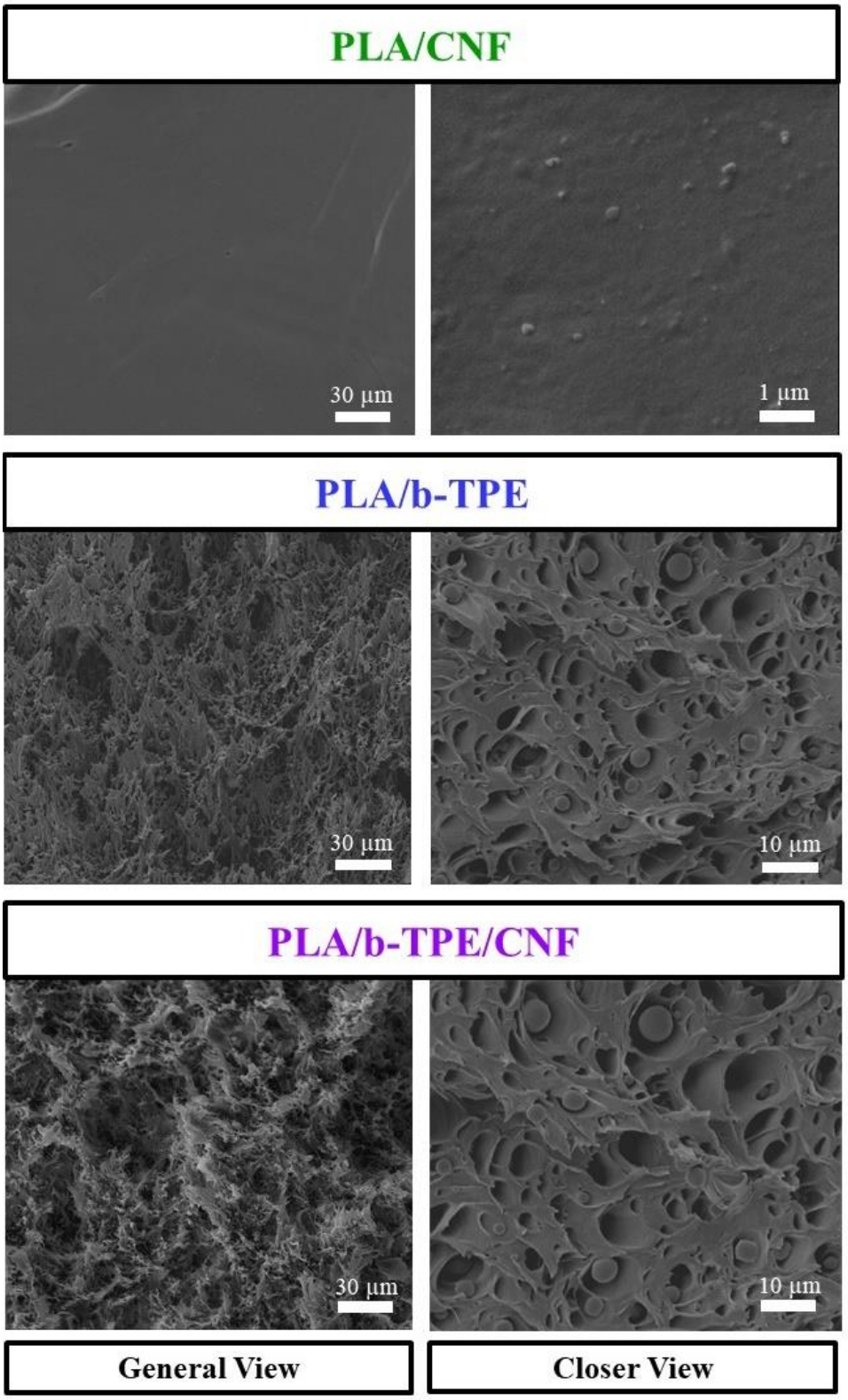

Figure 3.3 General and closer view SEM images showing fracture surface morphology of bioblend and biocomposite specimens

3.7 Thermal Behavior of Bioblends and Biocomposites

In order to observe thermal behavior of all specimens produced by melt-mixing and then shaped by compression molding, both DSC and TGA analyses were conducted.

(i) DSC

First heating DSC thermograms were illustrated in Figure 3.4. Then, values of glass transition temperature (T_g), cold crystallization temperature (T_{cc}), melting temperature (T_m), enthalpies during melting (ΔH_m) and cold crystallization (ΔH_{cc}) determined from thermograms were tabulated in Table 3.1. In this table, percent crystallinity (X_c) of all specimens was also given, which were determined by using the values of ΔH_m, ΔH_{cc} and the weight fraction of PLA (w_{PLA}) together with melting enthalpy of 100% crystalline PLA (ΔH_m^o) cited as 93.7 J/g in the literature [141].

It was observed that use of 1 wt% CNF reinforcement in neat PLA matrix played no significant role in the transition temperatures T_g, T_{cc}, T_m and the degree of crystallinity (X_c).

Contrarily, blending of PLA with 10 phr b-TPE resulted in an increase of glass transition temperature by 10ºC. This improvement in T_g value of PLA could be related to especially hard segments of the block copolymer structure of b-TPE. Moreover, Table 3.1 also indicated that cold crystallization temperature of PLA decreased by around 10ºC. Consequently, this decrease in T_{cc} was an indication of earlier start of heterogeneous nucleation of crystallites at the interfacial boundaries of homogenously distributed micron sized b-TPE domains in the PLA matrix. Thus, blending of PLA with b-TPE resulted in almost four times increase in X_c crystallinity amount. Similar observations were cited in the literature [122-124].

When 1 wt% CNF particles were incorporated together with 10 phr b-TPE, apart from higher degree of PLA crystallinity (X_c), no significant differences were observed.

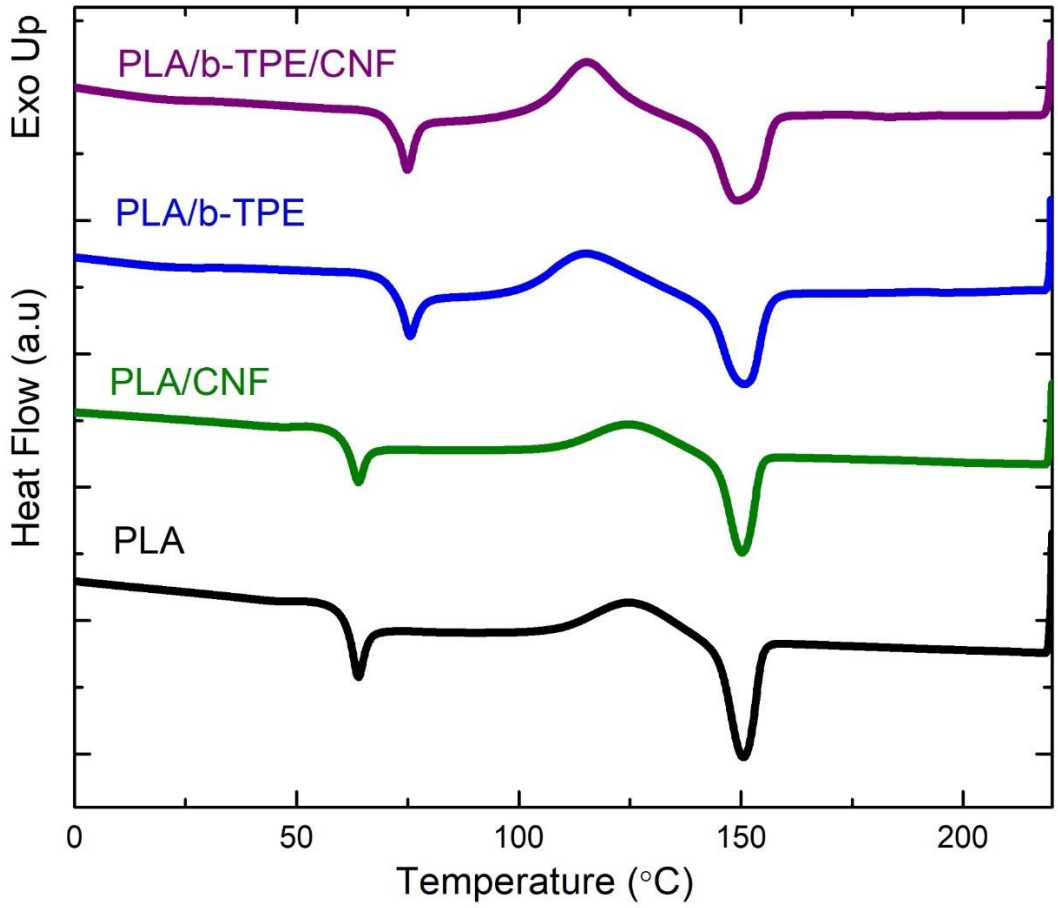

Figure 3.4 First heating DSC thermograms of bioblend and biocomposite specimens

Table 3. 1 Values of the transition temperatures, enthalpies and crystallinity amounts of bioblend and biocomposite specimens determined from first heating DSC thermograms.

Specimens	T_g **(°C)**	T_{cc} **(°C)**	T_m **(°C)**	ΔH_m **(J/g)**	ΔH_{cc} **(J/g)**	X_C **(%)**
PLA	63.9	124.8	150.5	29.4	22.5	7.38
PLA/CNF	64.1	124.7	150.2	23.7	16.1	8.25
PLA/b-TPE	75.6	115.2	150.7	37.7	17.6	21.6
PLA/b-TPE/CNF	75.0	115.3	149.1	43.2	15.9	29.4

(ii) TGA

Results of TGA as the second thermal analysis conducted for all specimens were illustrated in Figure 3.5 in the form of mass loss versus temperature curves. Then, thermal degradation temperatures ($T_{5\%}$, $T_{10\%,}$ $T_{25\%,}$ T_{max}) determined for the 5 wt%, 10 wt%, 25 wt%, and maximum wt% losses were tabulated in Table 3.2.

It is known that [126] since thermal degradation temperature levels of cellulose macromolecular structure of CNF reinforcements, and soft segment blocks of b-TPE elastomer structure are not higher than the PLA matrix structure; no improvements were observed in the $T_{5\%}$, $T_{10\%,}$ $T_{25\%,}$ T_{max} values of bioblend and biocomposite specimens.

Since all the ingredient materials used were bio-based macromolecules; another data i.e., *%Residue at 550ºC* determined in the thermogravimetric analyses revealed that residue amounts were negligible. Thus, contrary to the use of inorganic fillers in the PLA matrix, it could be stated that use of CNF and b-TPE would result in production of "fully green" bioblends and biocomposites.

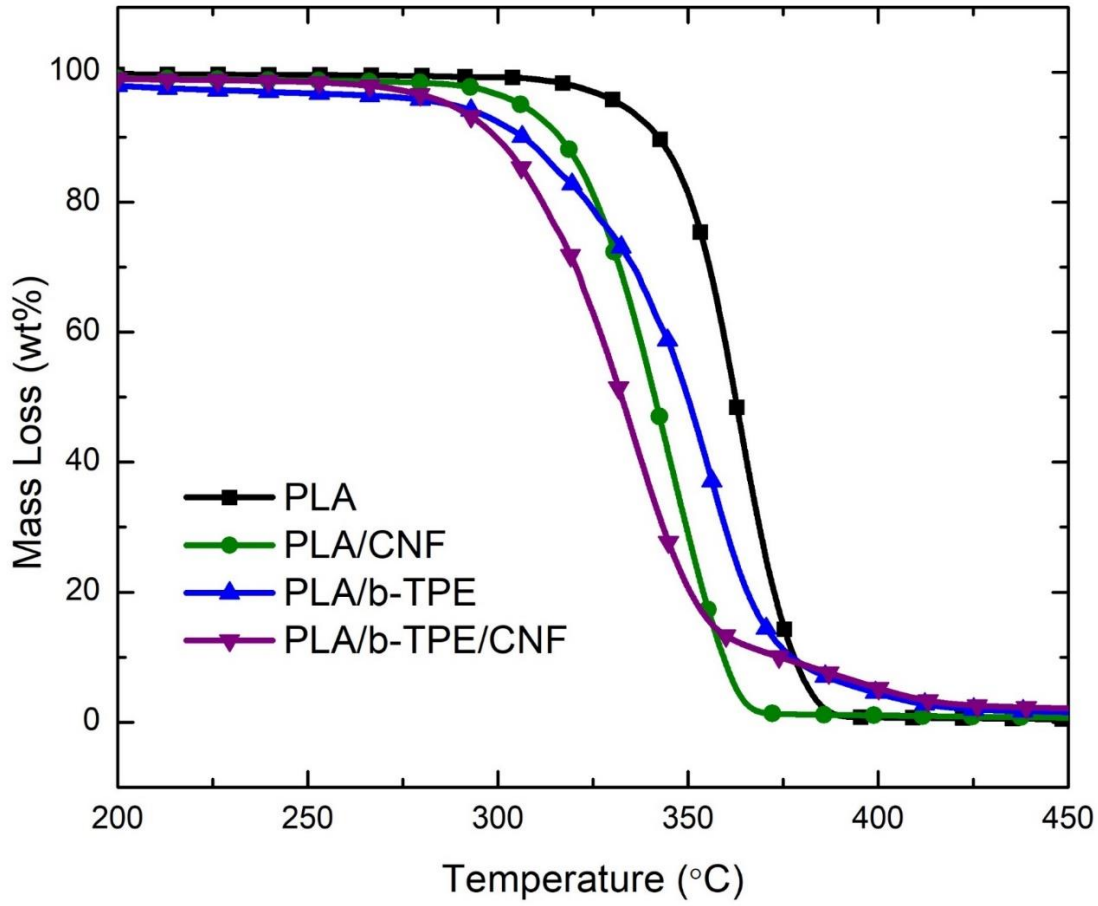

Figure 3.5 Thermogravimetric curves of bioblend and biocomposite specimens

Table 3.2 Values of the thermal degradation temperatures and %residue of the bioblend and biocomposite specimens determined from thermogravimetric curves.

Specimens	$T_{5\%}$ **(°C)**	$T_{10\%}$ **(°C)**	$T_{25\%}$ **(°C)**	T_{max} **(°C)**	**%Residue at 550ºC**
PLA	332	342	353	366	0.19
PLA/CNF	306	316	329	352	0.22
PLA/b-TPE	287	306	330	360	0.90
PLA/b-TPE/CNF	270	300	316	341	1.57

3.8 Contribution of CNF on the Strengthening of Neat and Blended PLA

It is known that strengthening and stiffening of polymer materials could be evidenced by the increase in the values of Strength and Elastic Modulus. Thus, in order to reveal contribution of CNF on the strengthening and stiffening of neat and blended PLA, three-point bending tests were performed for all specimens. Flexural stress-strain curves obtained from these tests were illustrated in Figure 3.6. Then, values of "Flexural Strength (σ_{Flex})" and "Flexural Modulus (E_{Flex})" determined from these curves were compared in Figure 3.7.

It was apparent that when neat PLA was reinforced with only 1 wt% CNF, significant degree of strengthening and stiffening took place; being 33% increase in σ_{Flex} and 43% increase in E_{Flex} values. Because, due to the stronger cellulose structure and extremely high surface area/volume ratio of their nano-size, use of CNF was very efficient in the well-known strengthening mechanisms of "decreased molecular mobility" of polymer matrix and "load transfer" mechanism from the matrix to the reinforcement.

Of course, for the efficient strengthening mechanisms of "decreased matrix mobility" and "load transfer from the matrix"; a certain degree of interfacial bond between the matrix and the reinforcement would be necessary. In this system, interfacial attraction between CNF and PLA could be attributed to polar interactions that might form between the extensive number of hydroxyl groups in the cellulose structure and the carboxyl, hydroxyl end groups, and ester carbonyl groups of PLA macromolecules.

On the other hand, Figure 3.7 indicated that when PLA was blended with 10 phr b-TPE, reduction in the strength and stiffness occurred, being 25% decrease in σ_{Flex} and 17% decrease in E_{Flex} values, which was expected. Because, as would be discussed in the next section, the main purpose of blending inherently brittle polymers with elastomers is to improve "toughness", not strength and stiffness. It is known that [122, 123] especially due to the very low T_g soft segments present in the block copolymer structure of thermoplastic elastomers, they act as plasticizers when blended with PLA. Consequently, they reduce strength and stiffness of the blends.

However, Figure 3.7 also revealed that, when 1 wt% CNF was incorporated into the PLA/b-TPE bioblend, reductions in the strength and stiffness values were recovered significantly. It was observed that σ_{Flex} and E_{Flex} values of the PLA/b-TPE/CNF specimen approached the values of PLA/CNF; and both values were higher than the values of neat PLA. Thus, it could be stated that, addition of only 1 wt% CNF also contributed to recover strength and stiffness losses in the PLA/b-TPE bioblend specimen.

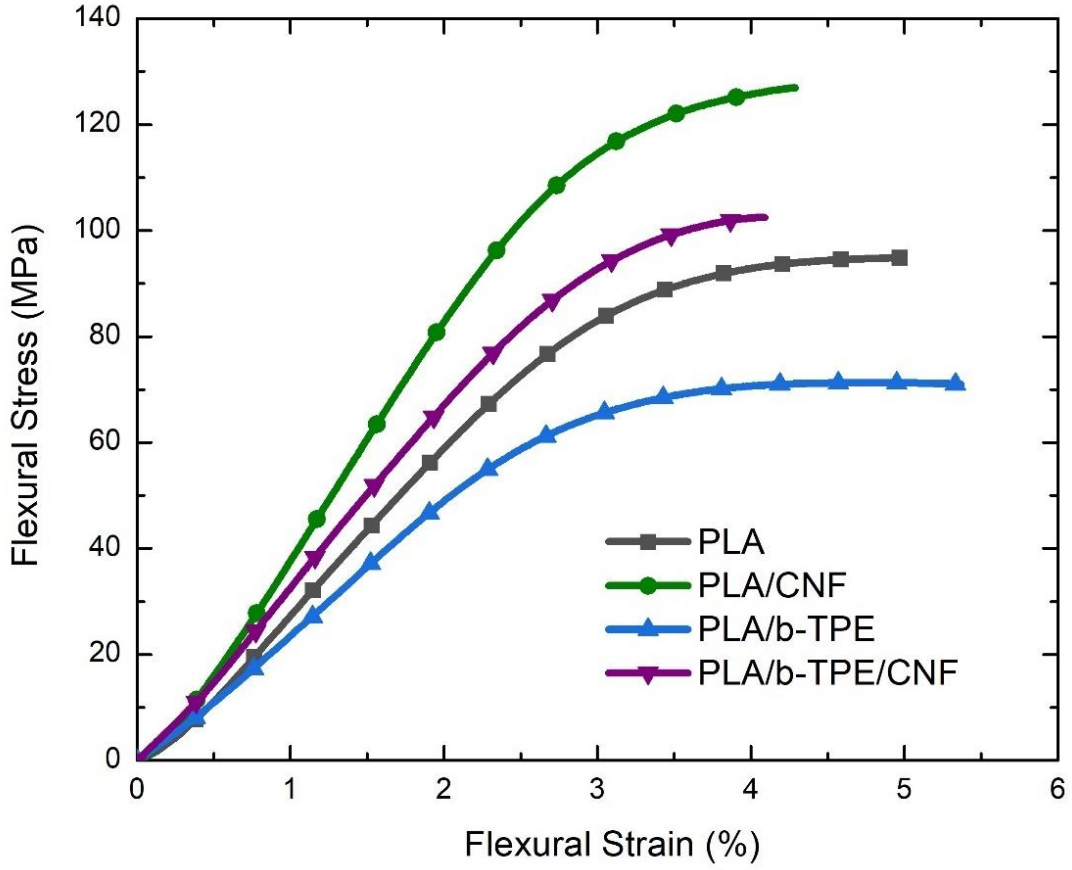

Figure 3.6 Flexural stress-strain curves of bioblend and biocomposite specimens

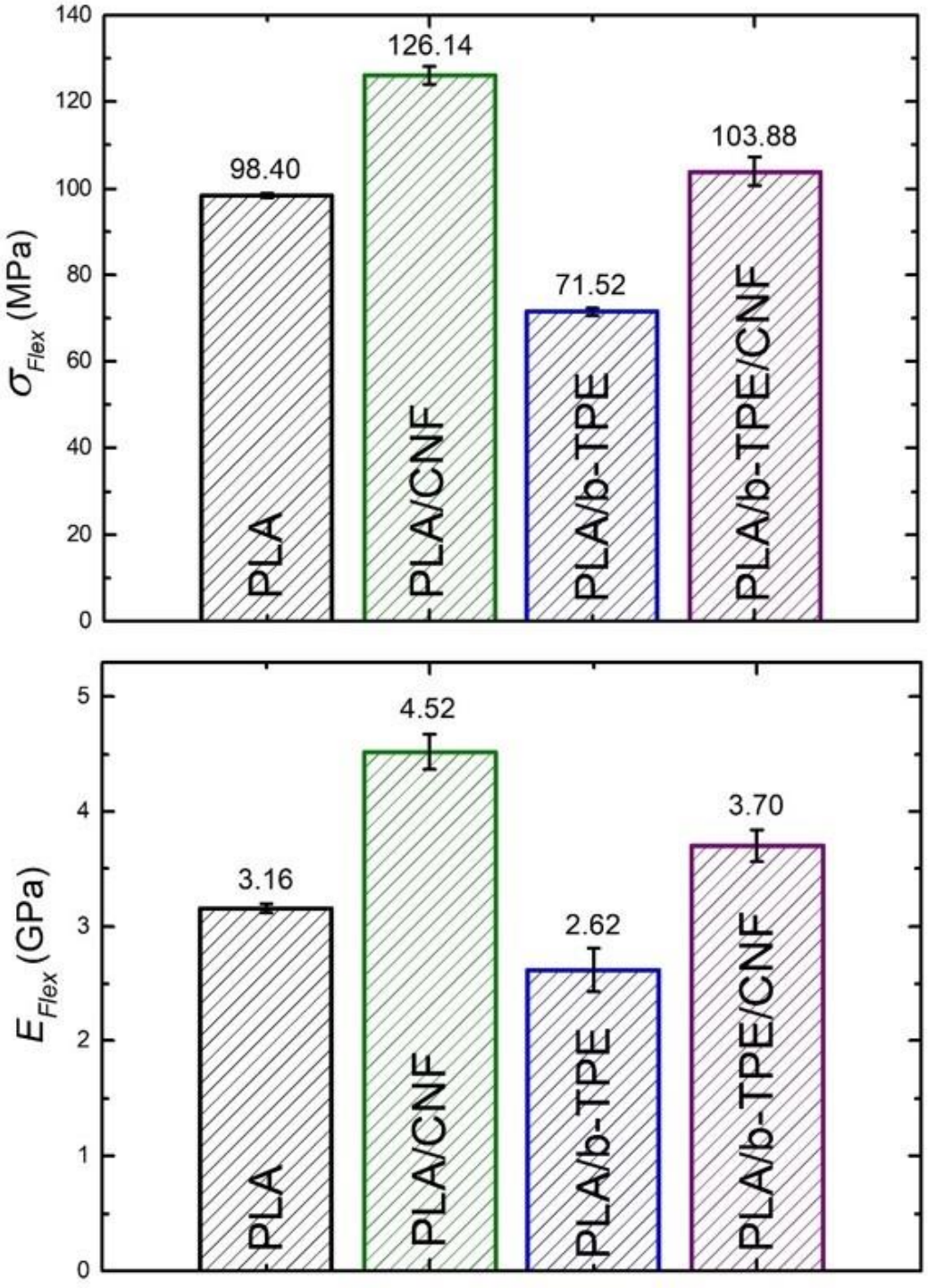

Figure 3.7 Contribution of CNF on the strengthening and stiffening of neat and blended PLA

3.9 Contribution of CNF on the Toughening of Neat and Blended PLA

One of the best methods to investigate toughening of brittle polymer materials is to perform Fracture Toughness tests for the determination of "Critical Stress Intensity Factor (K_{IC})" and "Critical Strain Energy Release Rate (G_{IC})" values. Thus, K_{IC} and G_{IC} fracture toughness values determined for all specimens were compared in Figure 3.8.

When only 1 wt% CNF was incorporated, Figure 3.8 revealed that toughening of brittle PLA matrix occurred, being 9% increase in K_{IC} and 45% increase in G_{IC} fracture toughness values. Because, one of the well-known toughening mechanisms named as "crack pinning" or "crack deflection" would take place at the interface of PLA matrix and CNF reinforcements leading to significant decreases in the propagation rate of cracks.

Figure 3.8 also revealed that when 10 phr b-TPE was blended with PLA, "rubber toughening" phenomenon occurred increasing the values of K_{IC} and G_{IC} as 5% and 104%, respectively. The main mechanism in rubber toughening was the excessive amount of "shear yielding", i.e., plastic deformation due to the presence of b-TPE round elastomeric domains homogenously distributed in the PLA matrix. Thus, high degree of shearing resulted in very rough fracture surface as evidenced in the SEM images of Figure 3.3. Apart from excessive shear yielding mechanism which retarded crack propagation rate by absorbing the energy required for crack growth, it could be pointed out that another rubber toughening mechanism occurring was the "cavity formation" around rubber domains, as seen in Figure 3.3. This mechanism also named as "debonding" is the separation at the interface between the immiscible rubber domains of b-TPE and PLA matrix, which absorb the energy of propagating cracks, and then decrease their growth rate, consequently resulting in higher fracture toughness values.

It was observed in Figure 3.8 that, the highest degree of toughening was obtained when PLA matrix was reinforced with 1 wt% CNF together with blending by 10 phr b-TPE.

Due to a kind of toughening synergism, K_{IC} and G_{IC} fracture toughness values of the PLA/b-TPE/CNF specimen increased by as much as 12% and 114% in K_{IC} and G_{IC} fracture toughness values, respectively.

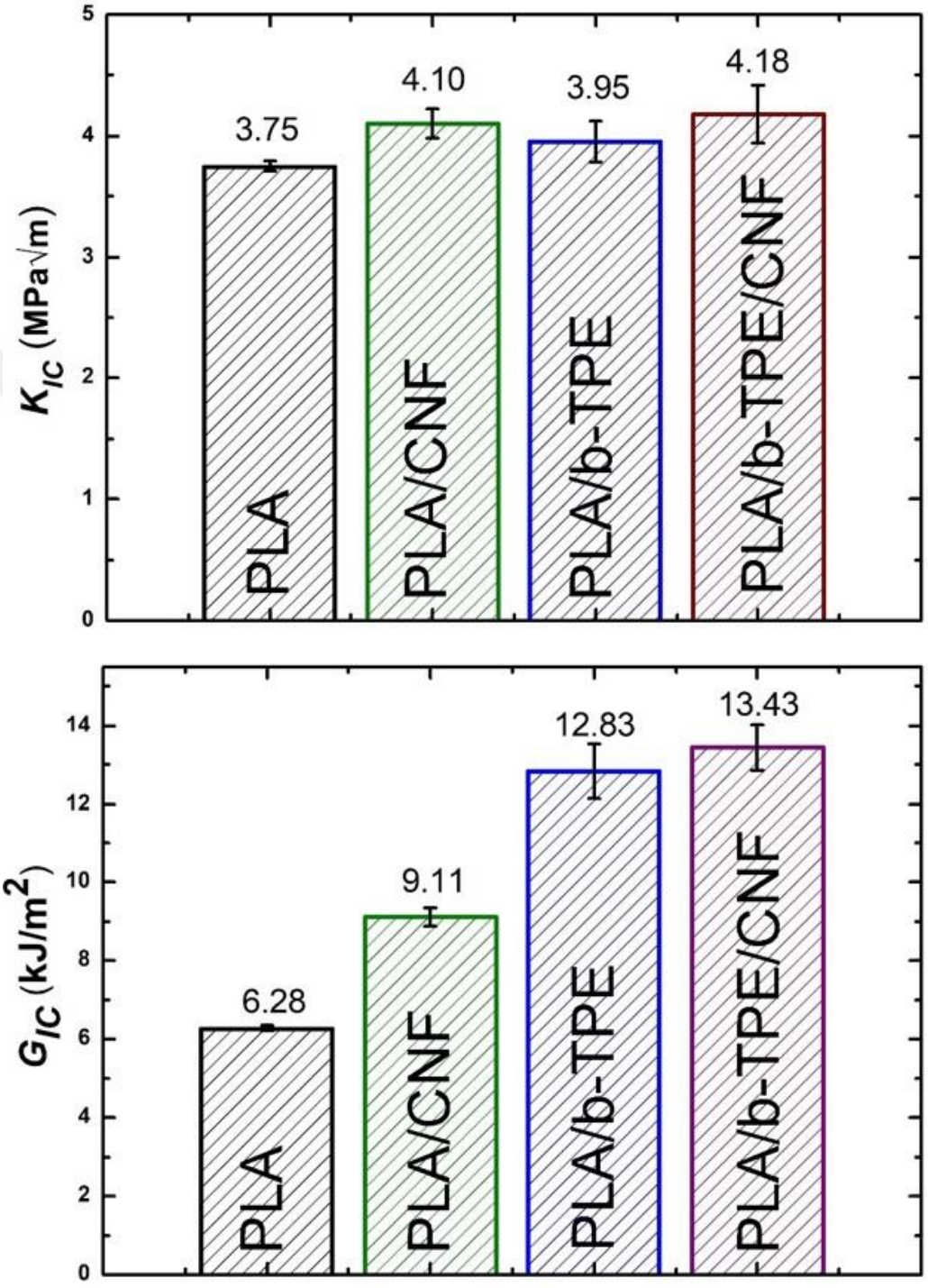

Figure 3.8 Contribution of CNF on the toughening of neat and blended PLA

3.10 Differences in Strengthening and Toughening of Specimens After 3D-Printing

Due to various advantages of additive manufacturing techniques compared to conventional molding techniques, FDM-type 3D-printers were frequently used during shaping of many biomedical components made from bioblends and biocomposites. Therefore, in order to reveal whether there would be any difference in the degree of strengthening and toughening of 3D-printed specimens compared to compression molded ones discussed above, three-point bending and fracture toughness tests were once more performed this time when the specimens were shaped by 3D-printing.

Then, Strength and Stiffness (σ_{Flex} and E_{Flex}) values of 3D-printed and compression molded specimens were compared in Figure 3.9; while Fracture Toughness (K_{IC} and G_{IC}) values were compared in Figure 3.10. All mechanical properties were also compared in Table 3.3 with ± standard deviations.

Figures 3.9 and 3.10, and Table 3.3 revealed that for the 3D-printed specimens; those increasing and decreasing trends due to use of CNF and b-TPE on the mechanical properties of PLA were all the same compared to the compression molded specimens discussed in the previous sections. This could be interpreted that there would be no change in the contribution trend of CNF to all mechanical properties of neat and blended PLA when components were shaped by 3D-printing.

On the other hand, Figure 3.9 indicated that flexural strength and modulus values of 3D-printed specimens were approximately 20% and 34% lower compared to compression molded specimens. Oppositely, Figure 3.10 indicated that K_{IC} and G_{IC} fracture toughness values of 3D-printed specimens were approximately 31% and 20% higher compared to compression molded specimens.

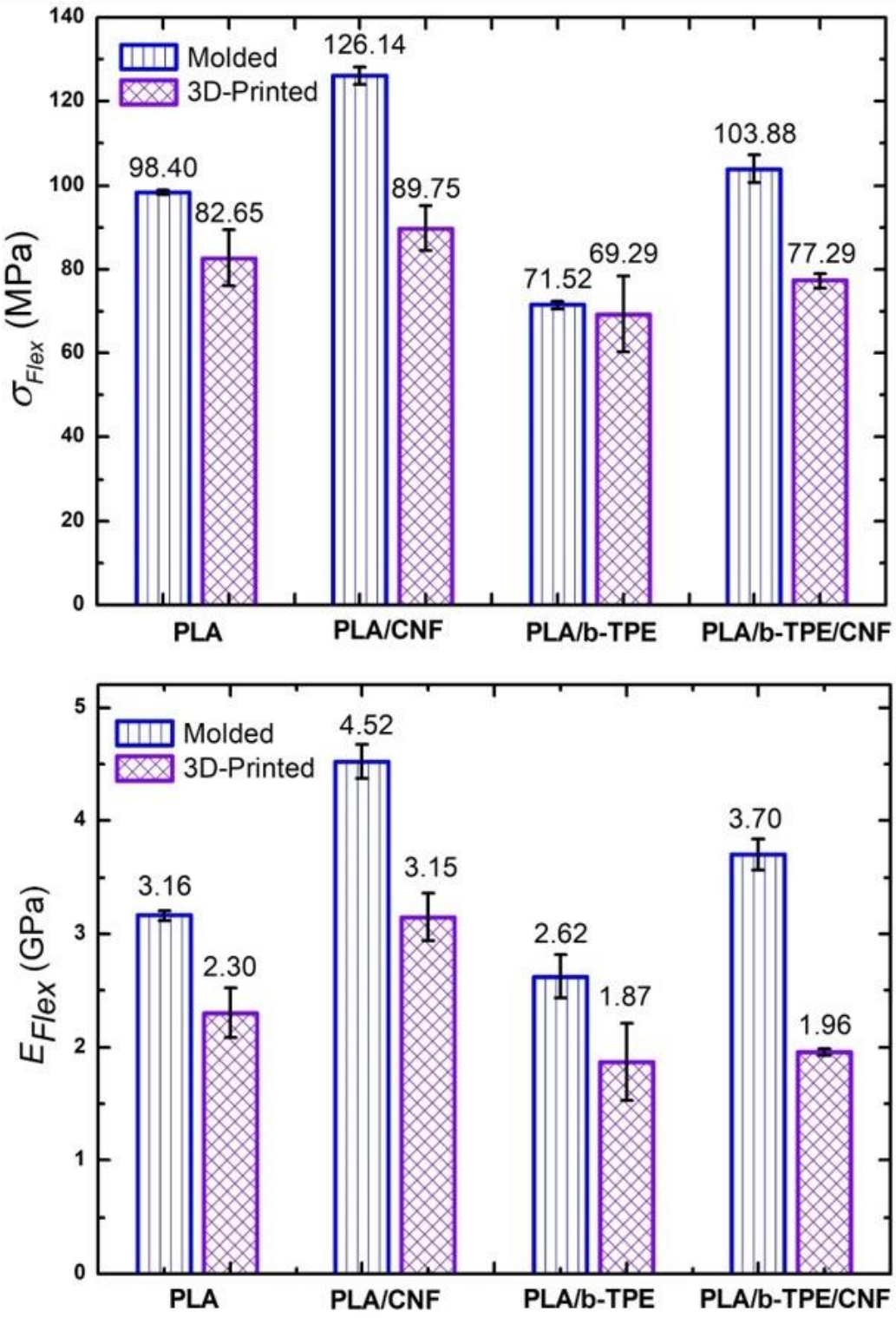

Figure 3.9 Differences in the flexural strength and modulus values of 3D-printed and compression molded specimens

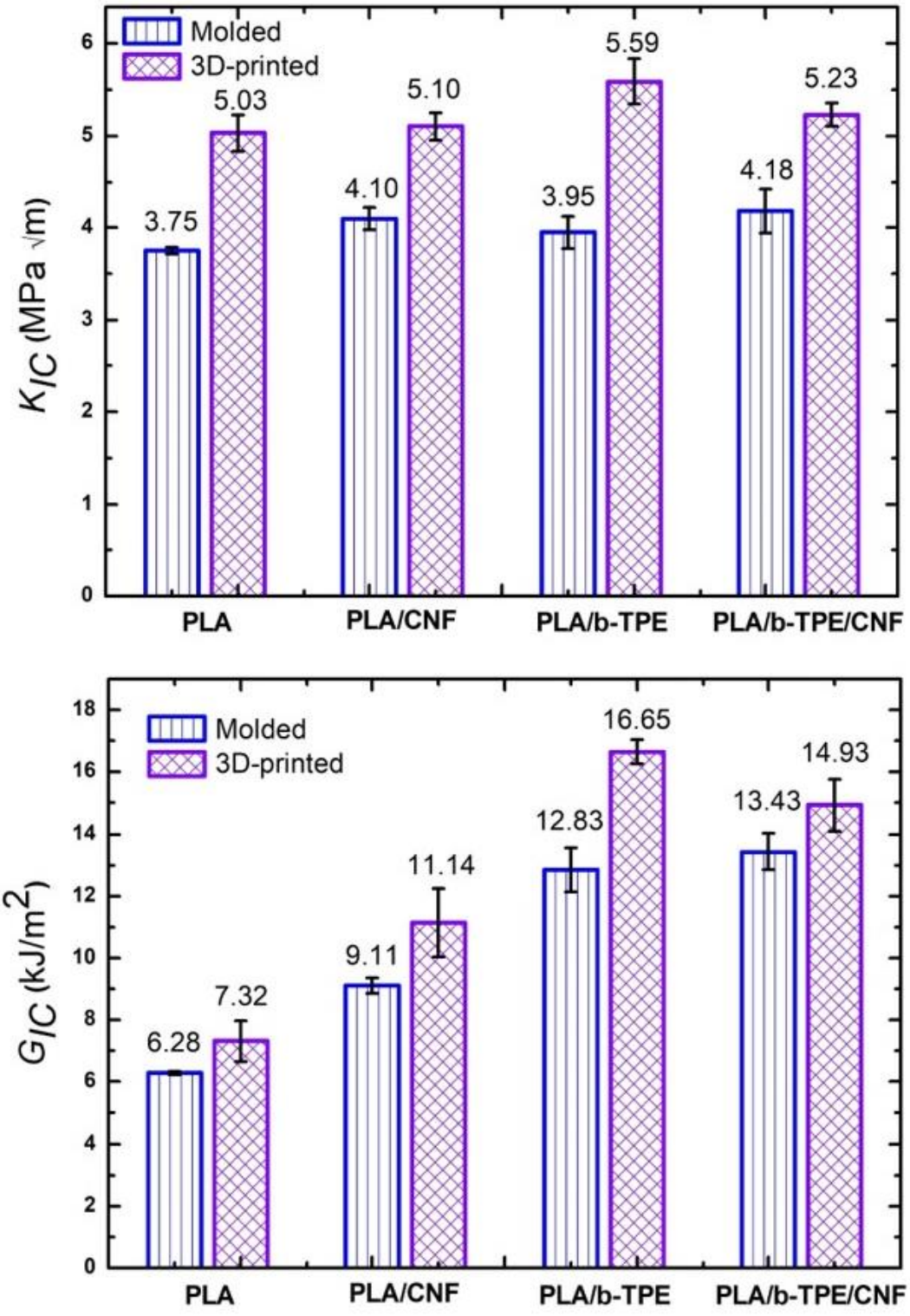

Figure 3.10 Differences in the fracture toughness values of 3D-printed and compression molded specimens

Table 3.3 Differences in the values of all mechanical properties of 3D-printed and compression molded specimens.

Specimens	σ_{Flex} (MPa)		E_{Flex} (GPa)		K_{IC} (MPa$\sqrt{m}$)		G_{IC} (kJ/m^2)	
	Molded	**3D-Printed**	**Molded**	**3D-Printed**	**Molded**	**3D-Printed**	**Molded**	**3D-Printed**
PLA	98.40±0.50	82.65±6.73	3.16±0.04	2.30±0.22	3.75±0.04	5.03±0.20	6.28±0.07	7.32±0.66
PLA/CNF	126.14±2.05	89.75±5.29	4.52±0.15	3.15±0.21	4.10±0.12	5.10±0.15	9.11±0.24	11.14±1.09
PLA/b-TPE	71.52±0.97	69.30±8.98	2.62±0.19	1.87±0.34	3.95±0.17	5.59±0.25	12.83±0.71	16.65±0.40
PLA/b-TPE/CNF	103.88±3.30	77.30±1.70	3.70±0.14	1.96±0.03	4.18±0.24	5.23±0.13	13.43±0.58	14.93±0.83

In order to reveal reasons of lower performance in the strengthening degree and higher performance in the toughening degree of 3D-printed specimens, visual inspection was conducted for the structural appearance of three-point bending and fracture toughness test specimens. In Figure 3.11, images of only neat PLA specimens were given. Because, compared to others, neat PLA specimens were rather semi-transparent, so that it was possible to make visual inspection.

Figure 3.11 revealed that there were certain differences in the appearances of 3D-printed and compression molded specimens. Compared to the rather smooth and uniform structure of compression molded specimens, a kind of "textured" structure appeared in the 3D-printed ones. The main reason for the formation of textured structure was use of ± 45° raster angle orientation during layer-by-layer production of 3D-printing.

Therefore, it could be stated that lower strength and stiffness (σ_{Flex} and E_{Flex}) values of 3D-printed specimens could be due to the detrimental effect of textured structure on the strengthening and stiffening mechanisms; via certain differences in the degree of orientation and distribution of CNF reinforcements and b-TPE domains in the PLA matrix.

On the other hand, it was apparent that textured structure resulted in higher fracture toughness (K_{IC} and G_{IC}) values of 3D-printed specimens, which could be due to additional crack deflection action of ±45° textures in terms of the decreased crack propagation rate toughening mechanism discussed before.

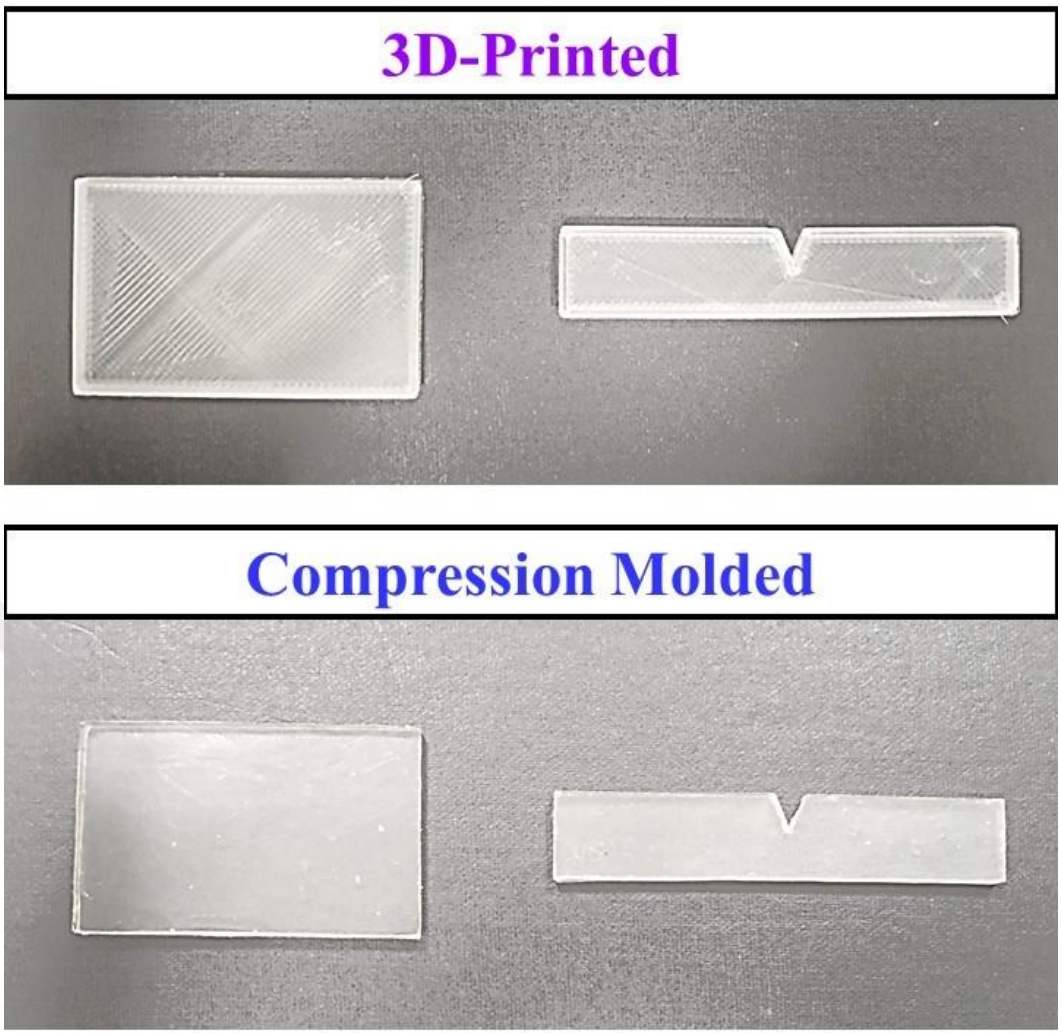

Figure 3.11 Images of the semi-transparent neat PLA mechanical test specimens showing rather textured structure of 3D-printed ones compared to compression molded ones

CHAPTER 4

USE OF CELLULOSE NANOFIBRILS AND NANOCRYSTALS IN ELECTROSPINNING OF POLYLACTIDE NANOFIBERS

Cellulose is the most abundant, renewable and sustainable biomaterial on Earth; being the basic constituent of all plants. For instance, it is present in the cell wall of wood along with hemicellulose and lignin. Although, there are various industrial applications of macro and micron sized cellulose fibrous forms; use of nano-sized cellulose structures as the biofillers of biopolymer matrices in the production of bio-nanocomposites is emerging [142-145].

As shown in Figure 4.1, two basic nanocellulose structures obtained by using mechanical and chemical top-down processing techniques are cellulose nanofibrils (CNF) and cellulose nanocrystals (CNC) with diameters up to 100 nm. CNF composed of both amorphous and crystalline regions in its fibrous form has rather a high aspect ratio, while CNC consists of low aspect ratio crystalline particles with very little amorphous part [146-148].

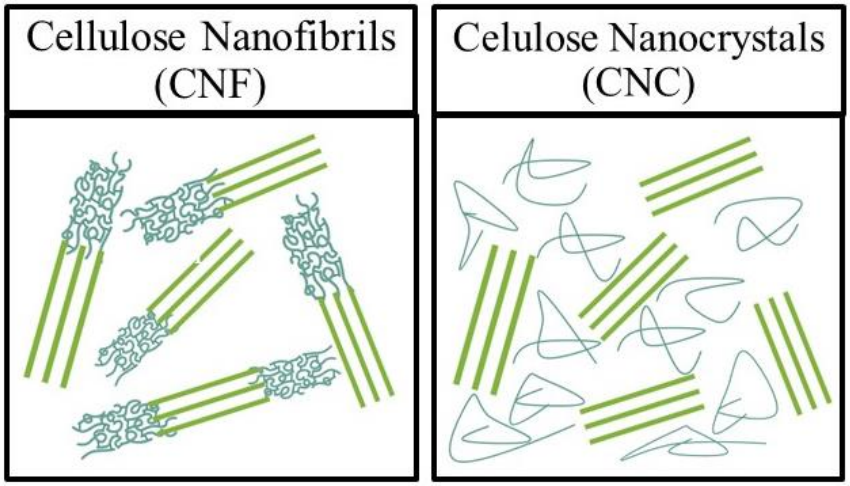

Figure 4.1 Two different nanocellulose structures (CNF and CNC) used as fillers in biocomposites

In the production of fully “green composites”; both the polymer matrix and the reinforcing fillers should be bio-sourced renewable ones. Although there are other alternatives, the most widely used biopolymer matrix selected in the bio-nanocomposite studies is polylactide (PLA) [149-151].

CNF or CNC filled PLA bio-nanocomposites could be obtained by using certain techniques such as “melt mixing” or “solution mixing” for various purposes. On the other hand, for certain biomedical applications such as wound dressing; fibrous forms would be necessary. For this purpose, “electrospinning” is being considered as the most effective nanofiber production technique [152].

As illustrated in Figure 4.2, during pumping the polymer solution to the feeding tip, high voltage power supply creates electrostatic field that charges the polymer solution. At this point, charged polymer solution droplets would be under opposite forces of viscoelastic forces and surface tension. When the first one exceeds the other one, solution droplets would transform into a conical form (Taylor Cone). During the upward whipping motion of the solution jet, solvents would evaporate. Then, electrospun nanofibers would be deposited on a grounded collector [153, 154].

It is known that, in many biomedical applications, use of electrospun nanofibers with as much as lower diameter would be advantageous. Because, decreasing the fiber diameter would increase their total surface area required for certain chemical or biological interactions. It should be noted that, decreasing fiber diameter could also increase the degradation rate.

Therefore, the main purpose of this chapter was to investigate the effects of various parameters on the morphology and diameter of nanocellulose (CNF and CNC) filled polylactide (PLA) electrospun nanofibers. For this purpose, first of all effects of three important electrospinning parameters (Solution Concentration, Solution Rate, Collector Distance) were studied for the 1 wt% CNF filled PLA. Then, effects of 3 wt% CNF use compared to 1 wt%; effects of CNC use compared to CNF; and effects of KCl salt addition for all combinations were also investigated. Moreover, *in vitro* degradation rate of all types of electrospun nanofiber mats was compared.

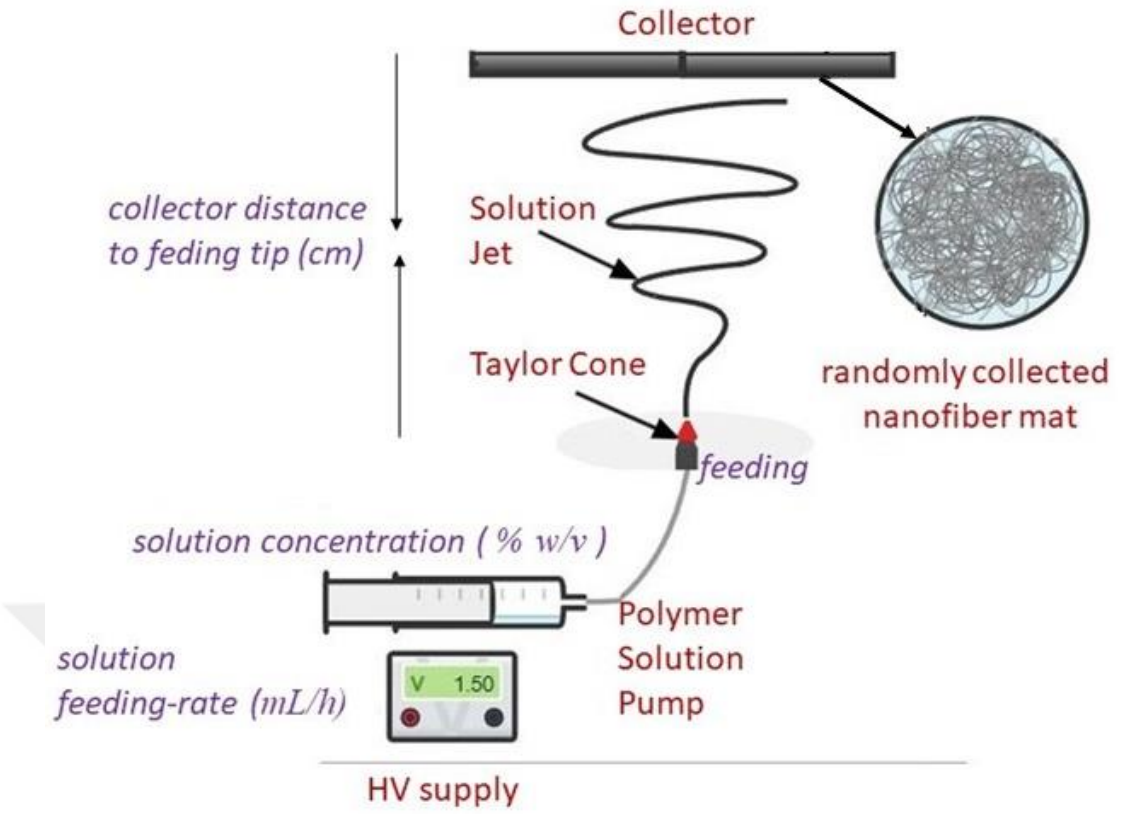

Figure 4.2 Typical electrospinning system indicating important processing parameters

Literature survey indicated that although there are several numbers of studies [155-162] on the various aspects of electrospinning of PLA/CNF and PLA/CNC; only very limited number of them were focused on the effects of certain parameters influencing diameter of their electrospun fibers.

For example, Yang *et al*. [163, 164], studied effects of different amounts of CNF; while Xiang *et al*. [165], Liu *et al*. [166], Patel *et al*. [167], Rahmat *et al*. [168] and Shi *et al*. [169] studied effects of different amounts of CNC on the diameter of PLA based electrospun fibers. They generally indicated that increasing the amount of CNF or CNC in the polymer solution decreased the diameter of electrospun fibers; mainly due to the increased charge density of the polymer solution having higher amount of hydroxyl groups present in the cellulose structures.

It is known that, in order to increase electrical conductivity of polymer solutions, organic or inorganic salts could be added. In the literature, there are certain number of studies [170-172] adding certain salts into neat or filled PLA solutions to observe their effects on the electrospun fibers. However, no studies were reported for CNF and CNC filled PLA solutions. Therefore, in this study adding KCl salt into PLA/CNF and PLA/CNC solutions would be the first one in the literature.

As stated above, size of the electrospun fibers plays critical role in terms of *in vitro* degradation behavior. In the literature although there are limited number of degradation studies [173-177] conducted for neat and filled PLA based electrospun fibers; no research was reported for the *in vitro* degradation of PLA/CNF, and only one study was reported for PLA/CNC by Shi *et al.* [169]. Thus, this study would be a pioneering one also from this point of view.

In this chapter, in order to fulfil these aims, following experimental procedures were conducted.

4.1 Materials Used

The base biopolymer used in the electrospinning solution was polylactide (PLA) having L-lactic acid macromolecular structure (NaturePlast PLE 001, France). It has a density of 1.25 g/cm^3, melting temperature range of 145-155°C, degradation temperature range of 240-250°C, melt flow index range of 2-8 g/10 min at 190°C under 2.16 kg, and weight average molecular weight of 101x10^3 g/mol.

Two different nanocellulose particles added to the PLA based electrospinning polymer solution were nanocellulose fibrils (CNF) and nanocellulose crystals (CNC). Diameter range of the particles given by the supplier (Guilin Qihong Technology, China) was 20-100 nm, in which CNF particles having slightly higher aspect ratio compared to CNC.

Other chemicals used in the preparation of electrospinning solution, i.e. chloroform (CF), dimethylformamide (DMF) and potassium chloride (KCl) were all high purity grade (Fluka, Germany).

Generally, in nanocomposite studies, the amount of the filler incorporated into the matrix polymer is around 1 wt%. Consequently, the amount of both CNF and CNC added into the PLA matrix solution was chosen as 1 wt%; i.e., 99 wt% PLA and 1 wt% CNF or CNC. For simplicity, these combinations were designated as PLA/CNF and PLA/CNC through the manuscript. Effects of using 3 wt% CNF were also investigated.

4.2 Electrospinning Procedures

(i) Equipment

As shown in Figure 4.3, electrospun nanofibers were obtained by using a single-nozzle vertical electrospinning equipment (NanoSpinner Ne100, Inovenso Inc., Turkey). The capacity of high voltage power supply was up to 40 kV, while the capacity of the polymer solution pump via a disposable syringe was up to 10 mL/h, so that it was possible to investigate effects of “Solution Feeding Rate”. A polyethylene capillary tube connects the syringe and the needle having inner diameter of 0.8 mm. Between the collector and feeding tip of the polymer solution jet, the distance was 25 cm so that another important electrospinning parameter “Collector Distance to Feeding Tip” could be investigated. The collector of the equipment was stationary type round aluminum plate. In order to collect electrospun nanofibers easily; collector was also covered with aluminum foils. By using the air ventilation system of the equipment, it was possible to keep temperature and relative humidity of the cabin at about 30°C and 40%, respectively.

(ii) Preparation of the Polymer Solutions

It is known that use of CF and DMF as 75/25 v/v solvent ratio is very effective during electrospinning of PLA based polymer solutions. Therefore first, CF/DMF solvent mixtures (3:1) were prepared as 10 mL, which was the capacity of polymer syringe of the equipment. Then, certain amount of PLA granules was dissolved in this mixture by magnetic agitation at 30°C with 600 rpm for 4 hours. After that, required amounts of nanocellulose particles were added to the dissolved PLA solution with further mixing of 2 hours. Moreover, PLA/nanocellulose solutions were also ultrasonicated to obtain well-dispersed cellulose nanoparticles just before the start of electrospinning process.

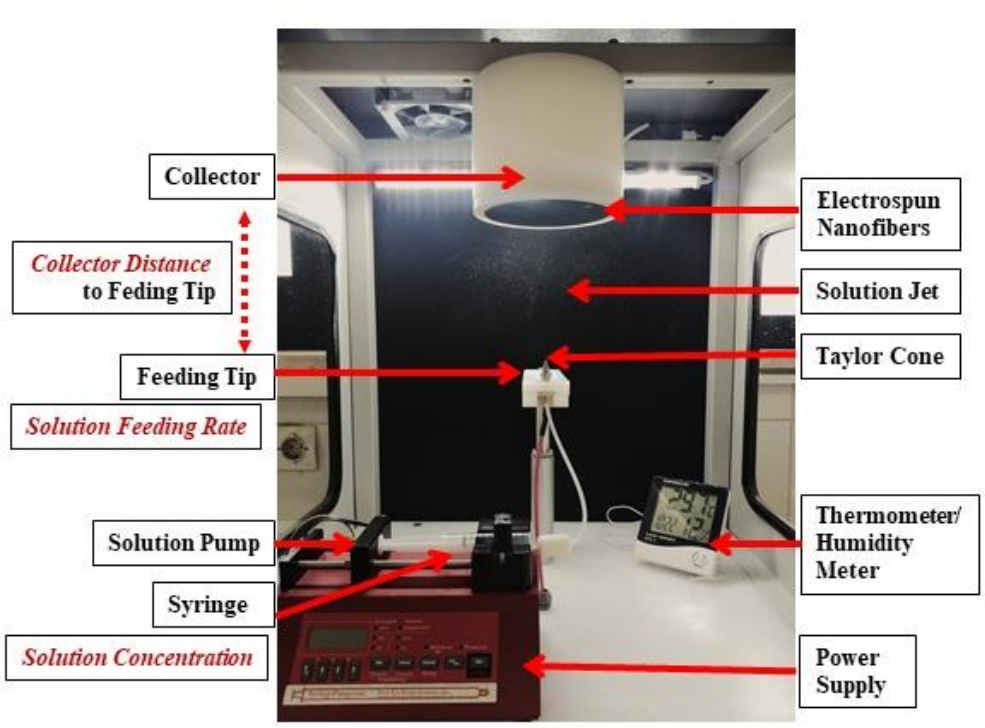

Figure 4.3 General view of the electrospinning equipment used

(iii) Viscosity and Conductivity Measurements of the Polymer Solutions

Since viscosity (i.e., polymer concentration) and charge density (i.e., electrical conductivity) of polymer solutions influence morphology and diameter of the

electrospun fibers, these two parameters were also measured at 25°C before the start of electrospinning. Viscosities of polymer solutions were measured using a digital viscosimeter (Brookfield DV-II+ Pro, USA) under 42.4 s^{-1} shear rate; while electrical conductivities were measured via a benchtop conductivity meter (Hanna HI 2315, USA).

(iv) Obtaining Electrospun Nanofibers

After preparing PLA/nanocellulose polymer solutions properly, and measuring their viscosity and conductivity, electrospinning processes were conducted by using different process parameters as would be discussed later in the manuscript. After each experiment, electrospun nanofibers were collected in the form of "mats" on the aluminum foil surface covering the collector. In order to use these electrospun fiber mats in further analysis, their thickness and amount should be similar. For this reason, electrospinning period used during each experiment was determined according to the Solution Feeding Rate. For instance, for the Feeding Rates of 0.9, 1.5, 1.8 mL/h; total electrospinning period used were 30, 18 and 15 minutes, respectively.

4.3 Diameter Analysis of Electrospun Fibers

Before diameter determination, it should be stated that scanning electron microscopy (FEI Nova Nano 430, USA) analysis was first conducted for the surface morphology of electrospun fibers including bead formation.

Diameter analysis of electrospun fibers was conducted in two steps. First, scanning electron microscopy was used to take various numbers of general and closer view SEM images of electrospun fibers collected in the form of mats on aluminum foil surfaces. Then, average diameter of the electrospun fibers was measured by using an image analysis software (ImageJ, USA) on at least 300 randomly selected individual fibers present on the SEM images.

4.4 *In Vitro* Degradation Analysis of Electrospun Fibers

Since electrospun biocomposite fibers have been considered for many biomedical applications, it is important to analyze *in vitro* degradation behavior of these electrospun samples in a simulated human body fluid. For this purpose, electrospun fibers in the form of mats were cut into 15x15 mm square samples. Then, samples were immersed in a physiological saline solution for up to 12 weeks in an oven at 37°C human body temperature (Figure 4.4).

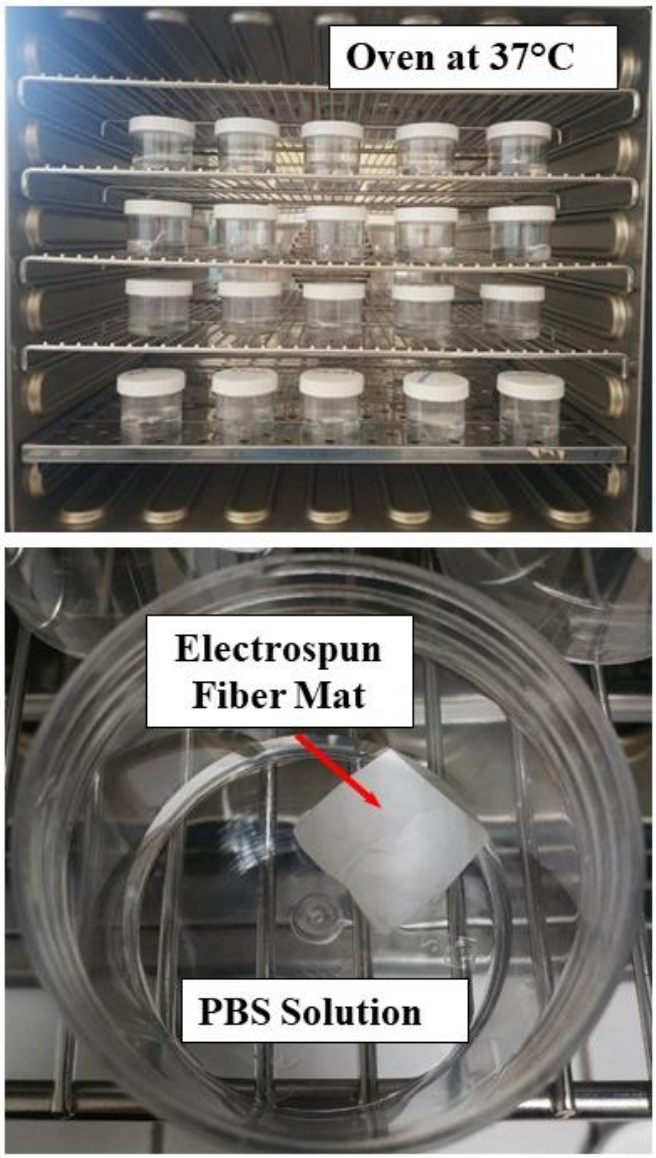

Figure 4.4 General and closer views of *in vitro* degradation of electrospun fiber mats

Before that, phosphate-buffered saline (PBS) tablets (Sigma Aldrich, USA) were dissolved in 200 mL deionized water to prepare the solution, so that it would be composed of 0.01 M phosphate buffer, 0.0027 M potassium chloride and 0.137 M sodium chloride with the required pH value of 7.38 at 25 °C.

At the end of each week, in order to determine degree of degradation, certain number of the electrospun fiber mat samples were taken out of their solution bottles, dried and then weighed with a precision balance to calculate "% weight loss" values.

It is known that the most critical four processing parameters during electrospinning of polymer solutions are;

(i) Applied Voltage (kV)
(ii) Polymer Concentration in the Solution (%w/v)
(iii) Solution Feeding Rate (mL/h)
(iv) Collector Distance to Feeding Tip (cm)

Depending on the electrospinning equipment, the most widely used "Applied Voltage" for many polymer solutions was in the range of 10-20 kV; being generally around 15 kV for neat and filled PLA based solutions [165, 166, 169, 172]. Thus in this study, Applied Voltage level selected was also 15 kV for the electrospinning of PLA/CNF solutions. For the three other critical processing parameters, various experimental procedures applied were discussed in the following sections.

4.5 Effects of PLA/CNF Concentration in the Solution

Electrospinability of polymer solutions first of all depends on mainly formation of "proper Taylor Cone" and "stable Polymer Solution Jet"; in which both of them are influenced directly by the "viscosity" that is "polymer concentration" of the solution. Otherwise, it would be very difficult for the polymer solution jet to reach the collector and form nanofibers.

Studies [155, 160, 172] on the neat and filled PLA based solutions indicated that typical range for the polymer solution concentrations was 5-15 %w/v. In this study, it was decided to try three different PLA/CNF concentration values as 6, 8 and 10 %w/v. Before electrospinning, viscosity values of these three solutions were measured in terms of cP.

Figure 4.5 shows conditions of "Taylor Cone" and "Solution Jet" formations together with the concentration and viscosity values of PLA/CNF solutions. It was observed that when PLA/CNF concentration was 10 %w/v (viscosity 308 cP), there was significant degree of clogging at the solution "Feeding Tip" blocking the formation of Taylor Cone and polymer Solution Jet, so that electrospinning was not possible.

When PLA/CNF concentration was 6 %w/v (viscosity 53 cP) or 8 %w/v (viscosity 124 cP); then formation of Taylor Cone and Solution Jet was possible. On the other hand, it was revealed that when concentration was 8 %w/v, more proper Taylor Cone and more stable Solution Jets were formed compared to the concentration of 6 %w/v. Then, in order to choose PLA/CNF concentration as 6 or 8 %w/v to use in the further experiments, electrospun fiber mat samples formed on the collector were examined under SEM.

Figure 4.6 indicated that when concentration was 6 %w/v, there was mainly formation of "droplets", not fibrous form. Because, it was discussed that [178] use of lower polymer concentration or lower solution viscosity might prevent getting sufficient amount of polymer macromolecules to overcome electrostatic stretching forces. Then, polymer jets split up leading to formation of droplets.

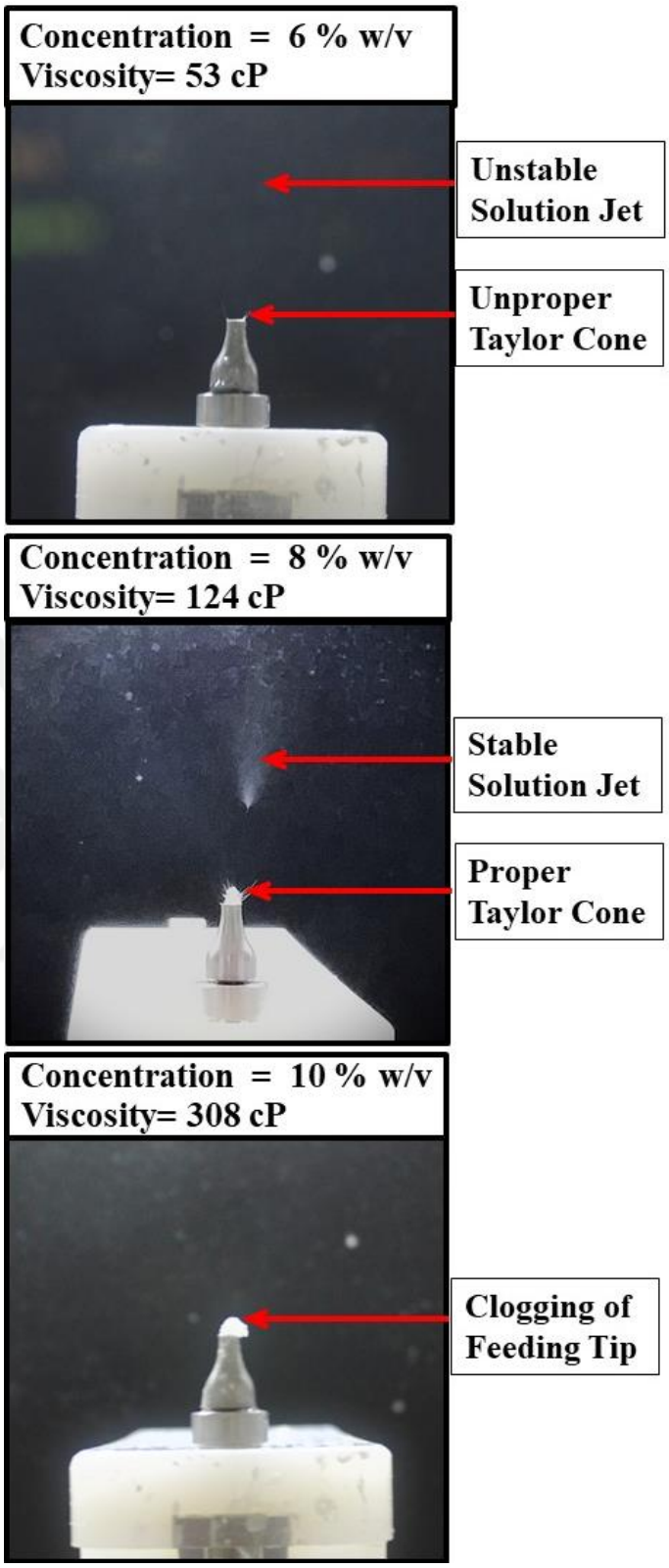

Figure 4.5 Images showing effects of PLA/CNF concentration or viscosity of the solution on the formation of Taylor Cone and polymer Solution Jet

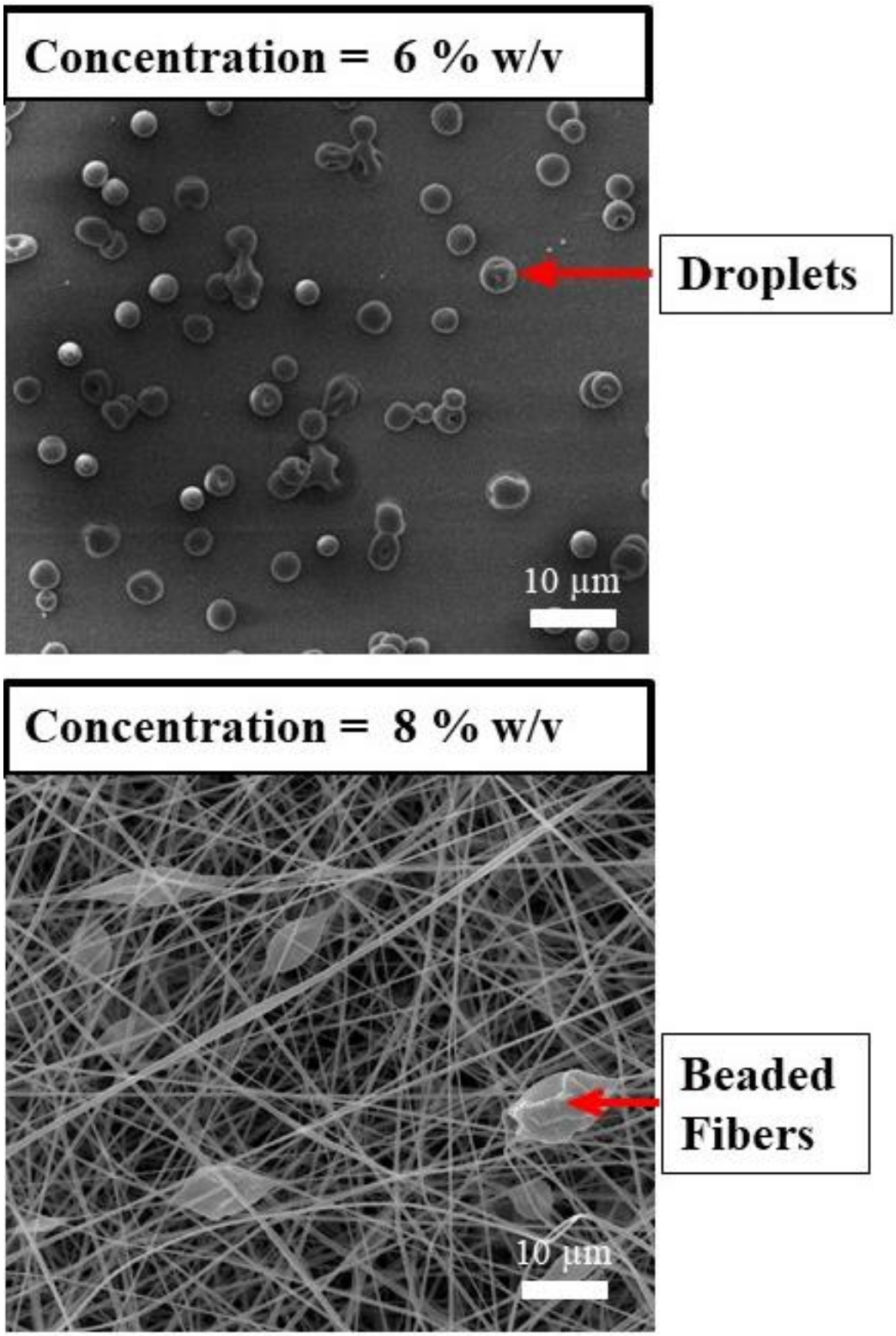

Figure 4.6 SEM images showing effects of solution concentration on the formation of PLA/CNF "droplets" or "beaded fibers"

On the other hand, use of 8 % w/v concentration resulted in formation of "fibrous" morphology. It was seen in Figure 4.6 that, many of the electrospun fibrous forms have no smooth structure; instead, there were so many numbers of "beads" on their surfaces. Thus, it was interpreted that in order to obtain "bead-free" PLA/CNF electrospun fibers, other processing parameters should be studied; as discussed in the next section.

4.6 Effects of Solution Rate and Collector Distance on the Bead-Free PLA/CNF Fibers

Researchers [167, 168, 172] on the electrospinability of neat and filled PLA based solutions revealed that when polymer concentration was around 8 %w/v, then in order to obtain electrospun fibers with smooth surfaces; typical range used for Solution Rate parameter was between 0.5-2.0 mL/h, while typical range for Collector Distance parameter was 10-25 cm. Thus, in this study to obtain "bead-free" smooth electrospun PLA/CNF fiber morphology, various experiments were conducted by using the following three different values for each processing parameter:

- PLA/CNF Solution Feeding Rate: 0.9, 1.5, 1.8 mL/h
- Collector Distance to Feeding Tip: 15, 18, 20 cm

After electrospinning of PLA/CNF solutions with various combinations of these two parameters, it was generally observed that increasing the Solution Rate and increasing the Collector Distance both resulted in formation of certain numbers of beads. From this point of view, it could be stated that the worst combination leading to "beaded" morphology was Solution Rate of 1.8 mL/h and Collector Distance of 20 cm. For the almost "bead-free" morphology, the best combination was Solution Rate of 1.5 mL/h and Collector Distance of 15 cm. Example SEM images for each combination were illustrated in Figure 4.7.

As would be discussed in the next sections, main reasons for the beaded morphology and thicker diameter levels observed for the electrospun PLA/CNF fibers were similar.

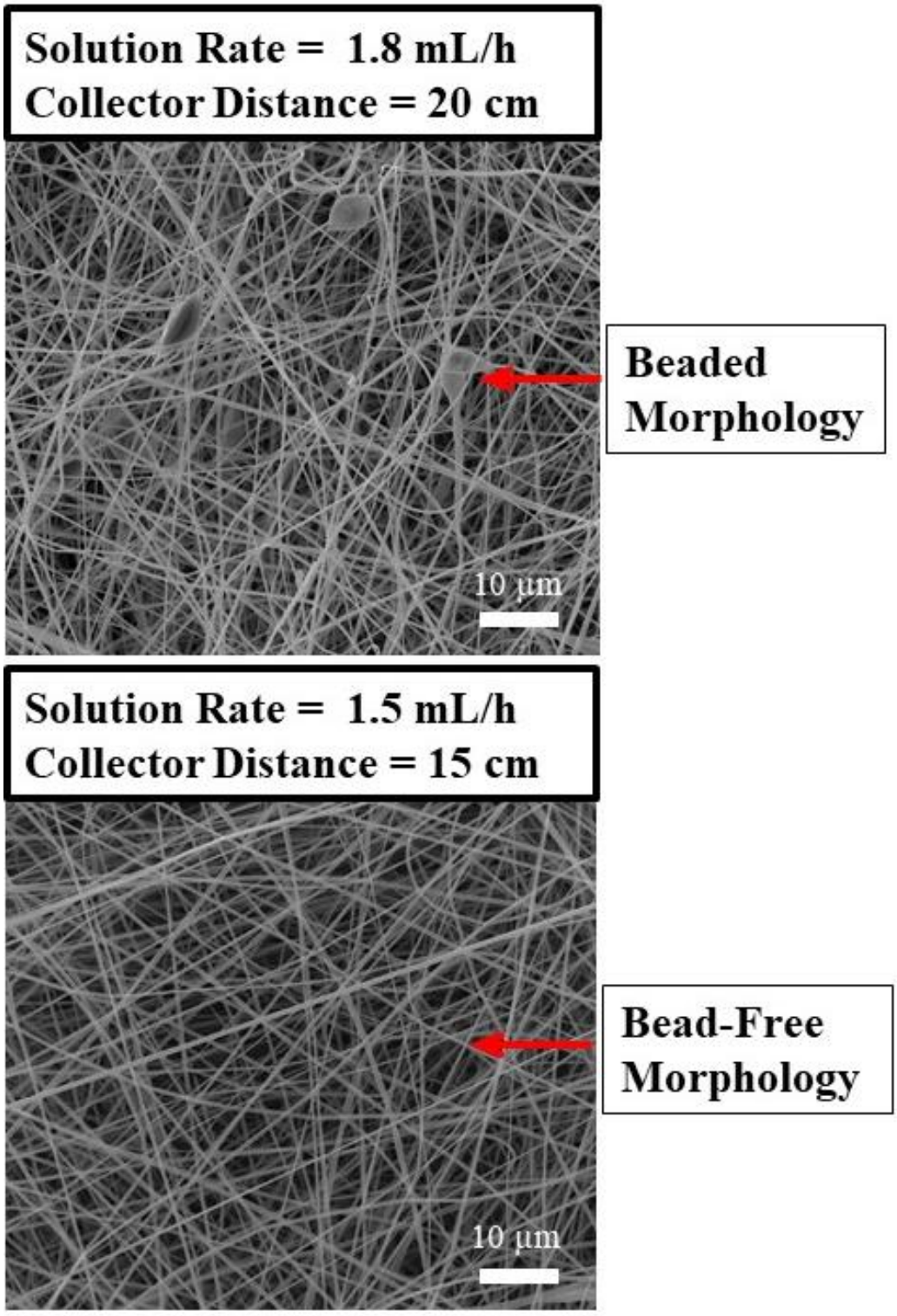

Figure 4.7 SEM images showing effects of solution rate and collector distance on the formation of "beaded" and "bead-free" electrospun PLA/CNF fibers

4.7 Effects of Solution Rate and Collector Distance on the Diameter of PLA/CNF Fibers

Since the optimum combination for the “bead-free” morphology of electrospun fibers was Solution Rate of 1.5 mL/h and Collector Distance of 15 cm, then effects of these two parameters on the “diameter” of PLA/CNF nanofibers were investigated by keeping one of these optimum values as constant and changing the other; which made up six different combinations. Then, average diameter analysis for these combinations was conducted as described in the experimental work section.

In order to reveal effects of Solution Rate parameter, Figure 4.8 shows general and closer SEM images including measured average fiber diameters obtained by increasing the Solution Rate values while keeping the Collector Distance value constant at 15 cm. Similarly, for the effects of Collector Distance, Figure 4.9 indicates SEM images and average fiber diameters obtained by increasing the Collector Distance values while keeping the Solution Rate value constant at 1.5 mL/h.

As revealed in Figures 4.7, 4.8, 4.9; it could be stated that to obtain rather bead-free and smooth PLA/CNF electrospun fibers with fine sized diameters; an optimum Solution Rate and Collector Distance values of 1.5 mL/h and 15 cm could be used. It was observed that use of higher values resulted in larger diameters.

According to similar observations reported [172, 179], it could be indicated that Solution Rate and Collector Distance parameters significantly influence the balance of electrostatic repulsion, surface tension and viscoelastic forces in the electrospinning solution. They are all very critical conditions for the required solution jet velocity, solvent evaporation time and sufficient polymer transfer rate. When Solution Rate and Collector Distance parameters are over an optimum value, then beaded morphology and larger diameter fiber formation would take place.

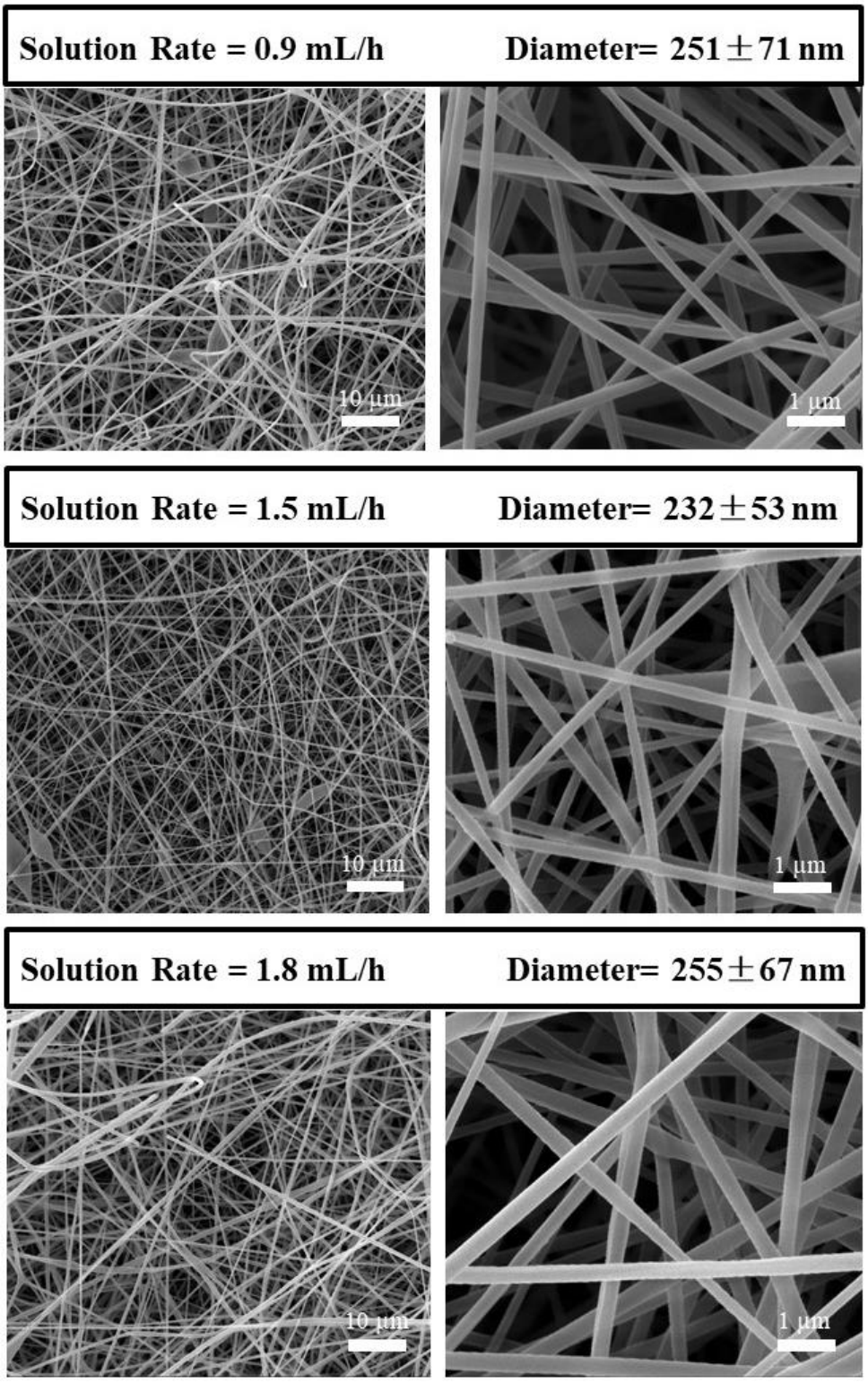

Figure 4.8 General and closer SEM images showing effects of Solution Rate on the average diameter of PLA/CNF electrospun fibers when Collector Distance was kept as 15 cm

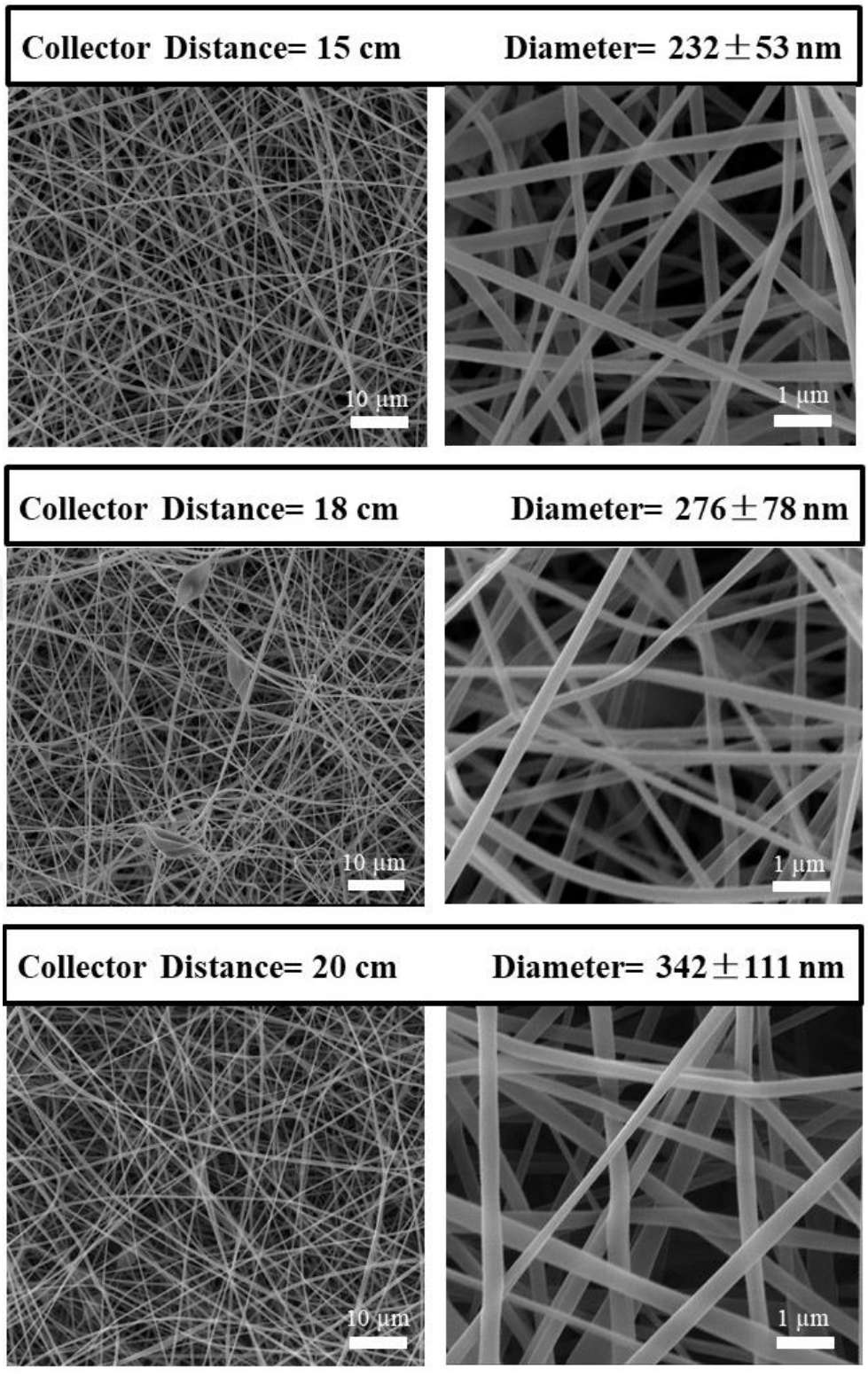

Figure 4.9 General and closer SEM images showing effects of Collector Distance on the average diameter of PLA/CNF electrospun fibers when Solution Rate was kept as 1.5 mL/h

4.8 Effects of 3 wt% CNF Use Compared to 1 wt% on the Diameter of Electrospun Fibers

In order to observe use of higher amount of nanocellulose particles on the diameter of electrospun fibers, this time PLA based electrospinning solution was prepared with 3 wt% CNF. Optimum processing parameters determined for the PLA solution with 1 wt% CNF discussed in the previous sections were applied without any change. Then, diameter analysis via SEM was conducted for each PLA/CNF electrospun fiber obtained. Figure 4.10 indicated that when polymer solution was filled with 3 wt% CNF compared to 1 wt% CNF, average diameter of electrospun fibers decreased significantly from 232 nm down to 175 nm.

It is known that in the cellulose structure including CNF, there are plenty of hydroxyl groups which have the ability to increase charge density of the polymer solutions significantly. Thus, it was stated that [163, 164, 167] higher charge density leads to increased electrostatic forces allowing the polymer solution jet to break into smaller segments and then formation of electrospun fibers with finer diameters.

Thus, compared to 1 wt% CNF, use of 3 wt% CNF resulted in higher charge density in the electrospinning solution leading to much finer diameter distribution of PLA/CNF nanofibers obtained. On the other hand, effects of using more than 3 wt% CNF were not investigated. Although, several trials were conducted, due to the feeding tip clogging and other processing problems, it was difficult to obtain proper electrospun fiber morphology.

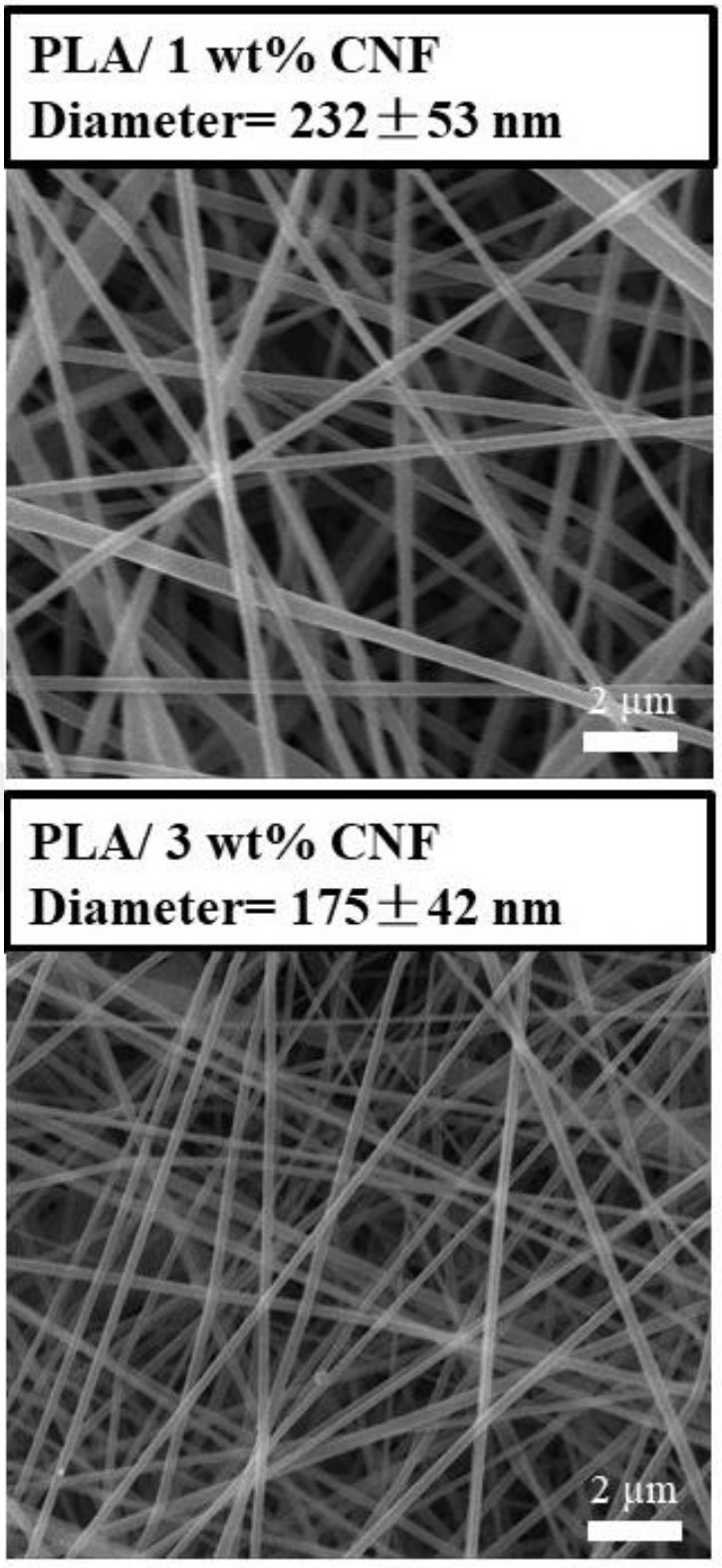

Figure 4.10 SEM images showing effects of higher CNF amount on the diameter of PLA/CNF electrospun fibers

4.9 Effects of CNC Use Compared to CNF on the Diameter of Electrospun Fibers

In order to compare whether there would be any difference when 1 wt% cellulose nanofibril (CNF) particles were replaced with 1 wt% cellulose nanocrystal (CNC) particles in the PLA solution, electrospinning experiments were repeated by using again the same optimum processing parameters to analyze and compare PLA/CNC electrospun fibers.

It was reported that [167, 166] apart from the extensive hydroxyl groups in the structure of all cellulose particles, additional sulfate ester groups would be present on the CNC surfaces; which were formed during H_2SO_4 acid hydrolysis technique used in their production. Consequently, charge density and electrical conductivity of PLA/CNC solution would be higher than the PLA/CNF solution, leading to finer diameter electrospun fibers as discussed above.

Thus, Figure 4.11 shows that due to higher conductivity of PLA/CNC solution (2.7 μS/cm) compared to conductivity of PLA/CNF solution (2.3 μS/cm); average PLA/CNC electrospun fiber diameter was 209 nm, while for PLA/CNF fibers it was 232 nm.

4.10 Effects of KCl Salt Addition on the Diameter of Electrospun Fibers

Since higher charge density or conductivity of the polymer solution leads to greater elongation forces and higher overall tension in the polymer solution jet resulting in bead-free fine diameter electrospun fibers; researchers [150-172] investigated effects of organic or inorganic salt additions for various neat and filled PLA solutions, but not for PLA/CNC and PLA/CNF.

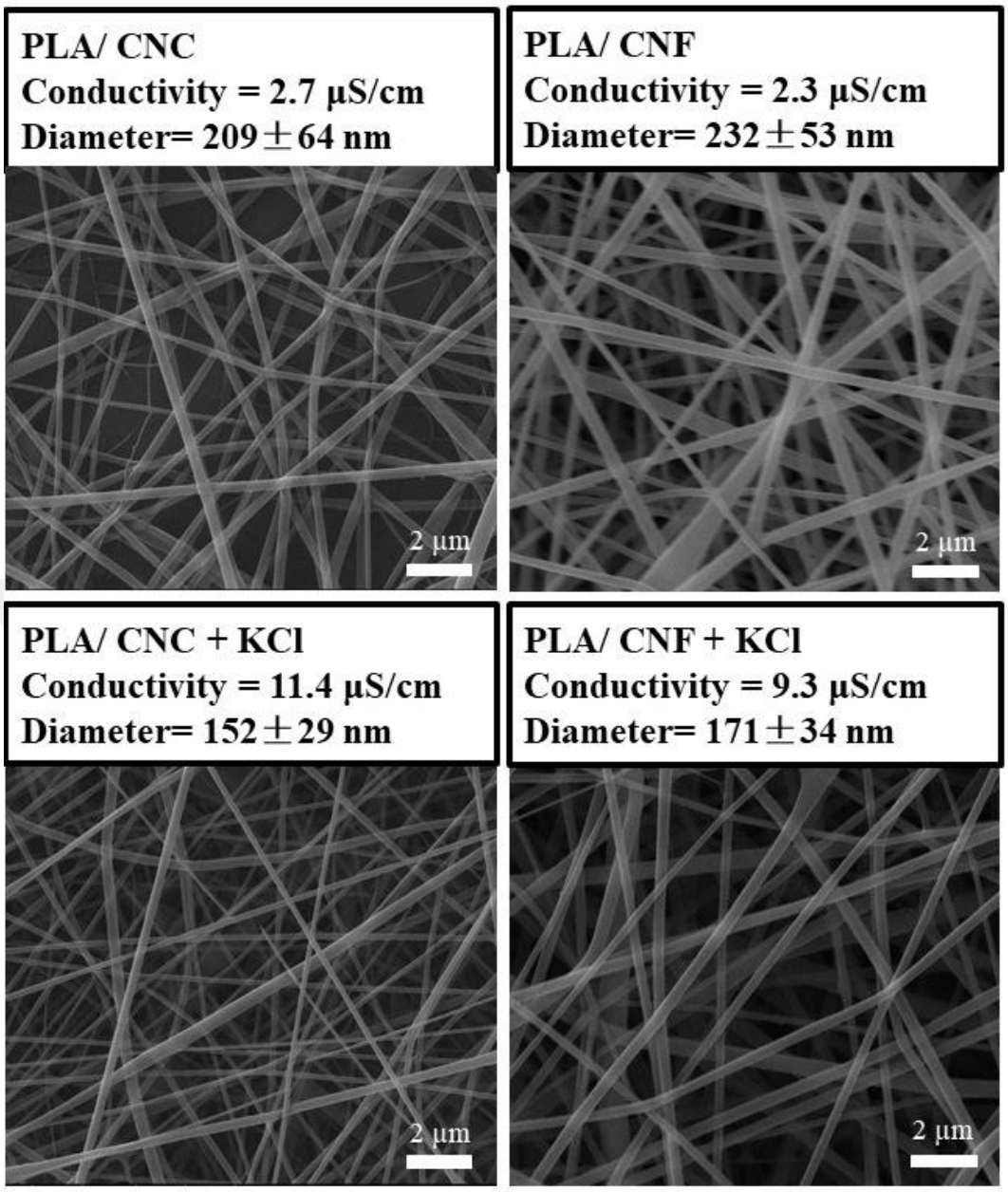

Figure 4.11 SEM images showing effects of CNC use and KCl salt addition on the diameter of electrospun fibers

Thus, by using again the same processing parameters discussed before, electrospinning experiments for both PLA/CNC and PLA/CNF solutions were repeated this time by adding 3 wt% KCl salt into their solutions. It could be observed in Figure 4.11 that when KCl salt was added to PLA/CNC solution, its conductivity increased from 2.7 to 11.4 μS/cm leading to the finest average diameter of 152 nm. Similarly, conductivity of PLA/CNF solution was increased from 2.3 to 9.3 μS/cm again resulting in finer average diameter of 171 nm.

4.11 Effects of Electrospun Fiber Diameters on the *In Vitro* Degradation Rate

It is known that biopolymer based electrospun fibers in mat or other forms have significant biomedical applications such as wound dressing; in which a controllable biodegradation rate would be required. Although *in vitro* degradation behavior of various neat and filled PLA based electrospun fiber mats was investigated [173-177], no study for PLA/CNF and only one study for PLA/CNC [169] was reported.

Therefore, according to the procedures explained in experimental work section, *in vitro* degradation rate of the electrospun fiber mats was investigated by immersing them in PBS simulated body fluid for 12 weeks. Apart from electrospun fiber mats of PLA/CNF, PLA/CNC, PLA/CNF + KCl and PLA/CNC + KCl; neat PLA samples were also produced and investigated for comparative reasons. Degradation degree in the mats was determined by measuring their "% weight loss" values after each week of PBS immersion. Figure 4.12 indicated that increasing the immersion period increased the degradation amount of all electrospun fiber mats.

It is known that [173-175], the main degradation mechanism of PLA based materials in PBS solution was "hydrolysis" leading to cleavage of the ester backbone of PLA chains into carboxylate and hydroxyl groups. Although PLA is hydrophobic biopolymer, cellulose nanostructures are hydrophilic; thus, immersion in PBS solution would increase *in vitro* degradation rate.

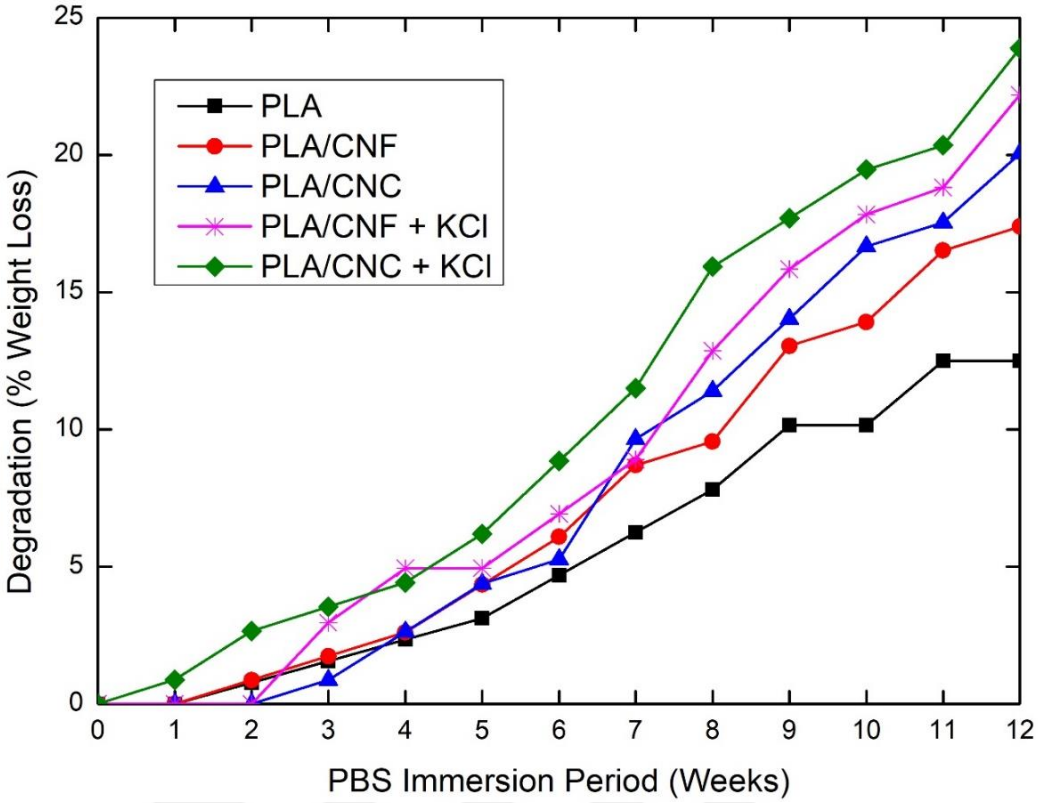

Figure 4.12 Increase of degradation degrees with increasing PBS immersion period for all electrospun fiber mats

Of course, hydrolytic degradation rate of electrospun fibers would be influenced by the total surface area exposed to PBS solution. Since decreasing the electrospun fiber diameter would increase total surface area exposed, then a higher degree of degradation would be expected. In order to observe that behavior, Table 4.1 was constructed to tabulate and compare effects of fiber diameter on the monthly *in vitro* degradation (in terms of % weight loss) of neat and all CNF and CNC filled PLA mats.

Table 4.1 revealed that decreasing the electrospun fiber diameter increased the *in vitro* degradation rate of their mats. For instance, after three months, neat PLA mat having largest average fiber diameter of 345 nm resulted in lowest degradation amount of 12.5 % weight loss; on the other hand, PLA/CNC + KCl mat having lowest average fiber damage of 152 nm resulted in highest degradation degree with 23.9 % weight loss.

Table 4.1 Effects of average fiber diameters on the *in vitro* degradation degree of all electrospun fiber mats after each month.

Electrospun Fiber Mats	**Average Electrospun Fiber Diameter (nm)**	***In Vitro* Degradation Degree (% Weight Loss)**		
		1st Month	2nd Month	3rd Month
PLA	345 ± 69	2.34	7.81	12.50
PLA/CNF	232 ± 53	2.61	9.56	17.39
PLA/CNC	209 ± 64	2.63	11.40	20.05
PLA/CNF + KCl	171 ± 34	4.95	12.87	22.18
PLA/CNC + KCl	152 ± 29	4.43	15.93	23.89

CHAPTER 5

CONCLUSIONS AND FUTURE RECOMMENDATIONS

Since there were three main parts in this dissertation, main conclusions obtained from these parts were as follows;

5.1 Use of Acid Hydrolysis to Obtain Cellulose Nanocrystals for Reinforcing Polylactide Biocomposites

- SEM analysis indicated that diameter range of round shaped CNC particles obtained was 15-55 nm; while DLS analysis revealed that their average size was 38 nm, having average Zeta potential value of -30.4 mV.

- Higher degree of hydroxyl groups and presence of sulfate half-ester groups on the surfaces of CNC particles observed by FTIR analysis might play a significant role in terms of interfacial interactions between the polymer matrix when used as reinforcement phase.

- XRD analyses showed that obtained CNC particles have monoclinic *Cellulose-I* crystal structure with *Crystallinity Index* of 80.6% and *Crystallite Size* of 3.39 nm. According to TG analyses, their maximum thermal degradation temperature was 307ºC with 23 wt% residue at 800ºC.

- Mechanical tests revealed that when only 1 wt% CNC particles were incorporated into PLA matrix, increases in flexural strength and modulus were 29% and 51%, respectively, while increases in fracture toughness values were as much as 105%.

- According to the observations under SEM analysis, there was certain degree of agglomeration of CNC particles when incorporated as 2 wt% and 3 wt%, leading to decline in all mechanical properties; because of their lower efficiency in strengthening and toughening mechanisms.

- Since CNC particles had lower thermal degradation temperatures compared to PLA matrix, TG analysis resulted in no improvements in the thermal behaviors of biocomposites.

5.2 Use of Cellulose Nanofibrils for Strengthening and Toughening of Neat and Blended Polylactide Biocomposites

- Fracture surface morphology analyses revealed that use of 1 wt% CNF and 10 phr b-TPE, separately or together, resulted in rather uniformly distributed reinforcements and round elastomer domains in PLA matrix.

- Thermal analyses indicated that use of 1 wt% CNF played no significant role in the thermal behaviors; while 10 phr b-TPE resulted in four times increase in crystallinity amount of PLA matrix by acting as heterogeneous nucleation of crystallites.

- Three-point bending tests revealed that due to the stronger cellulose structure and extremely high surface area/volume ratio of their nano-size, use of only 1 wt% CNF was very efficient in strengthening mechanisms of “decreased molecular mobility” of polymer matrix and “load transfer” mechanism from the matrix to the reinforcement; leading to 33% increase in flexural strength.

- On the other hand, due to the soft segments present in the block copolymer structure of thermoplastic elastomers, acting as plasticizers, blending with 10 phr b-TPE resulted in 25% decrease in flexural strength. However, when 1 wt%

CNF was incorporated into the PLA/b-TPE bioblend, reduction in flexural strength was recovered significantly, being higher than the value of neat PLA.

- Fracture toughness tests indicated that due to the certain efficiency of 1 wt% CNF on the "crack pinning" or "crack deflection" toughening mechanisms, the increase in G_{IC} fracture toughness was 45%.

- When PLA was blended with 10 phr b-TPE, "rubber toughening" phenomenon led to very efficient toughening mechanisms of "shear yielding" and "cavity formation" around rubber domains; G_{IC} fracture toughness value was increased as much as 104%. Moreover, when CNF and b-TPE were incorporated together, due to a kind of toughening synergism, G_{IC} fracture toughness increased by 114%.

- Mechanical tests of all specimens shaped by 3D-printing revealed that, compared to the values obtained from compression molded specimens; flexural strength values were approximately 20% lower, while G_{IC} fracture toughness values were approximately 20% higher. Differences in the values were due to the "textured" structure of 3D-printed specimens formed by the ± 45° raster angle orientation used during layer-by-layer production.

- It could be stated that lower strength values of 3D-printed specimens could be due to the detrimental effect of textured structure leading to certain differences in the degree of orientation and distribution of CNF reinforcements and b-TPE domains in the PLA matrix. On the other hand, higher fracture toughness values could be due to additional crack deflection action of ±45° textures in terms of decreased crack propagation rate.

5.3 Use of Cellulose Nanofibrils and Nanocrystals in Electrospinning of Polylactide Nanofibers

- It was observed that when “Solution Concentration” of PLA/CNF was 8 %w/v (viscosity 124 cP); due to proper “Taylor Cone” and stable “Solution Jet” formation, it was possible to obtain “fibrous” morphology rather than occurrence of droplets.

- In order to obtain almost “bead-free” morphology and “finest” average diameter (232 nm) for these PLA/CNF electrospun fibers, several trials indicated that the best processing parameter combination for “Solution Rate” and “Collector Distance” was 1.5 mL/h and 15 cm, respectively. Increasing values of these two parameters resulted in bead formation and thicker diameters.

- When polymer solution was filled with 3 wt% CNF rather than 1 wt%, average diameter of electrospun fibers decreased significantly from 232 nm down to 175 nm. It was basically due to the higher amount of hydroxyl groups present in the cellulose structure resulting in increased charge density of the polymer solution.

- When polymer solution was filled with 1 wt% CNC particles rather than 1 wt% CNF, average diameter of electrospun fibers decreased this time from 232 nm down to 209 nm. Because, additional sulfate ester groups present on CNC surfaces resulted in higher charge density and electrical conductivity of PLA/CNC solution (2.7 μS/cm) compared to conductivity of PLA/CNF solution (2.3 μS/cm).

- When 3 wt% KCl salt was added into PLA/CNC and PLA/CNF solutions; then due to the additional increased electrical conductivities, their average electrospun fiber diameters further decreased down to 152 nm and 171 nm, respectively.

- Moreover, *in vitro* degradation analysis of all electrospun fiber mats by immersing in a simulated body fluid revealed that increasing the immersion period increased their degradation rate in terms of "% weight loss". Since decreasing the electrospun fiber diameter would increase their total surface area exposed, it was also observed that mats with fine diameter fibers had higher degradation rate.

5.4 Future Recommendations

In this dissertation, polylactide based biocomposites by reinforcing two different cellulose structures (CNC and CNF) were investigated from three different aspects. It was basically observed that these biocomposites with improved mechanical properties either in the bulk form or nanofiber form could be used for various purposes. However, to obtain higher performance biocomposites by using these nanocellulose structures in a more efficient way, a number of difficulties should be surmounted.

Since higher performance and repeatability of these nanocellulose particles or fibrils mainly depend on the starting cellulose source and the production method; future works might investigate usability of new and alternative cellulose sources leading to more efficient and economical nanocellulose structures. Of course, new production methods and optimization studies could provide large-scale supply required for the mass production of biocomposites.

Surface functionalization is another challenging issue in nanocellulose studies, due to rather weak interactions between nanocellulose and many biopolymer matrices. To improve compatibility, certain interfacial studies could be conducted, such as use of "green" coupling agents.

Although there has been significant progress in the use of additive manufacturing techniques as the practical shaping method of many biomedical parts, there are still many parameters to be investigated for the PLA /nanocellulose filaments. Moreover,

4D-printing techniques have been considered as a new technology to obtain many other desired properties for the functional components. Thus, apart from 3D-printing studies, 4D-printing studies could be also conducted for the PLA /nanocellulose structures.

To produce “fully green composites”, it is necessary to determine the life cycle and environmental impact assessment concerning green chemistry. From extraction of nanocellulose to end-of-life disposal, it is necessary to apply a more holistic perspicacity.

To achieve wider commercial use of electrospun nanofiber forms, improvements in the conventional electrospinning equipment would be necessary, for instance use of new technology “needleless” and/or “rotary spinneret” electrospinning approaches. Thus, it could be another future perspective to try these systems for the PLA /nanocellulose structures.

Since PLA /nanocellulose biocomposites are considered as one of the most efficient materials for many biomedical applications, it would be a necessity to conduct extensive research on their toxicity, biocompatibility, in vivo biodegradation, and other clinical studies.

REFERENCES

[1] Ji, Q.; Zhou, C.; Li, Z.; Boateng, I. D.; Liu, X. Is Nanocellulose a Good Substitute for Non-Renewable Raw Materials? A Comprehensive Review of the State of the Art, Preparations, and Industrial Applications. Industrial Crops and Products 2023, 202, 117093. https://doi.org/10.1016/j.indcrop.2023.117093.

[2] Noremylia, M. B.; Hassan, M. Z.; Ismail, Z. Recent Advancement in Isolation, Processing, Characterization and Applications of Emerging Nanocellulose: A Review. International Journal of Biological Macromolecules 2022, 206, 954–976. https://doi.org/10.1016/j.ijbiomac.2022.03.064.

[3] Randhawa, A.; Dutta, S. D.; Ganguly, K.; Patil, T. V.; Patel, D. K.; Lim, K.-T. A Review of Properties of Nanocellulose, Its Synthesis, and Potential in Biomedical Applications. Applied Sciences 2022, 12 (14), 7090. https://doi.org/10.3390/app12147090.

[4] Chagas, J. S.; Almeida, J. N. S.; Pereira, A. C. L.; Silva, N. F. I.; Raimundo, R. A.; Medeiros, E. S.; Lima, B. A. S. G.; Galvão, L. S.; Santos, A. S. F.; Silva, F. I. Evaluation of the Kinetics of Low Intensity Ultrasound-Assisted Sulfuric Acid Hydrolysis to Obtain Cellulose Nanocrystals (CNCs) from Microcrystalline Cellulose (MCC). Cellulose 2023, 30 (18), 11455–11472. https://doi.org/10.1007/s10570-023-05580-3.

[5] Nechyporchuk, O.; Belgacem, M. N.; Bras, J. Production of Cellulose Nanofibrils: A Review of Recent Advances. Industrial Crops and Products 2016, 93, 2–25. https://doi.org/10.1016/j.indcrop.2016.02.016.

[6] Römling, U.; Galperin, M. Y. Bacterial Cellulose Biosynthesis: Diversity of Operons, Subunits, Products, and Functions. Trends in Microbiology 2015, 23 (9), 545–557. https://doi.org/10.1016/j.tim.2015.05.005.

[7] Petersen, N.; Gatenholm, P. Bacterial Cellulose-Based Materials and Medical Devices: Current State and Perspectives. Applied Microbiology and Biotechnology 2011, 91 (5), 1277–1286. https://doi.org/10.1007/s00253-011-3432-y.

[8] Kupnik, K.; Primožič, M.; Kokol, V.; Leitgeb, M. Nanocellulose in Drug Delivery and Antimicrobially Active Materials. Polymers 2020, 12 (12), 2825. https://doi.org/10.3390/polym12122825.

[9] Nicu, R.; Ciolacu, F.; Ciolacu, D. E. Advanced Functional Materials Based on Nanocellulose for Pharmaceutical/Medical Applications. Pharmaceutics 2021, 13 (8), 1125. https://doi.org/10.3390/pharmaceutics13081125.

[10] Chen, C.; Xi, Y.; Weng, Y. Recent Advances in Cellulose-Based Hydrogels for Tissue Engineering Applications. Polymers 2022, 14 (16), 3335. https://doi.org/10.3390/polym14163335.

[11] Ramezani, G.; Stiharu, I.; Van De Ven, T. G. M.; Nerguizian, V. Advancement in Biosensor Technologies of 2D MaterialIntegrated with Cellulose—Physical Properties. Micromachines 2023, 15 (1), 82. https://doi.org/10.3390/mi15010082.

[12] Liu, W.; Pang, B.; Zhang, M.; Lv, J.; Xu, T.; Bai, L.; Cai, X.; Yao, S.; Huan, S.; Si, C. Pickering Multiphase Materials Using Plant-based Cellulosic Micro/Nanoparticles. Aggregate 2024, e486. https://doi.org/10.1002/agt2.486.

[13] Choudhary, N.; Singh, S.; Bhardwaj, S.; Gupta, S.; Nandi, U.; Chandra, R.; Maji, P. K. Recent Advancements in Nanocellulose-Based Supercapacitors for Energy Storage Devices: A Review. Carbohydrate Polymer Technologies and Applications 2024, 7, 100416. https://doi.org/10.1016/j.carpta.2023.100416.

[14] Hoeng, F.; Denneulin, A.; Bras, J. Use of Nanocellulose in Printed Electronics:

A Review. Nanoscale 2016, 8 (27), 13131–13154. https://doi.org/10.1039/C6NR03054H.

[15] Roszowska-Jarosz, M.; Masiewicz, J.; Kostrzewa, M.; Kucharczyk, W.; Żurowski, W.; Kucińska-Lipka, J.; Przybyłek, P. Mechanical Properties of Bio-Composites Based on Epoxy Resin and Nanocellulose Fibres. Materials 2021, 14 (13), 3576. https://doi.org/10.3390/ma14133576.

[16] Noguchi, T.; Niihara, K.; Iwamoto, R.; Matsuda, G.; Endo, M.; Isogai, A. Nanocellulose/Polyethylene Nanocomposite Sheets Prepared from an Oven-Dried Nanocellulose by Elastic Kneading. Composites Science and Technology 2021, 207, 108734. https://doi.org/10.1016/j.compscitech.2021.108734.

[17] Zielińska, D.; Siwińska-Ciesielczyk, K.; Bula, K.; Peplińska, B.; Jesionowski, T.; Borysiak, S. Advanced Nanocellulose Hybrid Fillers for Sustainable Polypropylene Biomaterials with Enhanced Oxygen Barrier Properties. Applied Materials Today 2023, 34, 101897. https://doi.org/10.1016/j.apmt.2023.101897.

[18] Neves, R. M.; Ornaghi, H. L.; Ornaghi, F. G.; Amico, S. C.; Zattera, A. J. Degradation Kinetics and Lifetime Prediction for Polystyrene/Nanocellulose Nanocomposites. Journal of Thermal Analysis and Calorimetry 2022, 147 (1), 879–890. https://doi.org/10.1007/s10973-020-10316-7.

[19] Ribeiro, R. S. A.; Pohlmann, B. C.; Calado, V.; Bojorge, N.; Pereira, N. Production of Nanocellulose by Enzymatic Hydrolysis: Trends and Challenges. Engineering in Life Sciences 2019, 19 (4), 279–291. https://doi.org/10.1002/elsc.201800158.

[20] Bikiaris, N. D.; Koumentakou, I.; Samiotaki, C.; Meimaroglou, D.; Varytimidou, D.; Karatza, A.; Kalantzis, Z.; Roussou, M.; Bikiaris, R. D.; Papageorgiou, G. Z. Recent Advances in the Investigation of Poly(Lactic Acid) (PLA) Nanocomposites: Incorporation of Various Nanofillers and Their Properties and

Applications. Polymers 2023, 15 (5), 1196. https://doi.org/10.3390/polym15051196.

[21] Farahani, R. D.; Dubé, M.; Therriault, D. Three-Dimensional Printing of Multifunctional Nanocomposites: Manufacturing Techniques and Applications. Advanced Materials 2016, 28 (28), 5794–5821. https://doi.org/10.1002/adma.201506215.

[22] Venmathi Maran, B. A.; Jeyachandran, S.; Kimura, M. A Review on the Electrospinning of Polymer Nanofibers and Its Biomedical Applications. Journal of Composites Science 2024, 8 (1), 32. https://doi.org/10.3390/jcs8010032.

[23] Do, T. V. V.; Tran, N. B. A.; Nguyen-Thai, N. U. Preparation of Spherical Nanocellulose from Gai Bamboo and Mechanical Properties of Chitosan/Nanocellulose Composite. Polymer Composites 2023, 44 (4), 2287–2295. https://doi.org/10.1002/pc.27243.

[24] Seoane, I. T.; Cerrutti, P.; Vazquez, A.; Cyras, V. P.; Manfredi, L. B. Ternary Nanocomposites Based on Plasticized Poly(3-Hydroxybutyrate) and Nanocellulose. Polymer Bulletin 2019, 76 (2), 967–988. https://doi.org/10.1007/s00289-018-2421-z.

[25] A G Soares Da Silva, F.; Matos, M.; Dourado, F.; A M Reis, M.; C Branco, P.; Poças, F.; Gama, M. Development of a Layered Bacterial nanocellulose-PHBV Composite for Food Packaging. Journal of the Science of Food and Agriculture 2023, 103 (3), 1077–1087. https://doi.org/10.1002/jsfa.11839.

[26] Nabels-Sneiders, M.; Barkane, A.; Platnieks, O.; Orlova, L.; Gaidukovs, S. Biodegradable Poly(Butylene Succinate) Laminate with Nanocellulose Interphase Layer for High-Barrier Packaging Film Application. Foods 2023, 12 (22), 4136. https://doi.org/10.3390/foods12224136.

[27] Koeipudsa, N.; Phinyocheep, P. Cellulose Nanocrystals from Oil Palm Trunk Biomass as a Bio-reinforcing Filler for Improved Mechanical Properties of Modified Natural Rubber Composites. Polymer Composites 2024, pc.28078. https://doi.org/10.1002/pc.28078.

[28] Vatansever, E.; Arslan, D.; Nofar, M. Polylactide Cellulose-Based Nanocomposites. International Journal of Biological Macromolecules 2019, 137, 912–938. https://doi.org/10.1016/j.ijbiomac.2019.06.205.

[29] Ilyas, R. A.; Sapuan, S. M.; Harussani, M. M.; Hakimi, M. Y. A. Y.; Haziq, M. Z. M.; Atikah, M. S. N.; Asyraf, M. R. M.; Ishak, M. R.; Razman, M. R.; Nurazzi, N. M.; Norrrahim, M. N. F.; Abral, H.; Asrofi, M. Polylactic Acid (PLA) Biocomposite: Processing, Additive Manufacturing and Advanced Applications. Polymers 2021, 13 (8), 1326. https://doi.org/10.3390/polym13081326.

[30] Pirani, S.; Abushammala, H. M. N.; Hashaikeh, R. Preparation and Characterization of Electrospun PLA/Nanocrystalline Cellulose-based Composites. Journal of Applied Polymer Science 2013, 130 (5), 3345–3354. https://doi.org/10.1002/app.39576.

[31] Wu, H.; Liu, X.; Hua, X.; Zhang, J. Thermal-Oxidation Degradation of Polylactic Acid/Cellulose Nanocrystal Composites: Effects of Surface Chemistry. Industrial Crops and Products 2023, 202, 117008. https://doi.org/10.1016/j.indcrop.2023.117008.

[32] Tan, K.; Heo, S.; Foo, M.; Chew, I. M.; Yoo, C. An Insight into Nanocellulose as Soft Condensed Matter: Challenge and Future Prospective toward Environmental Sustainability. Science of The Total Environment 2019, 650, 1309–1326. https://doi.org/10.1016/j.scitotenv.2018.08.402.

[33] Salimi, S.; Sotudeh-Gharebagh, R.; Zarghami, R.; Chan, S. Y.; Yuen, K. H. Production of Nanocellulose and Its Applications in Drug Delivery: A Critical

Review. ACS Sustainable Chem. Eng. 2019, 7 (19), 15800–15827. https://doi.org/10.1021/acssuschemeng.9b02744.

[34] Yu, H.; Qin, Z.; Liang, B.; Liu, N.; Zhou, Z.; Chen, L. Facile Extraction of Thermally Stable Cellulose Nanocrystals with a High Yield of 93% through Hydrochloric Acid Hydrolysis under Hydrothermal Conditions. Journal of Materials Chemistry A 2013, 1 (12), 3938. https://doi.org/10.1039/c3ta01150j.

[35] Vanderfleet, O. M.; Osorio, D. A.; Cranston, E. D. Optimization of Cellulose Nanocrystal Length and Surface Charge Density through Phosphoric Acid Hydrolysis. Philosophical Transactions of the Royal Society A. 2018, 376 (2112), 20170041. https://doi.org/10.1098/rsta.2017.0041.

[36] Sadeghifar, H.; Filpponen, I.; Clarke, S. P.; Brougham, D. F.; Argyropoulos, D. S. Production of Cellulose Nanocrystals Using Hydrobromic Acid and Click Reactions on Their Surface. Journal of Materials Science 2011, 46 (22), 7344–7355. https://doi.org/10.1007/s10853-011-5696-0.

[37] Seta, F. T.; An, X.; Liu, L.; Zhang, H.; Yang, J.; Zhang, W.; Nie, S.; Yao, S.; Cao, H.; Xu, Q.; Bu, Y.; Liu, H. Preparation and Characterization of High Yield Cellulose Nanocrystals (CNC) Derived from Ball Mill Pretreatment and Maleic Acid Hydrolysis. Carbohydrate Polymers 2020, 234, 115942. https://doi.org/10.1016/j.carbpol.2020.115942.

[38] Sun, B.; Zhang, M.; Hou, Q.; Liu, R.; Wu, T.; Si, C. Further Characterization of Cellulose Nanocrystal (CNC) Preparation from Sulfuric Acid Hydrolysis of Cotton Fibers. Cellulose 2016, 23 (1), 439–450. https://doi.org/10.1007/s10570-015-0803-z.

[39] Brito, B. S. L.; Pereira, F. V.; Putaux, J.-L.; Jean, B. Preparation, Morphology and Structure of Cellulose Nanocrystals from Bamboo Fibers. Cellulose 2012, 19 (5), 1527–1536. https://doi.org/10.1007/s10570-012-9738-9.

[40] Khoo, R. Z.; Chow, W. S.; Ismail, H. Tensile, Thermal and Ultra-Violet Shielding Enhancement of Poly(Lactic Acid) Bionanocomposite Film Using Cellulose Nanocrystals Extracted from Sugarcane Bagasse. Journal of Thermoplastic Composite Materials 2023, 36 (6), 2543–2561. https://doi.org/10.1177/08927057221098972.

[41] Rana, Md. S.; Rahim, Md. A.; Mosharraf, Md. P.; Tipu, Md. F. K.; Chowdhury, J. A.; Haque, M. R.; Kabir, S.; Amran, Md. S.; Chowdhury, A. A. Morphological, Spectroscopic and Thermal Analysis of Cellulose Nanocrystals Extracted from Waste Jute Fiber by Acid Hydrolysis. Polymers 2023, 15 (6), 1530. https://doi.org/10.3390/polym15061530.

[42] Kassab, Z.; Abdellaoui, Y.; Salim, M. H.; Bouhfid, R.; Qaiss, A. E. K.; El Achaby, M. Micro- and Nano-Celluloses Derived from Hemp Stalks and Their Effect as Polymer Reinforcing Materials. Carbohydrate Polymers 2020, 245, 116506. https://doi.org/10.1016/j.carbpol.2020.116506.

[43] Kargarzadeh, H.; Ahmad, I.; Abdullah, I.; Dufresne, A.; Zainudin, S. Y.; Sheltami, R. M. Effects of Hydrolysis Conditions on the Morphology, Crystallinity, and Thermal Stability of Cellulose Nanocrystals Extracted from Kenaf Bast Fibers. Cellulose 2012, 19 (3), 855–866. https://doi.org/10.1007/s10570-012-9684-6.

[44] Dunlop, M. J.; Clemons, C.; Reiner, R.; Sabo, R.; Agarwal, U. P.; Bissessur, R.; Sojoudiasli, H.; Carreau, P. J.; Acharya, B. Towards the Scalable Isolation of Cellulose Nanocrystals from Tunicates. Scientific Reports 2020, 10 (1), 19090. https://doi.org/10.1038/s41598-020-76144-9.

[45] Lee, B.-M.; Kim, D.-Y.; Jeun, J.-P.; Kang, P.-H.; Hong, S.-K. A Facile Isolation Method of Cellulose Nanocrystals from Microcrystalline Cellulose. Journal of Materials Chemistry A 2013, 1, 3938

https://doi.org/10.1016/j.indcrop.2023.117867

[46] Chagas, J. S.; Almeida, J. N. S.; Pereira, A. C. L.; Silva, N. F. I.; Raimundo, R. A.; Medeiros, E. S.; Lima, B. A. S. G.; Galvão, L. S.; Santos, A. S. F.; Silva, F. I. Evaluation of the Kinetics of Low Intensity Ultrasound-Assisted Sulfuric Acid Hydrolysis to Obtain Cellulose Nanocrystals (CNCs) from Microcrystalline Cellulose (MCC). Cellulose 2023, 30 (18), 11455–11472. https://doi.org/10.1007/s10570-023-05580-3.

[47] Yi, X.; Liu, C.; Liu, X.; Wang, P.; Zhou, Z.; Liu, D. Magnetic Partially Carbonized Cellulose Nanocrystal-Based Magnetic Solid Phase Extraction for the Analysis of Triazine and Triazole Pesticides in Water. Microchimica Acta 2019, 186 (12), 825. https://doi.org/10.1007/s00604-019-3911-x.

[48] Leszczyńska, A.; Radzik, P.; Haraźna, K.; Pielichowski, K. Thermal Stability of Cellulose Nanocrystals Prepared by Succinic Anhydride Assisted Hydrolysis. Thermochimica Acta 2018, 663, 145–156. https://doi.org/10.1016/j.tca.2018.03.015.

[49] Seoane, I.; Manfredi, L.; Cyras, V.; Torre, L.; Fortunati, E.; Puglia, D. Effect of Cellulose Nanocrystals and Bacterial Cellulose on Disintegrability in Composting Conditions of Plasticized PHB Nanocomposites. Polymers 2017, 9 (11), 561. https://doi.org/10.3390/polym9110561.

[50] Wang, C.; Lu, L.; Liu, Z.; Lai, Y.; Li, J.; Xia, Z.; Cao, J.; Wang, X.; Lu, J.; Yang, W. Green Carbon Dots Illuminate Biogenic Nanohybrids toward Soft, Piezo/Photoactive, and Physically Transient Nanogenerators. ACS Sustainable Chemistry & Engineering. 2023, 11 (40), 14646–14658. https://doi.org/10.1021/acssuschemeng.3c00957.

[51] Kim, H. J.; Choi, Y. H.; Jeong, J. H.; Kim, H.; Yang, H. S.; Hwang, S. Y.; Koo, J. M.; Eom, Y. Rheological Percolation of Cellulose Nanocrystals in

Biodegradable Poly(Butylene Succinate) Nanocomposites: A Novel Approach for Tailoring the Mechanical and Hydrolytic Properties. Macromolecular Research 2021, 29 (10), 720–726. https://doi.org/10.1007/s13233-021-9080-x.

[52] Li, Y.-D.; Fu, Q.-Q.; Wang, M.; Zeng, J.-B. Morphology, Crystallization and Rheological Behavior in Poly(Butylene Succinate)/Cellulose Nanocrystal Nanocomposites Fabricated by Solution Coagulation. Carbohydrate Polymers 2017, 164, 75–82. https://doi.org/10.1016/j.carbpol.2017.01.089.

[53] Mi, H.-Y.; Jing, X.; Peng, J.; Salick, M. R.; Peng, X.-F.; Turng, L.-S. Poly(ε-Caprolactone) (PCL)/Cellulose Nano-Crystal (CNC) Nanocomposites and Foams. Cellulose 2014, 21 (4), 2727–2741. https://doi.org/10.1007/s10570-014-0327-y.

[54] Laghaei, R.; Fashandi, H.; Hejazi, S. M. Tailoring Surface Energy of Cellulose Nanocrystals (CNCs) via Low-Pressure Plasma Polymerization to Control the Interfacial Properties in Polycaprolactone (PCL)/CNC Nanocomposite. Cellulose 2024. https://doi.org/10.1007/s10570-023-05699-3

[55] Karkhanis, S. S.; Stark, N. M.; Sabo, R. C.; Matuana, L. M. Performance of Poly(Lactic Acid)/ Cellulose Nanocrystal Composite Blown Films Processed by Two Different Compounding Approaches. Polymer Engineering & Science 2018, 58 (11), 1965–1974. https://doi.org/10.1002/pen.24806.

[56] Kamal, M. R.; Khoshkava, V. Effect of Cellulose Nanocrystals (CNC) on Rheological and Mechanical Properties and Crystallization Behavior of PLA/CNC Nanocomposites. Carbohydrate Polymers 2015, 123, 105–114. https://doi.org/10.1016/j.carbpol.2015.01.012

[57] Oguz, O.; Candau, N.; Demongeot, A.; Citak, M. K.; Cetin, F. N.; Stoclet, G.; Michaud, V.; Menceloglu, Y. Z. Poly(Lactide)/Cellulose Nanocrystal Nanocomposites by High-shear Mixing. Polymer Engineering & Science 2021,

61 (4), 1028–1040. https://doi.org/10.1002/pen.25621.

[58] Kang, H.; Kim, D. S. A Study on the Crystallization and Melting of PLA Nanocomposites with Cellulose Nanocrystals by DSC. Polymer Composites 2023, 44 (11), 7727–7736. https://doi.org/10.1002/pc.27658.

[59] Sullivan, E.; Moon, R.; Kalaitzidou, K. Processing and Characterization of Cellulose Nanocrystals/Polylactic Acid Nanocomposite Films. Materials 2015, 8 (12), 8106–8116. https://doi.org/10.3390/ma8125447.

[60] Spinella, S.; Lo Re, G.; Liu, B.; Dorgan, J.; Habibi, Y.; Leclère, P.; Raquez, J.-M.; Dubois, P.; Gross, R. A. Polylactide/Cellulose Nanocrystal Nanocomposites: Efficient Routes for Nanofiber Modification and Effects of Nanofiber Chemistry on PLA Reinforcement. Polymer 2015, 65, 9–17. https://doi.org/10.1016/j.polymer.2015.02.048.

[61] Arslan, D.; Vatansever, E.; Sarul, D. S.; Kahraman, Y.; Gunes, G.; Durmus, A.; Nofar, M. Effect of Preparation Method on the Properties of Polylactide/Cellulose Nanocrystal Nanocomposites. Polymer Composites 2020, 41 (10), 4170–4180. https://doi.org/10.1002/pc.25701.

[62] Monika; Dhar, P.; Katiyar, V. Thermal Degradation Kinetics of Polylactic Acid/Acid Fabricated Cellulose Nanocrystal Based Bionanocomposites. International Journal of Biological Macromolecules 2017, 104, 827–836. https://doi.org/10.1016/j.ijbiomac.2017.06.039.

[63] Sung, S. H.; Chang, Y.; Han, J. Development of Polylactic Acid Nanocomposite Films Reinforced with Cellulose Nanocrystals Derived from Coffee Silverskin. Carbohydrate Polymers 2017, 169, 495–503. https://doi.org/10.1016/j.carbpol.2017.04.037.

[64] Lizundia, E.; Fortunati, E.; Dominici, F.; Vilas, J. L.; León, L. M.; Armentano,

I.; Torre, L.; Kenny, J. M. PLLA-Grafted Cellulose Nanocrystals: Role of the CNC Content and Grafting on the PLA Bionanocomposite Film Properties. Carbohydrate Polymers 2016, 142, 105–113. https://doi.org/10.1016/j.carbpol.2016.01.041.

[65] Cranston, E. D.; Gray, D. G. Morphological and Optical Characterization of Polyelectrolyte Multilayers Incorporating Nanocrystalline Cellulose. Biomacromolecules 2006, 7 (9), 2522–2530. https://doi.org/10.1021/bm0602886.

[66] Wang, N.; Ding, E.; Cheng, R. Thermal Degradation Behaviors of Spherical Cellulose Nanocrystals with Sulfate Groups. Polymer 2007, 48 (12), 3486–3493. https://doi.org/10.1016/j.polymer.2007.03.062.

[67] Xiong, R.; Zhang, X.; Tian, D.; Zhou, Z.; Lu, C. Comparing Microcrystalline with Spherical Nanocrystalline Cellulose from Waste Cotton Fabrics. Cellulose 2012, 19 (4), 1189–1198. https://doi.org/10.1007/s10570-012-9730-4.

[68] Doan, T. K. Q.; Chiang, K. Y. Characteristics and Kinetics Study of Spherical Cellulose Nanocrystal Extracted from Cotton Cloth Waste by Acid Hydrolysis. Sustainable Environment Research 2022, 32 (1), 26. https://doi.org/10.1186/s42834-022-00136-9.

[69] Naduparambath, S.; T.V., J.; V., S.; M.P., S.; Balan, A. K.; E., P. Isolation and Characterisation of Cellulose Nanocrystals from Sago Seed Shells. Carbohydrate Polymers 2018, 180, 13–20. https://doi.org/10.1016/j.carbpol.2017.09.088.

[70] Astruc, J.; Nagalakshmaiah, M.; Laroche, G.; Grandbois, M.; Elkoun, S.; Robert, M. Isolation of Cellulose-II Nanospheres from Flax Stems and Their Physical and Morphological Properties. Carbohydrate Polymers 2017, 178, 352–359. https://doi.org/10.1016/j.carbpol.2017.08.138.

[71] Qi, W.; Yu, J.; Zhang, Z.; Xu, H.-N. Effect of pH on the Aggregation Behavior of Cellulose Nanocrystals in Aqueous Medium. Materials Research Express 2019, 6 (12), 125078. https://doi.org/10.1088/2053-1591/ab5974.

[72] Schwanninger, M.; Rodrigues, J. C.; Pereira, H.; Hinterstoisser, B. Effects of Short-Time Vibratory Ball Milling on the Shape of FT-IR Spectra of Wood and Cellulose. Vibrational Spectroscopy 2004, 36 (1), 23–40. https://doi.org/10.1016/j.vibspec.2004.02.003.

[73] Nascimento, N. R. D.; Pinheiro, I. F.; Alves, G. F.; Mei, L. H. I.; Macedo Neto, J. C. D.; Morales, A. R. Role of Cellulose Nanocrystals in Epoxy-Based Nanocomposites: Mechanical Properties, Morphology and Thermal Behavior. Polímeros 2021, 31 (3), e2021034. https://doi.org/10.1590/0104-1428.20210057.

[74] Bhiogade, A.; Kannan, M. Studies on Thermal and Degradation Kinetics of Cellulose Micro/Nanoparticle Filled Polylactic Acid (PLA) Based Nanocomposites. Polymers and Polymer Composites 2021, 29, 85–98. https://doi.org/10.1177/0967391120987170.

[75] Yudhanto, F.; Sosiati, H.; Yudha, V.; Syafri, E. A Preliminary Study of Isolation and Characterization of Nanocrystalline Cellulose from Microcrystalline Cellulose by Acid Hydrolysis Process. MSF 2022, 1057, 11–18. https://doi.org/10.4028/p-45x464.

[76] Aggarwal, R.; Garg, A. K.; Saini, D.; Sonkar, S. K.; Sonker, A. K.; Westman, G. Cellulose Nanocrystals Derived from Microcrystalline Cellulose for Selective Removal of Janus Green Azo Dye. Industrial & Engineering Chemistry Research 2023, 62 (1), 649–659. https://doi.org/10.1021/acs.iecr.2c03365.

[77] Zhao, G.; Zhang, S.; Zhai, S.; Pan, M. Fabrication and Characterization of Photonic Cellulose Nanocrystal Films with Structural Colors Covering Full Visible Light. Journal of Materials Science 2020, 55 (20), 8756–8767.

https://doi.org/10.1007/s10853-020-04616-4.

[78] Mamudu, U.; Hussin, M. R.; Santos, J. H.; Lim, R. C. Synthesis and Characterisation of Sulfated-Nanocrystalline Cellulose in Epoxy Coatings for Corrosion Protection of Mild Steel from Sodium Chloride Solution. Carbohydrate Polymer Technologies and Applications 2023, 5, 100306. https://doi.org/10.1016/j.carpta.2023.100306.

[79] Rosli, N. A.; Wan Ishak, W. H.; Darwis, S. S.; Ahmad, I.; Mohd Khairudin, M. F. A. Bio-Nanocomposites Based on Compatibilized Poly(Lactic Acid) Blend-Reinforced Agave Cellulose Nanocrystals. BioResources 2021, 16 (3), 5538–5555. https://doi.org/10.15376/biores.16.3.5538-5555.

[80] N'Gatta, K. M.; Belaid, H.; El Hayek, J.; Assanvo, E. F.; Kajdan, M.; Masquelez, N.; Boa, D.; Cavaillès, V.; Bechelany, M.; Salameh, C. 3D Printing of Cellulose Nanocrystals Based Composites to Build Robust Biomimetic Scaffolds for Bone Tissue Engineering. Scientific Reports 2022, 12 (1), 21244. https://doi.org/10.1038/s41598-022-25652-x.

[81] Dos Santos, F. A.; Iulianelli, G. C. V.; Tavares, M. I. B. Effect of Microcrystalline and Nanocrystals Cellulose Fillers in Materials Based on PLA Matrix. Polymer Testing 2017, 61, 280–288. https://doi.org/10.1016/j.polymertesting.2017.05.028.

[82] Najafi, N.; Heuzey, M. C.; Carreau, P. J. Polylactide (PLA)-Clay Nanocomposites Pre-pared by Melt Compounding in the Presence of a Chain Extender. Composites Science and Technology 2012, 72 (5), 608–615. https://doi.org/10.1016/j.compscitech.2012.01.005.

[83] Zhou, Y.; Lei, L.; Yang, B.; Li, J.; Ren, J. Preparation and Characterization of Polylactic Acid (PLA) Carbon Nanotube Nanocomposites. Polymer Testing 2018, 68, 34–38. https://doi.org/10.1016/j.polymertesting.2018.03.044.

[84] Vidakis, N.; Petousis, M.; Savvakis, K.; Maniadi, A.; Koudoumas, E. A Comprehensive Investigation of the Mechanical Behavior and the Dielectrics of Pure Polylactic Acid (PLA) and PLA with Graphene (GnP) in Fused Deposition Modeling (FDM). International Journal of Plastics Technology 2019, 23 (2), 195–206. https://doi.org/10.1007/s12588-019-09248-1.

[85] Wang, Q.; Ji, C.; Sun, J.; Zhu, Q.; Liu, J. Structure and Properties of Polylactic Acid Bio-composite Films Reinforced with Cellulose Nanofibrils. Molecules 2020, 25 (14), 3306. https://doi.org/10.3390/molecules25143306.

[86] Lafia-Araga, R. A.; Sabo, R.; Nabinejad, O.; Matuana, L.; Stark, N. Influence of Lactic Acid Surface Modification of Cellulose Nanofibrils on the Properties of Cellulose Nanofibril Films and Cellulose Nanofibril–Poly(Lactic Acid) Composites. Biomolecules 2021, 11 (9), 1346. https://doi.org/10.3390/biom11091346.

[87] Asada, C.; Seno, M.; Nakamura Y. Preparation of Biopolymer Composite Using Cedar-Derived Cellulose Nanofiber Waste and Biomass Valorization 2021 12:6245–6254 https://doi.org/10.1007/s12649-021-01436-8

[88] Le Gars, M.; Dhuiège, B.; Delvart, A.; Belgacem, M. N.; Missoum, K.; Bras, J. High-Barrier and Antioxidant Poly(Lactic Acid)/Nanocellulose Multilayered Materials for Packaging. ACS Omega 2020, 5 (36), 22816–22826. https://doi.org/10.1021/acsomega.0c01955.

[89] Gitari, B.; Chang, B. P.; Misra, M.; Navabi, A.; Mohanty, A. K. A Comparative Study on the Mechanical, Thermal, and Water Barrier Properties of PLA Nanocomposite Films Pre-pared with Bacterial Nanocellulose and Cellulose Nanofibrils. BioResources 2019, 14 (1), 1867–1889. https://doi.org/10.15376/biores.14.1.1867-1889.

[90] Ghasemi, S.; Behrooz, R.; Ghasemi, I.; Yassar, R. S.; Long, F. Development of nanocellu-lose-reinforced PLA nanocomposite by using maleated PLA (PLA-g-MA). Journal of Thermoplastic Composite Materials 2018 31(8), 1090-1101. https://doi.org/10.1177/0892705717734600

[91] Sheikh, K.; Shahrajabian, H. Experimental Study on Mechanical, Thermal and Antibacterial Properties of Hybrid Nanocomposites of PLA/CNF/Ag. International Journal of Engi-neering 2021, 34 (1). https://doi.org/10.5829/ije.2021.34.02b.23.

[92] Gazzotti, S.; Rampazzo, R.; Hakkarainen, M.; Bussini, D.; Ortenzi, M. A.; Farina, H.; Lesma, G.; Silvani, A. Cellulose Nanofibrils as Reinforcing Agents for PLA-Based Nano-composites: An in-Situ Approach. Composites Science and Technology 2019, 171, 94–102. https://doi.org/10.1016/j.compscitech.2018.12.015.

[93] Shazleen, S. S.; Yasim-Anuar, T. A. T.; Ibrahim, N. A.; Hassan, M. A.; Ariffin, H. Functionality of Cellulose Nanofiber as Bio-Based Nucleating Agent and Nano-Reinforcement Material to Enhance Crystallization and Mechanical Properties of Polylactic Acid Nanocomposite. Polymers 2021, 13 (3), 389. https://doi.org/10.3390/polym13030389.

[94] Revati, R.; Majid, M. S. A.; Ridzuan, M. J. M.; Mamat, N.; Cheng, E. M.; Alshahrani, H. A. *In Vitro* Biodegradation, Cytotoxicity, and Biocompatibility of Polylactic Acid/Napier Cellulose Nanofiber Scaffold Composites. International Journal of Biological Macromolecules 2022, 223, 479–489. https://doi.org/10.1016/j.ijbiomac.2022.11.041.

[95] Ren, Q.; Wu, M.; Wang, L.; Zheng, W.; Hikima, Y.; Semba, T.; Ohshima, M. Light and Strong Poly (Lactic Acid)/ Cellulose Nanofiber Nanocomposite Foams with Enhanced Rheological and Crystallization Property. The Journal of Supercritical Fluids 2022, 190, 105758.

https://doi.org/10.1016/j.supflu.2022.105758.

[96] Clarkson, C. M.; El Awad Azrak, S. M.; Schueneman, G. T.; Snyder, J. F.; Youngblood, J. P. Crystallization Kinetics and Morphology of Small Concentrations of Cellulose Nano-fibrils (CNFs) and Cellulose Nanocrystals (CNCs) Melt-Compounded into Poly(Lactic Acid) (PLA) with Plasticizer. Polymer 2020, 187, 122101. https://doi.org/10.1016/j.polymer.2019.122101.

[97] Bitinis, N.; Verdejo, R.; Cassagnau, P.; Lopez-Manchado, M. A. Structure and Properties of Polylactide/Natural Rubber Blends. Materials Chemistry and Physics 2011, 129 (3), 823–831. https://doi.org/10.1016/j.matchemphys.2011.05.016.

[98] Phattarateera, S.; Pattamaprom, C. The Viscosity Effect of Masticated Natural vs. Syn-thetic Isoprene Rubber on Toughening of Polylactic Acid. International Journal of Polymer Science 2019, 2019, 1–9. https://doi.org/10.1155/2019/5679871.

[99] Han, D.-H.; Choi, M.-C.; Jeong, J.-H.; Choi, K.-M.; Kim, H.-S. Properties of Acryloni-trile Butadiene Rubber (NBR)/Poly(Lactic Acid) (PLA) Blends and Their Foams. Composite Interfaces 2016, 23 (8), 771–780. https://doi.org/10.1080/09276440.2016.1170518.

[100] Xiao, R. Z.; Zeng, Z. W.; Zhou, G. L.; Wang, J. J.; Li, F. Z.; Wang, A. M. Recent Advances in PEG-PLA Block Copolymer Nanoparticles. International Journal of Nanomedicine 2010, 1057. https://doi.org/10.2147/IJN.S14912.

[101] Cao, L.; Liu, C.; Zou, D.; Zhang, S.; Chen, Y. Using Cellulose Nanocrystals as Sustainable Additive to Enhance Mechanical and Shape Memory Properties of PLA/ENR Thermo-plastic Vulcanizates. Carbohydrate Polymers 2020, 230, 115618. https://doi.org/10.1016/j.carbpol.2019.115618.

[102] Huang, J.; Cao, L.; Yuan, D.; Chen, Y. Design of Multi-Stimuli-Responsive Shape Memory Biobased PLA/ENR/Fe3O4 TPVs with Balanced Stiffness–Toughness Based on Selective Distribution of Fe3O4. ACS Sustainable Chemistry & Engineering 2019, 7 (2), 2304–2315. https://doi.org/10.1021/acssuschemeng.8b05025.

[103] Gong, Z.; Wang, X.; Chen, X.; Chen, Y. Biobased Foamed Thermoplastic Vulcanizate with Good Electromagnetic Interference and Self-Healing Performance. ACS Sustainable Chemistry & Engineering 2023, 11 (24), 9243–9254. https://doi.org/10.1021/acssuschemeng.3c02507.

[104] Wang, W.; Huang, J.; Gong, Z.; Fan, J.; Cao, L.; Chen, Y. Biobased PLA/NR-PMMA TPV with Balanced Stiffness-Toughness: In-Situ Interfacial Compatibilization, Performance and Toughening Model. Polymer Testing 2020, 81, 106268. https://doi.org/10.1016/j.polymertesting.2019.106268.

[105] Wang, Y.; Liu, J.; Xia, L.; Shen, M.; Wei, L.; Xin, Z.; Kim, J. Fully Biobased Shape Memory Thermoplastic Vulcanizates from Poly(Lactic Acid) and Modified Natural Eucommia Ulmoides Gum with Co-Continuous Structure and Super Toughness. Polymers 2019, 11 (12), 2040. https://doi.org/10.3390/polym11122040.

[106] Hu, X.; Kang, H.; Li, Y.; Geng, Y.; Wang, R.; Zhang, L. Preparation, Morphology and Superior Performances of Biobased Thermoplastic Elastomer by *in Situ* Dynamical Vulcanization for 3D-Printed Materials. Polymer 2017, 108, 11–20. https://doi.org/10.1016/j.polymer.2016.11.045.

[107] Liu, G.-C.; He, Y.-S.; Zeng, J.-B.; Li, Q.-T.; Wang, Y.-Z. Fully Biobased and Super-tough Polylactide-Based Thermoplastic Vulcanizates Fabricated by Peroxide-Induced Dynamic Vulcanization and Interfacial Compatibilization. Biomacromolecules 2014, 15 (11), 4260–4271. https://doi.org/10.1021/bm5012739.

[108] Kang, H.; Hu, X.; Li, M.; Zhang, L.; Wu, Y.; Ning, N.; Tian, M. Novel Biobased Thermoplastic Elastomer Consisting of Synthetic Polyester Elastomer and Polylactide by in Situ Dynamical Crosslinking Method. RSC Advances 2015, 5 (30), 23498–23507. https://doi.org/10.1039/C4RA17024E.

[109] Da Costa, F. A. T.; Parra, D. F.; Cardoso, E. C. L.; Güven, O. PLA, PBAT, Cellulose Nanocrystals (CNCs), and Their Blends: Biodegradation, Compatibilization, and Nanoparticle Interactions. Journal of Polymers and the Environment 2023, 31 (11), 4662–4690. https://doi.org/10.1007/s10924-023-02899-7.

[110] Andrade, M. S.; Ishikawa, O. H.; Costa, R. S.; Seixas, M. V. S.; Rodrigues, R. C. L. B.; Moura, E. A. B. Development of Sustainable Food Packaging Material Based on Biodegradable Polymer Reinforced with Cellulose Nanocrystals. Food Packaging and Shelf Life 2022, 31, 100807. https://doi.org/10.1016/j.fpsl.2021.100807.

[111] Nazrin, A.; Sapuan, S. M.; Zuhri, M. Y. M. Mechanical, Physical and Thermal Properties of Sugar Palm Nanocellulose Reinforced Thermoplastic Starch (TPS)/Poly (Lactic Acid) (PLA) Blend Bionanocomposites. Polymers 2020, 12 (10), 2216. https://doi.org/10.3390/polym12102216.

[112] Nazrin, A.; Sapuan, S. M.; Zuhri, M. Y. M.; Tawakkal, I. S. M. A.; Ilyas, R. A. Water Barrier and Mechanical Properties of Sugar Palm Crystalline Nanocellulose Reinforced Thermoplastic Sugar Palm Starch (TPS)/Poly(Lactic Acid) (PLA) Blend Bionanocomposites. Nanotechnology Reviews 2021, 10 (1), 431–442. https://doi.org/10.1515/ntrev-2021-0033.

[113] Nazrin, A.; Sapuan, S. M.; Zuhri, M. Y. M.; Tawakkal, I. S. M. A.; Ilyas, R. A. Flammability and Physical Stability of Sugar Palm Crystalline Nanocellulose Reinforced Thermo-plastic Sugar Palm Starch/Poly(Lactic Acid) Blend

Bionanocomposites. Nanotechnology Re-views 2021, 11 (1), 86–95. https://doi.org/10.1515/ntrev-2022-0007.

[114] Dasan, Y. K.; Bhat, A. H.; Ahmad, F. Polymer Blend of PLA/PHBV Based Bionanocomposites Reinforced with Nanocrystalline Cellulose for Potential Application as Packaging Material. Carbohydrate Polymers 2017, 157, 1323–1332. https://doi.org/10.1016/j.carbpol.2016.11.012.

[115] Choi, J.-H.; Kim, J.-H.; Lee, S. Y.; Jang, S.-K.; Kwak, H. W.; Kim, H.; Choi, I.-G. Thermoplasticity Reinforcement of Ethanol Organosolv Lignin to Improve Compatibility in PLA-Based LignoBioplastics: Focusing on the Structural Characteristics of Lignin. International Journal of Biological Macromolecules 2022, 209, 1638–1647. https://doi.org/10.1016/j.ijbiomac.2022.04.090.

[116] Abdelwahab, M. A.; Jacob, S.; Misra, M.; Mohanty, A. K. Super-Tough Sustainable Biobased Composites from Polylactide Bioplastic and Lignin for Bio-Elastomer Application. Polymer 2021, 212, 123153. https://doi.org/10.1016/j.polymer.2020.123153.

[117] Qahtani, M.; Wu, F.; Misra, M.; Gregori, S.; Mielewski, D. F.; Mohanty, A. K. Experimental Design of Sustainable 3D-Printed Poly(Lactic Acid)/Biobased Poly(Butylene Succinate) Blends via Fused Deposition Modeling. ACS Sustainable Chemistry & Engineering 2019, 7 (17), 14460–14470. https://doi.org/10.1021/acssuschemeng.9b01830.

[118] You, X.; Snowdon, M. R.; Misra, M.; Mohanty, A. K. Poly(Ethylene Terephthalate)/Poly(Lactic Acid) Blends Tailored with Epoxide Compatibilizers. ACS Omega 2018, 3 (9), 11759–11769. https://doi.org/10.1021/acsomega.8b01353.

[119] [119] Quiles-Carrillo, L.; Montanes, N.; Pineiro, F.; Jorda-Vilaplana, A.; Torres-Giner, S. Ductility and Toughness Improvement of Injection-Molded

Compostable Pieces of Polylactide by Melt Blending with Poly(ε-Caprolactone) and Thermoplastic Starch. Materials 2018, 11 (11), 2138. https://doi.org/10.3390/ma11112138.

[120] Si, W.-J.; Yang, L.; Weng, Y.-X.; Zhu, J.; Zeng, J.-B. Poly(Lactic Acid)/Biobased Polyurethane Blends with Balanced Mechanical Strength and Toughness. Polymer Testing 2018, 69, 9–15. https://doi.org/10.1016/j.polymertesting.2018.05.004.

[121] Chen, N.; Peng, C.; Chang, Y.-C.; Li, X.; Zhang, Y.; Liu, H.; Zhang, S.; Zhang, P. Supertough Poly (Lactic Acid)/Bio-Polyurethane Blends Fabricated by Dynamic Self-Vulcanization of Dual Difunctional Monomers. International Journal of Biological Macromolecules 2022, 222, 1314–1325. https://doi.org/10.1016/j.ijbiomac.2022.09.253.

[122] Gurunathan, T.; Chung, J. S.; Nayak, S. K. Reactive Compatibilization of Biobased Polyurethane Prepolymer Toughening Polylactide Prepared by Melt Blending. Journal of Polymers and the Environment 2016, 24 (4), 287–297. https://doi.org/10.1007/s10924-016-0771-x.

[123] Nagarajan, V.; Mohanty, A. K.; Misra, M. Blends of Polylactic Acid with Thermoplastic Copolyester Elastomer: Effect of Functionalized Terpolymer Type on Reactive Toughening. Polymer Engineering & Science 2018, 58 (3), 280–290. https://doi.org/10.1002/pen.24566.

[124] Meyva, Y.; Kaynak, C. Toughening of Polylactide by Bio-Based and Petroleum-Based Thermoplastic Elastomers. International Polymer Processing 2015, 30 (5), 593–602. https://doi.org/10.3139/217.3113.

[125] Sangeetha, V. H.; Varghese, T. O.; Nayak, S. K. Value Addition of Waste Cotton: Effect of Nanofibrillated Cellulose on EVA/EVOH Toughened Polylactic Acid System. Waste and Biomass Valorization 2020, 11 (8), 4119–4128.

https://doi.org/10.1007/s12649-019-00738-2.

[126] Aydemir, D.; Gardner, D. J. Biopolymer Blends of Polyhydroxybutyrate and Polylactic Acid Reinforced with Cellulose Nanofibrils. Carbohydrate Polymers 2020, 250, 116867. https://doi.org/10.1016/j.carbpol.2020.116867.

[127] Hosseinnezhad, R.; Vozniak, I.; Zaïri, F. In Situ Generation of Green Hybrid Nanofibril-lar Polymer-Polymer Composites—A Novel Approach to the Triple Shape Memory Polymer Formation. Polymers 2021, 13 (12), 1900. https://doi.org/10.3390/polym13121900.

[128] Agbakoba, V. C.; Mokhena, T. C.; Ferg, E. E.; Hlangothi, S. P.; John, M. J. PLA Bio-nanocomposites Reinforced with Cellulose Nanofibrils (CNFs) for 3D Printing Applications. Cellulose 2023 30, 11537–11559 https://doi.org/10.1007/s10570-023-05549-2

[129] Tekinalp, H. L.; Meng, X.; Lu, Y.; Kunc, V.; Love, L. J.; Peter, W. H.; Ozcan, S. High Modulus Biocomposites via Additive Manufacturing: Cellulose Nanofibril Networks as "Microsponges." Composites Part B: Engineering 2019, 173, 106817. https://doi.org/10.1016/j.compositesb.2019.05.028.

[130] Huan, S.; Ajdary, R.; Bai, L.; Klar, V.; Rojas, O. J. Low Solids Emulsion Gels Based on Nanocellulose for 3D-Printing. Biomacromolecules 2019, 20 (2), 635–644. https://doi.org/10.1021/acs.biomac.8b01224.

[131] Dong, J.; Mei, C.; Han, J.; Lee, S.; Wu, Q. 3D Printed Poly(Lactic Acid) Composites with Grafted Cellulose Nanofibers: Effect of Nanofiber and Post-Fabrication Annealing Treatment on Composite Flexural Properties. Additive Manufacturing 2019, 28, 621–628. https://doi.org/10.1016/j.addma.2019.06.004.

[132] Ambone, T.; Torris, A.; Shanmuganathan, K. Enhancing the Mechanical Properties of 3D Printed Polylactic Acid Using Nanocellulose. Polymer

Engineering & Science 2020, 60 (8), 1842–1855. https://doi.org/10.1002/pen.25421.

[133] Gomez-Maldonado, D.; Peresin, M. S.; Verdi, C.; Velarde, G.; Saloni, D. Thermal, Structural, and Mechanical Effects of Nanofibrillated Cellulose in Polylactic Acid Filaments for Additive Manufacturing. BioResources 2020, 15 (4), 7954–7964. https://doi.org/10.15376/biores.15.4.7954-7964.

[134] Perić, M.; Putz, R.; Paulik, C. 3D-Printed PLA Filaments Reinforced with Nanofibrillated Cellulose. Journal of Renewable Materials 2020, 8 (7), 759–772. https://doi.org/10.32604/jrm.2020.09284.

[135] Wang, Q.; Ji, C.; Sun, L.; Sun, J.; Liu, J. Cellulose Nanofibrils Filled Poly(Lactic Acid) Biocomposite Filament for FDM 3D Printing. Molecules 2020, 25 (10), 2319. https://doi.org/10.3390/molecules25102319.

[136] Petousis, M.; Vidakis, N.; Mountakis, N.; Papadakis, V.; Kanellopoulou, S.; Gaganatsiou, A.; Stefanoudakis, N.; Kechagias, J. Multifunctional Material Extrusion 3D-Printed Antibacterial Polylactic Acid (PLA) with Binary Inclusions: The Effect of Cuprous Oxide and Cellulose Nanofibers. Fibers 2022, 10 (6), 52. https://doi.org/10.3390/fib10060052.

[137] Gauss, C.; Pickering, K. L. A New Method for Producing Polylactic Acid Biocomposites for 3D Printing with Improved Tensile and Thermo-Mechanical Performance Using Grafted Nanofibrillated Cellulose. Additive Manufacturing 2023, 61, 103346. https://doi.org/10.1016/j.addma.2022.103346.

[138] Zhang, Z.; Cao, B.; Jiang, N. The Mechanical Properties and Degradation Behavior of 3D-Printed Cellulose Nanofiber/Polylactic Acid Composites. Materials 2023, 16 (18), 6197. https://doi.org/10.3390/ma16186197.

[139] Zhang, Z.; Wang, W.; Li, Y.; Fu, K.; Tong, X.; Cao, B.; Chen, B. 3D Printing of

Cellulose Nanofiber/Polylactic Acid Composites via an Efficient Dispersion Method. Composites Communications 2023, 43, 101731. https://doi.org/10.1016/j.coco.2023.101731.

[140] Matsumoto, K.; Takemura, K.; Kitamura, R.; Katogi, H.; Tanaka, T.; Takagi, H. Cellulose Nanofiber-Introduced Continuous-Ramie Yarn-Reinforced Polylactic Acid Filament for 3D Printing: Novel Fabrication Process and Mechanical Properties. Composites Part A: Applied Science and Manufacturing 2024, 176, 107836. https://doi.org/10.1016/j.compositesa.2023.107836.

[141] Fischer, E. W.; Sterzel, H. J.; Wegner, G. Investigation of the Structure of Solution Grown Crystals of Lactide Copolymers by Means of Chemical Reactions. Colloid and Polymer Science 1973, 251, 980-990. https://doi.org/10.1007/BF01498927

[142] Lan, G.-X.; Liu, Y.; Zhou, N.; Guo, D.-Q.; Ma, M.-G. Multifunctional Nanocellulose-Based Composites for Potential Environmental Applications. Cellulose 2023, 30 (1), 39–60. https://doi.org/10.1007/s10570-022-04918-7.

[143] R., R.; Philip, E.; Madhavan, A.; K.B., A.; Binod, P.; Pugazhendhi, A.; Awasthi, M. K.; Gnansounou, E.; Pandey, A.; Sindhu, R. Promising Eco-Friendly Biomaterials for Future Biomedicine: Cleaner Production and Applications of Nanocellulose. Environmental Technology & Innovation 2021, 24, 101855. https://doi.org/10.1016/j.eti.2021.101855.

[144] Zhai, S.; Chen, H.; Zhang, Y.; Li, P.; Wu, W. Nanocellulose: A Promising Nanomaterial for Fabricating Fluorescent Composites. Cellulose 2022, 29 (13), 7011–7035. https://doi.org/10.1007/s10570-022-04700-9

[145] Li, S.; Chen, H.; Liu, X.; Li, P.; Wu, W. Nanocellulose as a Promising Substrate for Advanced Sensors and Their Applications. International Journal of Biological Macromolecules 2022, 218, 473–487.

https://doi.org/10.1016/j.ijbiomac.2022.07.124.

[146] Zinge, C.; Kandasubramanian, B. Nanocellulose Based Biodegradable Polymers. European Polymer Journal 2020, 133, 109758. https://doi.org/10.1016/j.eurpolymj.2020.109758.

[147] Ma, T.; Hu, X.; Lu, S.; Liao, X.; Song, Y.; Hu, X. Nanocellulose: A Promising Green Treasure from Food Wastes to Available Food Materials. Critical Reviews in Food Science and Nutrition 2022, 62 (4), 989–1002. https://doi.org/10.1080/10408398.2020.1832440.

[148] Ng, H.-M.; Sin, L. T.; Bee, S.-T.; Tee, T.-T.; Rahmat, A. R. Review of Nanocellulose Polymer Composite Characteristics and Challenges. Polymer-Plastics Technology and Engineering 2017, 56 (7), 687–731. https://doi.org/10.1080/03602559.2016.1233277.

[149] Haider, T. P.; Völker, C.; Kramm, J.; Landfester, K.; Wurm, F. R. Plastics of the Future? The Impact of Biodegradable Polymers on the Environment and on Society. Angewandte Chemie International Edition 2019, 58 (1), 50–62. https://doi.org/10.1002/anie.201805766.

[150] Ranakoti, L.; Gangil, B.; Mishra, S. K.; Singh, T.; Sharma, S.; Ilyas, R. A.; El-Khatib, S. Critical Review on Polylactic Acid: Properties, Structure, Processing, Biocomposites, and Nanocomposites. Materials 2022, 15 (12), 4312. https://doi.org/10.3390/ma15124312.

[151] Akter, M.; Uddin, M. H.; Tania, I. S. Biocomposites Based on Natural Fibers and Polymers: A Review on Properties and Potential Applications. Journal of Reinforced Plastics and Composites 2022, 41 (17–18), 705–742. https://doi.org/10.1177/07316844211070609.

[152] Al-Abduljabbar, A.; Farooq, I. Electrospun Polymer Nanofibers: Processing,

Properties, and Applications. Polymers 2022, 15 (1), 65. https://doi.org/10.3390/polym15010065.

[153] Kong, L.; Ziegler, G. R. Quantitative Relationship between Electrospinning Parameters and Starch Fiber Diameter. Carbohydrate Polymers 2013, 92 (2), 1416–1422. https://doi.org/10.1016/j.carbpol.2012.09.026.

[154] Cramariuc, B.; Cramariuc, R.; Scarlet, R.; Manea, L. R.; Lupu, I. G.; Cramariuc, O. Fiber Diameter in Electrospinning Process. Journal of Electrostatics 2013, 71 (3), 189–198. https://doi.org/10.1016/j.elstat.2012.12.018.

[155] Wang, L.; Wang, C.; Zhang, Q.; Liu, J.; Xia, X. Comparison of Morphological, Structural and Antibacterial Properties of Different Apocynum Venetum Poly (Lactic Acid)/Nanocellulose Nanofiber Films. Textile Research Journal 2020, 90 (5–6), 593–605. https://doi.org/10.1177/0040517519873868.

[156] Abdullah, T.; Saeed, U.; Memic, A.; Gauthaman, K.; Hussain, M. A.; Al-Turaif, H. Electrospun Cellulose Nano Fibril Reinforced PLA/PBS Composite Scaffold for Vascular Tissue Engineering. Journal of Polymer Research 2019, 26 (5), 110. https://doi.org/10.1007/s10965-019-1772-y

[157] Huan, S.; Liu, G.; Cheng, W.; Han, G.; Bai, L. Electrospun Poly(Lactic Acid)-Based Fibrous Nanocomposite Reinforced by Cellulose Nanocrystals: Impact of Fiber Uniaxial Alignment on Microstructure and Mechanical Properties. Biomacromolecules 2018, 19 (3), 1037–1046. https://doi.org/10.1021/acs.biomac.8b00023.

[158] Zhou, C.; Shi, Q.; Guo, W.; Terrell, L.; Qureshi, A. T.; Hayes, D. J.; Wu, Q. Electrospun Bio-Nanocomposite Scaffolds for Bone Tissue Engineering by Cellulose Nanocrystals Reinforcing Maleic Anhydride Grafted PLA. ACS Applied Materials & Interfaces 2013, 5 (9), 3847–3854. https://doi.org/10.1021/am4005072.

[159] Peng, Q.; Cheng, J.; Lu, S.; Li, Y. Electrospun Hyperbranched Polylactic Acid–Modified Cellulose Nanocrystals/Polylactic Acid for Shape Memory Membranes with High Mechanical Properties. Polymers for Advanced Techs 2020, 31 (1), 15–24. https://doi.org/10.1002/pat.4743.

[160] Cacciotti, I.; Fortunati, E.; Puglia, D.; Kenny, J. M.; Nanni, F. Effect of Silver Nanoparticles and Cellulose Nanocrystals on Electrospun Poly(Lactic) Acid Mats: Morphology, Thermal Properties and Mechanical Behavior. Carbohydrate Polymers 2014, 103, 22–31. https://doi.org/10.1016/j.carbpol.2013.11.052.

[161] Arrieta, M. P.; López, J.; López, D.; Kenny, J. M.; Peponi, L. Biodegradable Electrospun Bionanocomposite Fibers Based on Plasticized PLA–PHB Blends Reinforced with Cellulose Nanocrystals. Industrial Crops and Products 2016, 93, 290–301. https://doi.org/10.1016/j.indcrop.2015.12.058.

[162] Leonés, A.; Salaris, V.; Mujica-Garcia, A.; Arrieta, M. P.; Lopez, D.; Lieblich, M.; Kenny, J. M.; Peponi, L. PLA Electrospun Fibers Reinforced with Organic and Inorganic Nanoparticles: A Comparative Study. Molecules 2021, 26 (16), 4925. https://doi.org/10.3390/molecules26164925.

[163] Yang, Z.; Si, J.; Cui, Z.; Ye, J.; Wang, X.; Wang, Q.; Peng, K.; Chen, W.; Chen, S.-C. Biomimetic Composite Scaffolds Based on Surface Modification of Polydopamine on Electrospun Poly (Lactic Acid)/Cellulose Nanofibrils. Carbohydrate Polymers 2017, 174, 750–759. https://doi.org/10.1016/j.carbpol.2017.07.010.

[164] Yang, Z.; Li, X.; Si, J.; Cui, Z.; Peng, K. Morphological, Mechanical and Thermal Properties of Poly (Lactic Acid) (PLA)/Cellulose Nanofibrils (CNF) Composites Nanofiber for Tissue Engineering. J. Journal Wuhan University of Technology, Materials Science Edition. 2019, 34 (1), 207–215. https://doi.org/10.1007/s11595-019-2037-7.

[165] Xiang, C.; Taylor, A. G.; Hinestroza, J. P.; Frey, M. W. Controlled Release of Nonionic Compounds from Poly(Lactic Acid)/Cellulose Nanocrystal Nanocomposite Fibers. Journal of Applied Polymer Science 2013, 127 (1), 79–86. https://doi.org/10.1002/app.36943.

[166] Liu, W.; Dong, Y.; Liu, D.; Bai, Y.; Lu, X. Polylactic Acid (PLA)/Cellulose Nanowhiskers (CNWs) Composite Nanofibers: Microstructural and Properties Analysis. Journal of Composites Science 2018, 2 (1), 4. https://doi.org/10.3390/jcs2010004.

[167] Patel, D. K.; Dutta, S. D.; Hexiu, J.; Ganguly, K.; Lim, K.-T. Bioactive Electrospun Nanocomposite Scaffolds of Poly (Lactic Acid)/Cellulose Nanocrystals for Bone Tissue Engineering. International Journal of Biological Macromolecules 2020, 162, 1429–1441. https://doi.org/10.1016/j.ijbiomac.2020.07.246.

[168] Rahmat, M.; Karrabi, M.; Ghasemi, I.; Zandi, M.; Azizi, H. Silane Crosslinking of Electrospun Poly (Lactic Acid)/Nanocrystalline Cellulose Bionanocomposite. Materials Science and Engineering: C 2016, 68, 397–405. https://doi.org/10.1016/j.msec.2016.05.111.

[169] Shi, Q.; Zhou, C.; Yue, Y.; Guo, W.; Wu, Y.; Wu, Q. Mechanical Properties and *in Vitro* Degradation of Electrospun Bio-Nanocomposite Mats from PLA and Cellulose Nanocrystals. Carbohydrate Polymers 2012, 90 (1), 301–308. https://doi.org/10.1016/j.carbpol.2012.05.042.

[170] Zong, X.; Kim, K.; Fang, D.; Ran, S.; Hsiao, B. S.; Chu, B. Structure and Process Relationship of Electrospun Bioabsorbable Nanofiber Membranes. Polymer 2002, 43 (16), 4403–4412. https://doi.org/10.1016/S0032-3861(02)00275-6.

[171] Yoon, C. K.; Ko, S. J.; Jeon, J. H.; Lee, W. I. Effect of Ammonium Polyphosphate and Acrylic Acid on NaCl Treated Electrospun PLA Microfiber Mat. Polymer

Engineering & Science 2020, 60 (10), 2448–2458. https://doi.org/10.1002/pen.25483.

[172] Meyva-Zeybek, Y.; Kaynak, C. Electrospinning of PLA and PLA / POSS Nanofibers: Use of Taguchi Optimization for Process Parameters. Journal of Applied Polymer Science 2021, 138 (3), 49685. https://doi.org/10.1002/app.49685.

[173] Kanak, N. A.; Shahruzzaman, Md.; Islam, Md. S.; Takafuji, M.; Rahman, M. M.; Kabir, S. F. Fabrication of Electrospun PLA-nHAp Nanocomposite for Sustained Drug Release in Dental and Orthopedic Applications. Materials 2023, 16 (10), 3691. https://doi.org/10.3390/ma16103691.

[174] Salaris, V.; San Félix García-Obregón, I.; López, D.; Peponi, L. Fabrication of PLA-Based Electrospun Nanofibers Reinforced with ZnO Nanoparticles *and In Vitro* Degradation Study. Nanomaterials 2023, 13 (15), 2236. https://doi.org/10.3390/nano13152236.

[175] Leonés, A.; Peponi, L.; Lieblich, M.; Benavente, R.; Fiori, S. *In Vitro* Degradation of Plasticized PLA Electrospun Fiber Mats: Morphological, Thermal and Crystalline Evolution. Polymers 2020, 12(12), 2975. https://doi.org/10.3390/polym12122975

[176] Peng, H.; Zhou, S.; Guo, T.; Li, Y.; Li, X.; Wang, J.; Weng, J. *In Vitro* Degradation and Release Profiles for Electrospun Polymeric Fibers Containing Paracetanol. Colloids and Surfaces B: Biointerfaces 2008, 66 (2), 206–212. https://doi.org/10.1016/j.colsurfb.2008.06.021.

[177] Injorhor, P.; Trongsatitkul, T.; Wittayakun, J.; Ruksakulpiwat, C.; Ruksakulpiwat, Y. Biodegradable Polylactic Acid-Polyhydroxyalkanoate-Based Nanocomposites with Bio-Hydroxyapatite: Preparation and Characterization. Polymers 2023, 15 (5), 1261. https://doi.org/10.3390/polym15051261.

[178] Klairutsamee, W.; Supaphol, P.; Jangchud, I. Electrospinnability of Poly (Butylene Succinate): Effects of Solvents and Organic Salt on the Fiber Size and Morphology. Journal of Applied Polymer Science 2015, 132 (43), n/a-n/a. https://doi.org/10.1002/app.42716.

[179] Ding, W.; Wei, S.; Zhu, J.; Chen, X.; Rutman, D.; Guo, Z. Manipulated Electrospun PVA Nanofibers with Inexpensive Salts. Macromolecular Materials and Engineering. 2010, 295 (10), 958–965. https://doi.org/10.1002/mame.201000188.

CURRICULUM VITAE

Burcu Sarı

Department of Metallurgical and Materials Engineering, Polymers and Nanocomposites Laboratory D-307, Middle East Technical University (METU), 06800, Ankara/Turkey

EDUCATION

Doctor of Philosophy (2024)
Department of Polymer and Science Technology
Middle East Technical University (METU), Ankara, Turkey
Dissertation Subject: Studies on the Nanocellulose Filled Polylactide Based Biocomposites
Advisor: Prof. Dr. Cevdet KAYNAK

Master of Science (2015)
Department of Polymer and Science Technology
Middle East Technical University (METU), Ankara, Turkey
Thesis Subject: Properties of Polylactide / Montmorillonite Nanocomposites: Before and After Weathering
Advisor: Prof. Dr. Cevdet KAYNAK

Bachelor of Science (2012)
Department of Materials Science and Engineering
Anadolu University, Eskişehir, Turkey
Thesis Subject: Mechanical Characterization of Polymer Matrix Composites Produced by Resin Transfer Molding
Advisor: Prof. Dr. Abdullah Tuğrul Seyhan

Associate Degree (2010)
Department of Business Administration
Anadolu University, Eskişehir, Turkey

PROFESSIONAL EXPERIENCE

09/2012 - 09/2022
Research Assistant
Polymer Science and Technology Department/METU

RESEARCH INTERESTS

Research & Engineering Projects, Materials Production and Characterization, Polymers, Composites, Nanotechnology, Biotechnology, Sustainability, Green Materials

INTERNATIONAL PUBLICATIONS (SCI)

1. B. Sari and C. Kaynak, "Obtaining Cellulose Nanocrystals by Acid Hydrolysis Procedure; and Their Use as Reinforcement in Polylactide Biocomposites", Journal of Thermoplastic Composite Materials,(submitted in February 2024, under review)

2. B. Sari and C. Kaynak, "Contribution of Cellulose Nanofibrils on the Strengthening and Toughening of Neat and Blended Polylactide Specimens; and the Differences After 3D-Printing", Journal of Thermoplastic Composite Materials, (accepted in March 2024) (available online), DOI: 10.1177/08927057241241499

3. B. Sari and C. Kaynak, "Parameters Influencing Electrospun Nanofiber Diameter of Polylactide Incorporated with Cellulose Nanofibrils and Nanocrystals", Journal of Thermoplastic Composite Materials, (accepted in February 2024) (available online), DOI: 10.1177/08927057241235650

4. B. Sari and C. Kaynak, "Effects of Montmorillonite Content and Maleic Anhydride Compatibilization on the Mechanical Behavior of Polylactide Nanocomposites", International Polymer Processing, 31 (4), 454-462 (August 2016)

5. C. Kaynak and B. Sari, "Accelerated Weathering Performance of Polylactide and its Montmorillonite Nanocomposite", Applied Clay Science, 121, 86-94 (March 2016)

INTERNATIONAL CONFERENCE PROCEEDINGS

1. B. Sari and C. Kaynak , "Effect of Electrospinning Parameters on Polylactic Acid / Nanocellulose Biocomposite Fibers", Congress Proceedings Book of the International Conference on Nanotechnology for Renewable Materials - TAPPI NANO - 2022, Technical Association of the Pulp and Paper Industry, Helsinki (13 – 18 June 2022)

2. B. Sari and C. Kaynak, "Characterization of Cellulose Nanocrystals Produced via Acid Hydrolysis Method", Congress Proceedings Book of the 20th International Metallurgy and Materials Congress - IMMC 2021, UCTEA Chamber of Metallurgical Engineers, Istanbul, 1 page on USB, (10 – 12 June 2021)

3. C. Kaynak and B. Sari, "Weathering Degradation of Polylactide / Montmorillonite Nanocomposites", Book of Abstracts of the 14th International Conference on Nanosciences & Nanotechnologies – NN17, Aristotle University of Thessaloniki, Thessaloniki, Greece, page 83, (4-7 July 2017)

4. B. Sari and C. Kaynak, "Behavior of Polylactide / Montmorillonite Nanocomposites", Congress Proceedings Book of the 18th International Metallurgy and Materials Congress - IMMC 2016, UCTEA Chamber of Metallurgical Engineers, Istanbul, pages: 258-260, (29 September – 1 October 2016)

CITATIONS (as 23.02.2024)

Sum of times cited (ISI Web of Science):	58
H-index (ISI Web of Science)	2

NATIONAL CONFERENCE PROCEEDINGS

1. B. Sarı, C. Kaynak, "Polilaktit/Montmorillonit Nanokompozitlerinin Mekanik ve Isıl Davranışları", 5. Ulusal Polimer Bilim ve Teknoloji Kongresi, Gaziosmanpaşa Üniversitesi, Tokat, Bildiri Özetleri, sayfa:78, (1-4 Eylül 2014)

AWARDS

Burcu Sarı, "ABS and Its' Biocomposites in Soft Tissue Engineering" SABIC, Innovate Your Idea, 3rd prize
Various Publication and Course Performance Awards

ASSISTED COURSES

- PST 502 Polymer Science and Technology (Coordinator)
- PST 508 Characterization Techniques for Polymeric Materials
- CHEM 101&102 General Chemistry Laboratory
- METE 215 Materials Processing Laboratory
- METE 470 Composite Materials
- METE 560 Polymer Nanocomposites

LANGUAGE

English: Fluent (METU EPE:84, YÖKDİL:86)